


# Evaluation of Corrosion Behaviour of Hot Dip Zn and Zn-Al Alloy Coatings on Steel Wire using Laboratory and Field Tests

Centre for Materials Engineering

Masters Dissertation

Student: Tapiwa Tevera

Supervisor: Prof. R.D. Knutsen

Final submission: 27 June 2014

# Plagiarism Declaration

I, Tapiwa Silas Tevera, know the meaning of plagiarism and declare that all the work in this document save for that which is properly acknowledged, is my own.

Signature:..Signed by candidate Signature Removed……

Date:……..27 June 2014……

# Abstract

The use of galvanised coatings on steel for structural ropes, bundles and wires has become standard practice as unprotected steel is prone to corrosion degradation. Galvanised coatings increase the service lifespan of steel by providing barrier and cathodic corrosion protection. Zinc (Zn) and zinc-aluminium (Zn-Al) alloys are the most commonly used metallic coatings on steel wire. Zn-Al coatings outperform Zn coatings, most notably in marine environments, as they combine the highly insulating oxide film associated with Al corrosion and the cathodic protection of Zn to the underlying steel.

Corrosion behaviour of hot dipped Zn Class A (235 g/m$^2$), Zn Class B (135 g/m$^2$), Zn-5Al (150 g/m$^2$), Zn-5Al-xMg (150 g/m$^2$) and Zn-10Al (300 g/m$^2$) coatings on various wire structures was investigated in this study with particular attention being given to wire configuration, wire diameter and coating mass distribution. Test specimens were exposed to corrosive environments represented by the continuous ASTM B117 salt spray test and the cyclic VW PV 1210 salt spray test, both carried out over a 12-week period. Environmental exposure tests were also carried out over a 16-month period at Chapman's Peak, a local coastal environment.

A qualitative examination of corrosion products on specimens exposed to laboratory tests revealed that corrosion was more prolific in steel rope, followed by the bundles and finally the wires, regardless of the coating applied on the materials. The high corrosion activity observed in ropes and bundles was due to the high prevalence of crevice corrosion in these systems owing to their construction.

On the basis of calculated corrosion rates of wires exposed to the salt spray tests a relative ranking of the coatings is as follows: Zn-10Al (300 g/m$^2$) > Zn-5Al-xMg (150 g/m$^2$) > Zn-5Al (150 g/m$^2$) > Zn Class A (235 g/m$^2$) > Zn Class B (135 g/m$^2$). The Zn-10Al (300g/m$^2$) coating outperformed the both Zn-5Al (150g/m$^2$) and Zn-5Al-xMg (150g/m$^2$) coatings owing to the higher Al content in the alloy. The presence of Mg in the Zn-5Al-xMg (150g/m$^2$) coating was responsible for its improved corrosion performance over the Zn-5Al (150g/m$^2$) coating. The high dissolution rates of the Zn Class A (235 g/m$^2$) and Zn Class B (135 g/m$^2$) coatings made them the least effective of all the coatings. However, Zn Class A (235 g/m$^2$) performed better than the Zn Class B (135 g/m$^2$) coating owing to its greater coating thickness.

The environmental exposure tests further supported the superiority of Zn-Al alloy coatings over Zn coatings. However it could not be determined from the 16-month study which of the Zn-Al alloy coatings performed better when exposed to the local coastal environment.

# Contents

# 1. Introduction

## 1.1 Subject of Study

The subject of this study is to evaluate the corrosion performance of select hot dip zinc (Zn) and zinc-aluminium (Zn-Al) alloy coatings on steel wire exposed to harsh environmental conditions represented by accelerated laboratory corrosion tests as well as an environmental exposure test carried out along Chapman's Peak Drive, Hout Bay near Cape Town.

## 1.2 Background to the Study

The use of hot dip coatings on steel for structural ropes, bundles and wires has become standard practice as unprotected steel is prone to corrosion degradation. Galvanised coatings increase service lifespan of steel by providing barrier and cathodic corrosion protection. Zn and Zn-Al alloy coatings are the most commonly used metallic coatings on steel wire. Zn-Al coatings outperform Zn coatings, most notably in marine environments, as they combine the highly insulating oxide film associated with Al corrosion and the cathodic protection of Zn to the underlying steel.

Catch fences, or rock fall barriers, have been installed along Chapman's Peak Drive to protect motorists from rock falls. These catch fences consist of steel components in the form of rope, bundles and wires. Chapman's Peak Drive is situated in a coastal environment where steel readily corrodes. Therefore, the use of galvanized coatings is critical in terms of protecting steel from corrosion in such environments. Zn-Al alloy coatings outperform Zn coatings owing to the superior barrier layer formed by corrosion products of Al.

## 1.3 Objectives of the Study

This study aims to achieve the following:

- Compare the relative corrosion resistance of different coating systems on steel wires, taking into account wire configuration, wire diameter and the coating mass distribution.
- Compare and contrast the experimental results obtained from the accelerated corrosion tests represented by the ASTM B117 and VW PV 1210 salt spray tests as well as environmental exposure tests carried out along Chapman's Peak Drive.
- Determine the usefulness of the ASTM B117 and VW PV 1210 salt spray tests in mimicking corrosion behaviour in the natural environment.
- Describe the mechanism of localised corrosion attack in Zn-Al alloy coatings on steel wire in a marine environment.

## 1.4 Scope and Limitations

(1) Samples were provided with the Zn and Zn-Al alloy coatings already having been applied on the material. The hot dipping procedure and constituents of the galvanizing baths were not revealed as this information is proprietary. (2) The samples had different coating mass distributions which complicated the assessment of relative corrosion performance of the coatings. Though the composition of a coating determines its corrosion rate, the lifespan of a coating is significantly impacted by its coating mass distribution. (3) The manufacturer stated that the substrate steel was a low carbon steel, however the chemical composition of the steel was not provided. (4) The environmental exposure tests were limited to 16 months, the maximum period during which the test could be run. Results of environmental corrosion tests are more meaningful when the tests are carried out over a much longer period of time.

## 1.5 Plan of Development

This report continues with a review of relevant literature in chapter 2, after which the experimental methods followed in the study are described in chapter 3. Chapter 4 through to chapter 8 report and discuss results of this study. The results chapters begin with a qualitative examination of corrosion performance of rope exposed to the ASTM B117 and VW PV 1210 tests on the basis of their coatings as well as the size of the rope. In chapter 5, a quantitative comparison of corrosion performance of Zn and Zn-Al coatings on wire is presented. The microstructure of the Zn-Al alloys coatings before and after the salt spray tests are the main focus of chapter 6. Chapters 7 and 8 deal with corrosion performance of wire in bundle configuration and results of environmental exposure test respectively. The conclusions of the study are summarized in Chapter 9 with recommendations highlighted in Chapter 10.

# 2. Literature Review

## 2.1 What is Steel?

The term 'steel' is used to describe alloys composed primarily of iron and carbon. Steel is the most widely used engineering material in the world due to its low price and favourable material properties, which include high strength and ductility [1]. The World Steel Association estimates that the global production of steel in 2012 exceeded 1,5 billion tonnes [1,2], which was over 30 times greater than aluminium production, the next second most used metal in the world [2]. A classification of steel is presented in **Table 2.1** on the basis of carbon composition with typical applications of the types of steel given [3].

**Table 2.1: Classification of steel based on carbon composition** [3]

| Name of steel | Carbon composition (wt. %) | Example of application |
|---|---|---|
| Ultra low carbon steel | 0.03 < | |
| Low carbon steel | 0.04 – 0.15 | Wire, tubing, car bodies |
| Mild | 0.15 – 0.30 | Buildings, bridges, piping |
| Medium | 0.30 – 0.60 | Machinery, tractors, mining equipment |
| High | 0.60 – 0.99 | Springs, railroad car wheels |
| Ultra high carbon steel | 1.0 – 2.0 | Ball bearings, drills, metal cutting tools |
| Cast iron | 2.0 – 4.0 | Engine cylinder blocks, |

## 2.2 Understanding Why Steel Corrodes

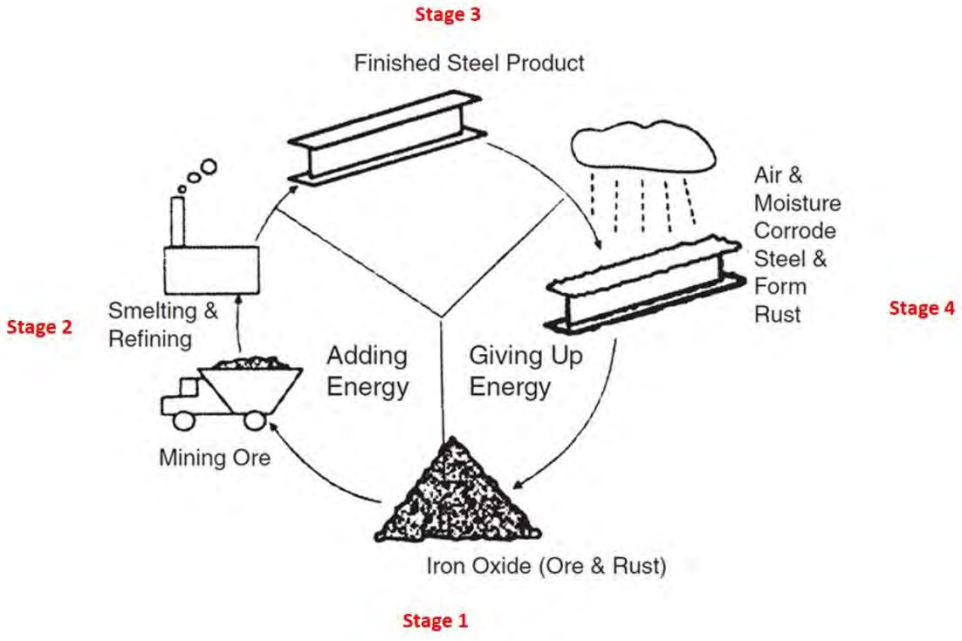


**Figure 2.1: Corrosion lifecycle of steel** [4]

A major disadvantage of steel is that it is oxidised under moist conditions to form red/brown corrosion products, or rust, in a process called corrosion [5]. Corrosion is defined as a chemical or electrochemical reaction between a metal or alloy and its environment [5]. The corrosion lifecycle of steel may be summarised in four simple stages (**Figure 2.1**):

**Stage 1** - Iron exists in nature mainly as oxide ores, which are chemical compounds largely composed of iron oxide [4].

**Stage 2** – During the energy consuming processes of smelting and refining, iron oxide is reduced to an iron-carbon alloy, generally referred to as pig iron or cast iron when used to produce engineering components [6]. This process leaves the iron in a thermodynamically unstable state [4,5]. Steel is, however, made in a secondary process after refining the hot metal (liquid iron) by reducing the carbon to levels $\leq 0.02\%$ in a convertor thereafter adjusting the composition of the other elements using appropriate ferroalloys that include manganese and silicon to obtain the desired steel grade [6].

**Stage 3** - Once in service, steel articles react with air and moisture in the environment in an energy releasing process [5].

**Stage 4** - The steel is subsequently converted to hydrated iron oxide, a more thermodynamically stable compound. This hydrated iron oxide is basically $Fe(OH)_3$, the red/brown coloured corrosion product that appears when iron or steel are exposed to oxygen in moist conditions [67-9].

## 2.3 Mechanisms by which Steel Corrodes

Corrosion is classified into various categories according to the morphology of corrosion damage which is largely determined by the environment the steel is exposed to [10]. The main mechanisms of corrosion are reviewed in this section.

### 2.3.1 Uniform or General Attack

Uniform corrosion is characterised by an even thinning of a metal or alloy which occurs over a large area at a relatively constant rate as illustrated in **Figure 2.2**. Factors affecting uniform corrosion include the nature of the exposed metal; with reference to shape, thickness, surface condition and chemistry of the metal. A shape that retains moisture, and as a result, does not drain properly will corrode faster than metals with shapes that do not retain moisture [8,11].

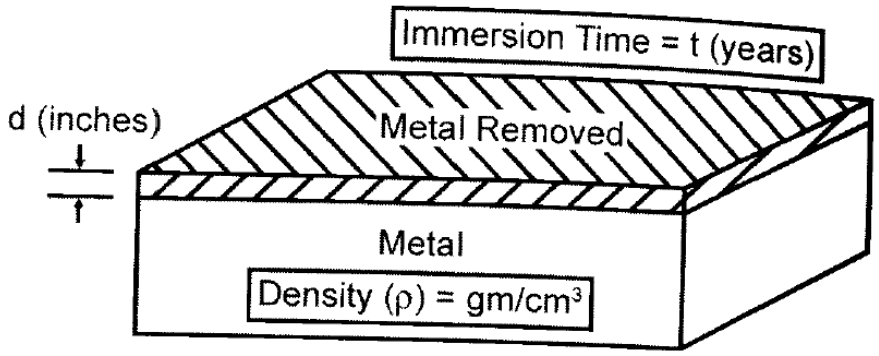


**Figure 2.2: Uniform corrosion of a metal showing a thickness (*d*) removed in time (*t*) [8].**

Thick metals are more susceptible to corrosion than thin metals. Section thickness affects the period of wetness, with thick sections maintaining a film of moisture on the metal's surface for a much longer period of time than thin sections. This is caused by an ambient temperature lag increase in the thicker metal. Pollutants such as chlorides, hydrogen, and sulphur containing compounds increase the oxidizing power of an environment which may lead to an increased rate of uniform corrosion [7,11,12].

### 2.3.2 Pitting Corrosion

Pitting corrosion refers to localised corrosion which selectively attacks areas of a metal surface where scratches or mechanically induced breaks exist in a protective film [10]. Compositional heterogeneity such as inclusions or precipitates and emerging dislocations caused by residual tensile stresses also contribute towards pitting [10]. **Figure 2.3** illustrates the process of pitting. General corrosion precedes pit initiation over an area of the wetted surface (**Figure 2.3a**). Oxygen consumption by normal cathode reactions in neutral solution creates an oxygen concentration gradient within the electrolyte [10,13]. This anodically polarises the central region which actively dissolves (**Figure 2.3b**) [10]. Hydroxyl ($OH^-$) ions, generated in the cathode region, diffuse inward and react with iron ($Fe^{2+}$) ions diffusing outwards (**Figure 2.3b**). This results in deposition of insoluble corrosion products around the pit [10]. Over time, the corrosion products form a scab over the pit which isolates its internal environment from the bulk environment (**Figure 2.3c**) [10,13]. Chlorides and oxidising agents in the environment are known to promote this mechanism of corrosion [7,10,11,13].

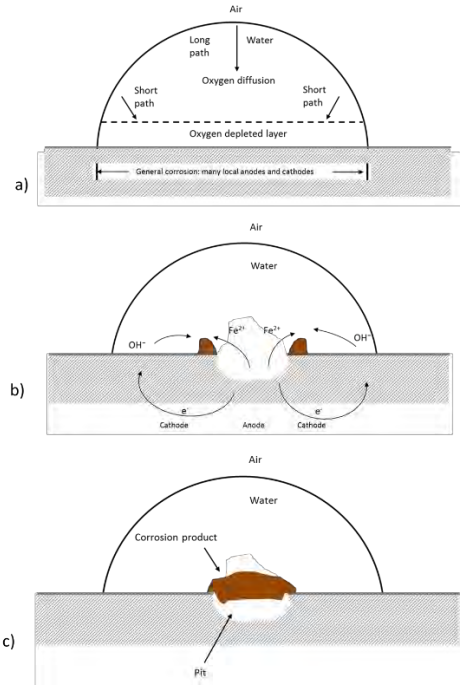


**Figure 2.3: Simple illustration of pitting corrosion mechanism. (a) General corrosion over wetted area results in oxygen depletion in adjacent electrolyte to steel surface. (b) Metal dissolution leads to corrosion product formation around the newly formed pit. (c) Corrosion products accumulate with time to cover the pit [10].**

### 2.2.3 Crevice Corrosion

Crevice corrosion occurs in regions of a metal that are shielded, or confined, from an electrolyte relative to the rest of the metal [13]. The geometry of metallic structures is therefore important in determining whether crevice corrosion is promoted or inhibited [13]. Examples of situations where crevice corrosion is predicted to occur are summarised in **Figure 2.4** [13].

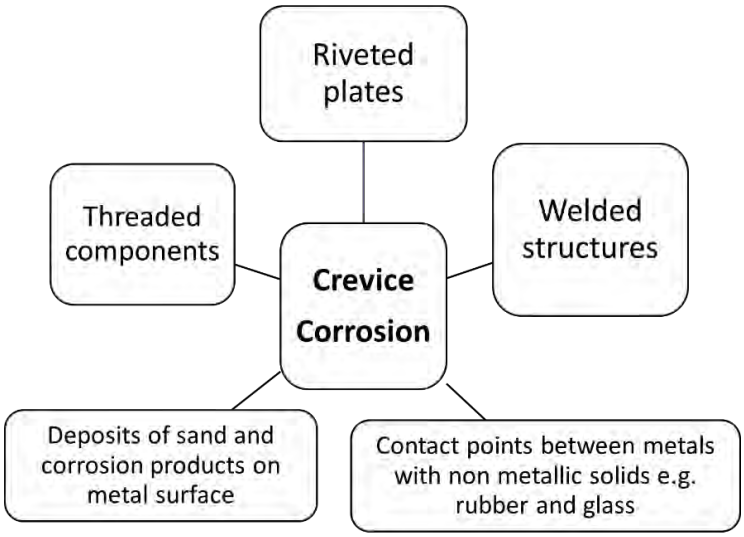


**Figure 2.4: Situations where crevice corrosion is prevalent**

A widely accepted mechanism for crevice corrosion has been proposed by Fontana-Greene which has been illustrated in **Figure 2.5**. Their mechanism may be summarised as follows [13]:

1. Corrosion occurs slowly over the entire exposed metal surface area. Normal anode and cathode processes occur whereby the generation of positive metal ions is counterbalanced by $OH^-$ ions (**Figure 2.5a**).
2. Dissolved oxygen is more readily replaced at metal surfaces in the bulk electrolyte as opposed to within crevices. The lack of oxygen within crevices impedes the cathodic process. As a result, generation of $OH^-$ ions is diminished.
3. Diffusion of negative ions occurs from the bulk electrolyte into the crevice, where there is an excess of positive ions, in order to maintain the potential energy at a minimum. The presence of chlorides promotes the development of low pH because of low tendency to associate with hydrogen ions in water.
4. The increase in hydrogen ion concentration accelerates the metal dissolution process within the crevice. Therefore, metal within the crevice will corrode rapidly while metal outside the crevice area will be catholically protected (**Figure 2.5b**).

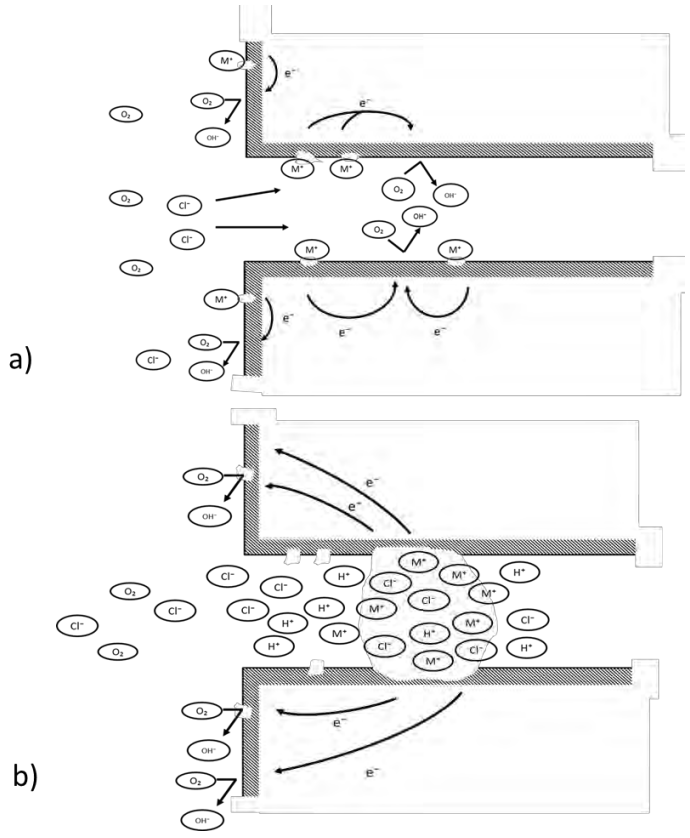


**Figure 2.5: The Fontana-Greene mechanism of crevice corrosion. (a) Initial corrosion occurs over the entire surface of the metal. (b) Metal dissolution only occurs within crevice where concentration of hydrogen and chloride ions is high [13].**

### 2.3.4 Intergranular Corrosion

Intergranular corrosion, or grain boundary corrosion, occurs when a grain boundary area is attacked because of the presence of precipitates in these regions. Grain boundaries are often the preferred sites for the precipitation and segregation (**Figure 2.6**) which become anodic relative to the interior of the grain [13,14].

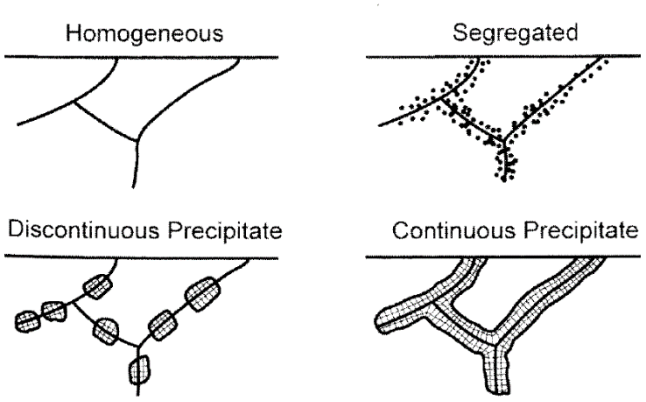


**Figure 2.6: Intergranular corrosion takes place when elements segregating or precipitating at grain boundaries cause the area to become anodic in relation to the interior of the grain [8].**

### 2.3.5 Galvanic Corrosion

Galvanic corrosion, which may also be referred to as dissimilar metal corrosion, occurs when the potential difference exists between two dissimilar metals immersed in a corrosive environment [7]. A galvanic couple may be the cause of premature failure in steel components; for example, when steel is in contact with copper. In such cases, steel will be anodic relative to copper, as predicted by the galvanic series, and thus will corrode preferentially as highlighted in **Figure 2.7**. Galvanic couples may be used advantageously to protect steel from corrosion, as described in **Section 2.5.1**.

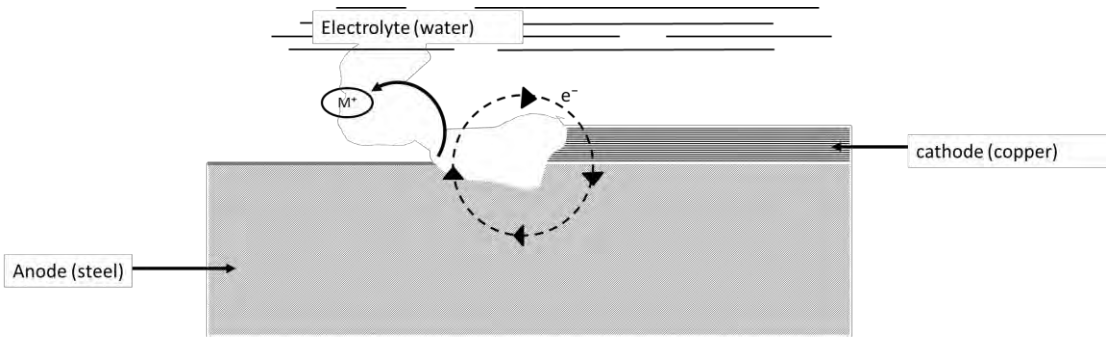


**Figure 2.7: Galvanic couple formed between steel and copper whereby steel is corroded in preference to copper [13].**

The potential difference available to promote the electrochemical corrosion reaction is reflected by the galvanic series shown in **Figure 2.8**. The galvanic series is simply a list of common metals and

alloys arranged according to their tendency to corrode galvanically in a particular environment [7,12,14]. The strongest galvanic couples are observed when metals and alloys are far apart from each other within the galvanic series [13,14]. The galvanic series is not be confused with the electrochemical series (**Table 2.2**), which shows exact potentials based on highly standardised conditions that rarely exist in nature [13]. A summary of the key differences between the galvanic and electrochemical series are shown in **Table 2.3**.

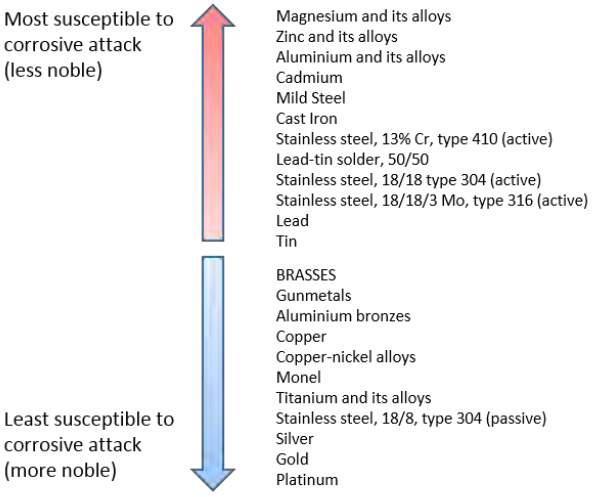


**Figure 2.8: Galvanic series of metals and their alloys in seawater** [13,14]

**Table 2.2: The electrochemical series** [10,13]

| Cathode (Reduction) | | | Half Reaction Standard Potential E° (V) |
|---|---|---|---|
| $F_2(g) + 2e^-$ | → | $2F^-(aq)$ | +2.87 |
| $Au^+(aq) + e^-$ | → | $Au(s)$ | +1.68 |
| $Cl_2(g) + 2e^-$ | → | $2Cl^-(aq)$ | +1.36 |
| $O_2(g) + 4H^+(aq) + 4e^-$ | → | $2H_2O(1)$ | +1.23 |
| $Ag^+(aq) + e^-$ | → | $Ag(s)$ | +0.80 |
| $Fe^{3+}(aq) + e^-$ | → | $Fe^{2+}(aq)$ | +0.77 |
| $I_2(s) + 2e^-$ | → | $2I^-(aq)$ | +0.54 |
| $O_2(g) + 2H_2O(l) + 4e^-$ | → | $4OH^-(aq)$ | +0.40 |
| $Cu^{2+}(aq) + 2e^-$ | → | $Cu(s)$ | +0.34 |
| $2H^+(aq) + 2e^-$ | → | $H_2(g)$ | 0.00 |
| $Pb^{2+}(aq) + 2e^-$ | → | $Pb(s)$ | −0.13 |
| $Sn^{2+}(aq) + 2e^-$ | → | $Sn(s)$ | −0.14 |
| $Ni^{2+}(aq) + 2e^-$ | → | $Ni(s)$ | −0.23 |
| $Co^{2+}(aq) + 2e^-$ | → | $Co(s)$ | −0.28 |
| $Fe^{2+}(aq) + 2e^-$ | → | $Fe(s)$ | −0.44 |
| $Zn^{2+}(aq) + 2e^-$ | → | $Zn(s)$ | −0.76 |
| $2H_2O(l) + 2e^-$ | → | $H_2(g) + 2OH^-(aq)$ | −0.83 |
| $Al^{3+}(aq) + 3e^-$ | → | $Al(s)$ | −1.67 |
| $Mg^{2+}(aq) + 2e^-$ | → | $Mg(s)$ | −2.34 |
| $Na^+(aq) + e^-$ | → | $Na(s)$ | −2.71 |
| $Ca^{2+}(aq) + 2e^-$ | → | $Ca(s)$ | −2.87 |
| $K^+(aq) + e^-$ | → | $K(s)$ | −2.93 |

**Table 2.3: Significant differences between galvanic and electrochemical series** [10,13]

| Galvanic series | Electrochemical series |
|---|---|
| 1. A relative **qualitative** series listing an experimental order of nobility/activity of metals | 1. An absolute **quantitative** series listing electrochemical data for use in precise calculations |
| 2. Lists data for both pure metals and alloys | 2. Only lists data for metal elements |
| 3. Measured under arbitrary (but specified) conditions of temperature, pressure and electrolyte | 3. Measured under standard conditions and is independent of other species in the environment |

## 2.4 The Need to Protect Steel from Corrosion Damage

Steel corrodes in all environments; however it is most prone to corrosion in harsh environments, such as marine and industrial settings [15]. Atmospheric corrosion of steel is one of the principle causes of economic losses in the automotive, construction, and manufacturing industries [16]. As a result, greater emphasis has gone into the design and protection of metal structures exposed to corrosive atmospheres [16].The corrosion performance of steel may be vastly improved by alloying it with elements such as chromium and nickel, as in the case of stainless steels [15]. However, it is expensive to do so and may not be practical for various applications [15]. Corrosion protection of steel by use of metallic coatings has proved to be a more affordable alternative [15].

## 2.5 Corrosion Protection by Metallic Coatings

Protective coatings are applied onto steel for three main reasons [15,17]:

1. To reduce corrosion of the substrate metal.
2. To modify the physical or mechanical properties of the substrate metal.
3. To achieve and maintain some desired decorative effect.

The relative importance of these criteria will determine the appropriate coating material used as well as its method of application [15]. In the case of steel, reducing the rate of corrosion, especially in harsh environments, is the most important reason for the use of coatings.

Metallic coatings offer the widest range of coating material, as well as coating techniques for application of a specific coating in comparison to non-metallic coatings such as paint and organic coatings [15]. **Table 2.4** summarizes the most important techniques for metallic coating application.

**Table 2.4: Techniques for metallic coating application** [15]

| Coating Techniques |
|---|
| Electrodeposition |
| Electroless |
| Electrophoretic |
| Hot dipping |
| Spraying |
| Cladding |
| Vacuum/Vapour |
| Vapour dissociation |
| Cementation and diffusion |

The properties and performance of metallic coatings need to be considered in combination with the coating/substrate interaction as it impacts the effectiveness of the coating in protecting the underlying metal from corrosion [15]. Metals that are more anodic relative to steel in the electrochemical series (**Table 2.2**) will corrode preferentially and will therefore sacrificially protect steel. Conversely, metals that are cathodic relative to steel cannot sacrificially protect steel [8,10,15]. It is important to note that these relationships cannot be considered on thermodynamic grounds alone as shown in the electrochemical series. Coating/substrate relationships must be considered for specific environments [13,15].

### 2.5.1 Use of Zn as a Protective Metallic Coating on Steel

Zn is used as a protective coating on steel more than any of the other non-ferrous metals [15]. It is a cheap metal which can be easily applied onto steel by a variety of coating processes (**Table 2.4**). Zn coatings protect steel by first serving as barriers which separate steel from a corrosive environment [18]. Secondly, Zn coatings also provide galvanic or sacrificial corrosion protection to the underlying steel at voids, scratches and cut edges of the coating [15,16,18]. Sacrificial corrosion is maintained until the exposed area of the substrate exceeds the area over which the electrochemical protective reaction can be maintained [15] .

During corrosion of Zn, a porous superficial oxide layer ($ZnO_2$) forms on the coating surface by a mechanism of dissolution and reprecipitation [18]. This leads to formation of preferential corrosion pathways across high porosity areas which account for the linear corrosion rate of Zn coatings [18]. $Zn(OH)_2$ may precipitate at the cathodic areas of the exposed steel, following dissolution of Zn, forming a secondary barrier layer [18]. The corrosion products of Zn are white in appearance and are commonly referred to as white rust [16]. A general darkening and roughening of the Zn coating surface is observed as a result of corrosion [15,16]. Apart from this, there is little deterioration in the appearance of the underlying steel as long as the Zn coating is able to sacrificially protect it. When a Zn coating eventually fails corrosion of steel will take place which is identified by the formation of red/brown corrosion products of steel [4,5,7,8].

### 2.5.2 Application of Zn Coatings onto Steel by Hot Dip Galvanizing

Hot dip galvanizing is one of the methods used to apply Zn coatings onto steel products as highlighted in **Table 2.4**. The process involves immersing a steel article into a molten Zn bath at temperatures between 445°C – 450°C, leading to metallurgical bond formation between the molten Zn and the surface of the steel article as a result of interfacial alloying [10]. As a result, when the steel article is removed from the bath its entire surface will be covered in a thin Zn overlay [10].

The coating mass distribution of a Zn hot dip coating is dependent on the classification of galvanizing process which refers to the manner in which the coating is processed after application. Coatings applied onto wire commonly fall into one or two categories; Class A or Class B coatings [19,20]. In Class A coatings, the hot dip process occurs after wire drawing which consequently makes diameter of the coating more difficult to control and limits tensile strength of the coated wire [20]. However, in Class B coatings the wire is drawn after the coating has been applied which gives better control of wire diameter and coating thickness [19,20].

Coating mass distribution generally increases with wire diameter as shown by guidelines in **Table 2.5** [18]. It is common practice for a wire manufacturer to provide wire with a coating significantly in excess of the minimum required by standards in order to allow for variation in the coating process[19].

**Table 2.5: Minimum weight of Zn coatings as specified by the EN 10244.2** [19,20]

| Wire Diameter, d (mm) | Class A coating ($g/m^2$) | Class B coating ($g/m^2$) |
|---|---|---|
| 0.15 ≤ d < 0.20 | - | 15 |
| 0.20 ≤ d < 0.25 | 30 | 20 |
| 0.25 ≤ d < 0.32 | 45 | 30 |
| 0.32 ≤ d < 0.40 | 60 | 30 |
| 0.40 ≤ d < 0.50 | 85 | 40 |
| 0.50 ≤ d < 0.60 | 100 | 50 |
| 0.60 ≤ d < 0.70 | 115 | 60 |
| 0.70 ≤ d < 0.80 | 130 | 60 |
| 0.80 ≤ d < 0.90 | 145 | 70 |
| 0.90 ≤ d < 1.00 | 155 | 70 |
| 1.00 ≤ d < 1.20 | 165 | 80 |
| 1.20 ≤ d < 1.40 | 180 | 90 |
| 1.40 ≤ d < 1.65 | 195 | 100 |
| 1.65 ≤ d < 1.85 | 205 | 100 |
| 1.85 ≤ d < 2.15 | 215 | 115 |
| 2.15 ≤ d < 2.50 | 230 | 125 |
| 2.50 ≤ d < 2.80 | 245 | 125 |
| 2.80 ≤ d < 3.20 | 255 | 135 |
| 3.20 ≤ d < 3.80 | 265 | 135 |
| 3.80 ≤ d < 4.40 | 275 | 135 |
| 4.40 ≤ d < 5.20 | 280 | 150 |
| 5.20 ≤ d < 8.20 | 290 | |
| 8.20 ≤ d < 10.00 | 300 | |

### 2.5.3 Review of Zn Hot Dip Galvanizing Process

The main steps in the Zn galvanizing process of steel articles include surface preparation of the steel, immersion of the steel article into a molten Zn bath, and inspection of the Zn coated steel article after galvanizing. Each of these steps has its own series of processes that are important in ensuring the success of the Zn galvanizing process [21-23].

**Step 1: Surface Preparation**

It is essential that the surface of the steel article is clean prior to hot dipping, as Zn will not react with an unclean steel surface. Surface preparation consists of three stages:

**Degreasing**. Grease, oil and paint are removed by immersing the steel article into a hot alkali solution, such as sodium hydroxide [16,22].

**Pickling**. Mill scale, rust and other surface oxides are removed by rinsing the steel article in hydrochloric or sulphuric acid [18,22].

**Fluxing.** The steel article is immersed in a hot zinc ammonium chloride solution which conditions the steel surface to react with molten Zn [16,21,22]. Fluxing specifically dissolves oxide films formed on the steel after pickling ensuring that the steel surface remains clean prior to immersion in the molten Zn bath [21].

**Step 2: Galvanizing**

Steel is completely immersed into the molten Zn bath maintained at temperatures between 445 - 450°C, which is the temperature range during which a metallurgical bond forming reaction between Zn and steel occurs [18]. Excess Zn is removed from the newly Zn coated steel article by draining, vibration or air blowing [18].

The Zn coated steel article is cooled by one of several approaches which include quenching in a passivation solution, quenching in water, furnace cooling, or cooling in the open air [16,18]. In addition to quickly cooling the steel, quenching in a passivation solution such as sodium dichromate provides temporary corrosion protection to the Zn coating [18].

**Step 3: Inspection**

Various physical as well as laboratory tests are carried out in order to examine coating thickness, coating adherence to the surface of the steel, coating uniformity as well as coating mass.

## 2.6 Fe-Zn Hot Dip Galvanizing Intermetallic Phases

A metallurgical reaction occurs when the steel is immersed into a molten Zn bath during the galvanizing process. Various Fe-Zn intermetallic phases (**Figure 2.9**) form on the surface of the steel as a result [10,21].

The gamma (Γ + $Γ_1$) phase layer is in immediate contact with the steel substrate and consists of the highest amount of Fe. It is the thinnest of Fe-Zn intermetallic layers [18]. Adjacent to the gamma (Γ) phase is the delta (δ) phase, which exhibits columnar morphology as a result of preferred growth perpendicular to the steel substrate [21]. A zeta (ζ) phase, observed directly on top of delta (δ) phase, grows in a columnar morphology which is quite distinct from columnar morphology of delta (δ) phase. Nucleation of small zeta (ζ) crystals may occur if the zinc melt is supersaturated with Fe [18]. Eta (η) phase is the outermost phase whose composition is almost entirely made up of Zn [18,24].

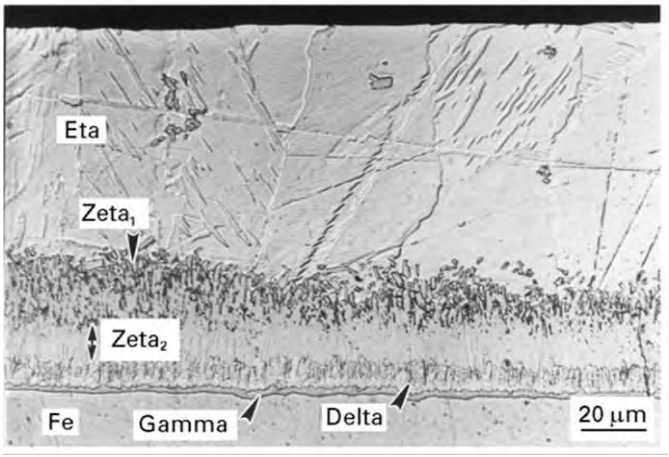


**Figure 2.9: Light micrograph of cross section through Zn hot dip galvanized coating on a steel substrate showing distinct Fe-Zn intermetallic phases. The microstructure formed after immersion of steel for 300s in a 450ºC Zn bath (0.00 wt % Al content) [25].**

The composition of Fe decreases from gamma (Γ + $Γ_1$) phase, adjacent to the steel substrate, to eta (η) phase furthest from the steel substrate. A summary of the characteristics of the Fe-Zn intermetallic phases according to formula, Fe composition and crystal structure are described in **Table 2.6**. The compositions of Fe and Zn in the intermetallic phases were determined by electron probe microanalysis at 1μm increments across the entire Fe-Zn alloy layer [26].

**Table 2.6: Identification of Fe-Zn intermetallic phases in hot dipped galvanized Zn coating on steel [18]**

| Phase | Formula | Iron (wt %) | Crystal Structure | Alloy Characteristics |
|---|---|---|---|---|
| Eta (η) | Zn | 0.03 ≤ | HCP | Soft, ductile |
| Zeta (ζ) | $FeZn_{13}$ | 5.7 – 6.3 | Monoclinic | Hard, brittle |
| Delta (δ) | $FeZn_7$ | 7 – 11 | Hexagonal | Ductile |
| Gamma ($Γ_1$) | $Fe_5Zn_{21}$ | 17 – 19.5 | FCC | Hard, brittle |
| Gamma (Γ) | $Fe_3Zn_{10}$ | 23.5 – 28.0 | BCC | Hard, brittle |

### 2.6.1 Fe-Zn Intermetallic Phase Formation during Zn Hot Dip Galvanizing of Steel

The Fe-Zn phase layer formation has been shown schematically (**Figure 2.10**). The reaction sequence is represented according to time so that $t_0 < t_1 < t_2 < t_3 < t_4$, where $t_0$ corresponds to time zero [18]. Zeta (ζ) phase layer nucleates first ($t_1$) at the steel/molten Zn interface. This is followed by delta (δ) phase formation ($t_2$) at the iron/zeta (ζ) interface. Gamma ($\Gamma + \Gamma_1$) phase was found to form after an incubation time of 30s ($t_3$). The last morphological feature to develop is the formation of a second zeta phase ($t_4$) between 30 – 60s reaction time at the delta (δ)/zeta (ζ) interface [18,26].

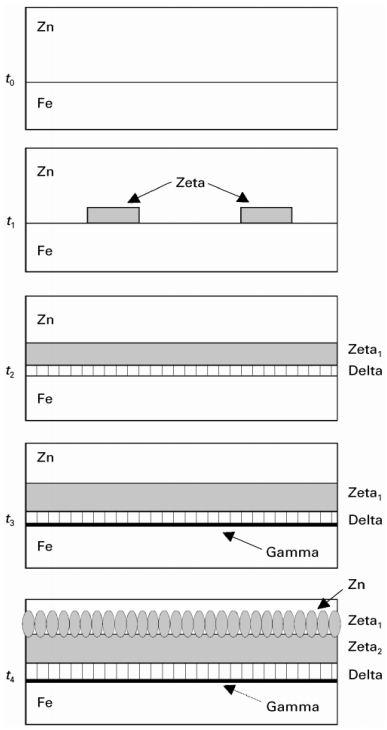


**Figure 2.10: Schematic representation of Fe-Zn phase layer formation in Zn galvanizing bath (0.00 wt% Al-Zn). $t_0$ corresponds to zero time, and development occurs according to time such that $t_1 < t_2 < t_3 < t_4$ [18].**

### 2.6.2 Control of Fe-Zn Intermetallic Phase Formation

The growth kinetics of the Fe-Zn intermetallic phases are mainly influenced by three factors; immersion temperature of the molten Zn bath, the duration of steel article immersion in the molten bath and the presence of elements such as Al in the molten Zn bath [18]. Studies have revealed that Fe-Zn growth kinetics in a molten Zn bath consisting of 0.20 wt% Al (**Figure 2.11**) differ significantly to Fe-Zn growth kinetics in a molten Zn bath with 0.00 wt% Al (**Figure 2.10**) [18]. Al has a greater affinity for Fe than Zn resulting in rapid formation of a thin $Fe_2Al_5$ intermetallic layer, with a fine granular structure, on the surface of a steel substrate in a Zn-0.20 wt% Al bath [18]. Delta (δ) phase is the first Fe-Zn intermetallic phase to form on the steel surface, followed by gamma ($\Gamma + \Gamma_1$) phase [18]. Zeta (ζ) phase did not form in Zn-0.20 wt% Al baths [18].

A study exploring the effect of immersion temperature on Fe-Zn intermetallic phase formation revealed that in short time immersions up to 300s at 450$^o$C (**Figure 2.12**) the zeta (ζ) phase layer grows rapidly initially before levelling off [18]. On the other hand, the delta (δ) phase layer grows

slowly before rapidly increasing in thickness after an immersion time of 180 seconds [18]. The gamma ($\Gamma + \Gamma_1$) phase layer developed slowest to yield a phase layer of approximately 1µm in thickness [18]. The study concluded that for short immersion times, less than 300s, the zeta phase dominated the coating morphology [18]. A separate investigation found that for long immersion times the delta (δ) phase layer dominated the coatings structure [18].

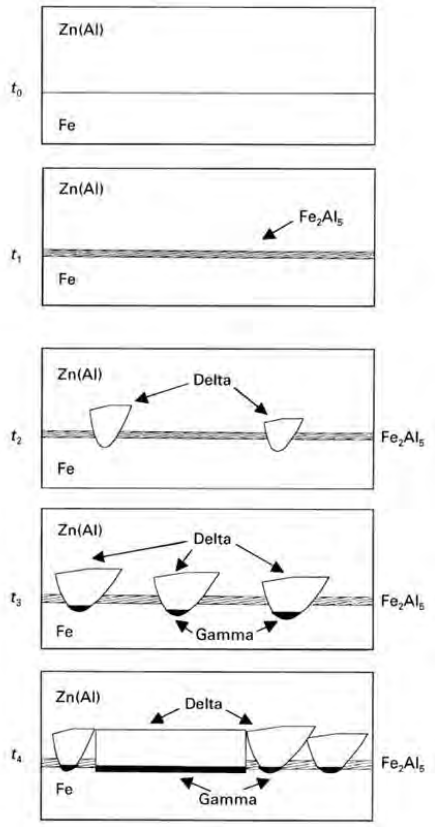


**Figure 2.11: A schematic representation of Fe-Zn phase layer formation in a 0.20 wt% Al-Zn galvanizing bath. $t_0$ corresponds to zero time, and development occurs according to time such that $t_1 < t_2 < t_3 < t_4$ [18].**

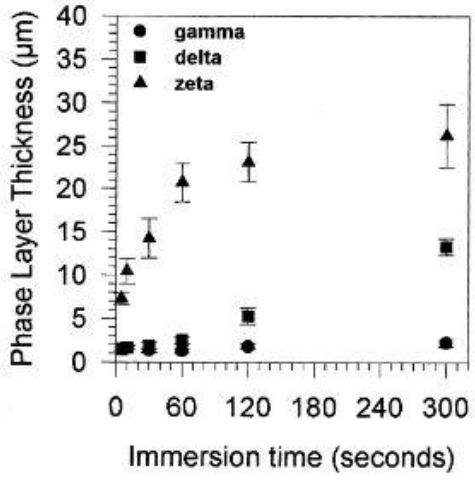


**Figure 2.12: Formation of zeta (ζ), delta (δ), and gamma ($\Gamma + \Gamma_1$) intermetallic phases on steel during immersion in 450°C Zn bath for 300s [18].**

### 2.6.3 Limitations in using Hot Dip Zn Coatings for Corrosion Protection

The list of corrosion products formed on Zn following exposure to the environment is large and includes hydroxides, oxides, carbonates, sulphates, chlorides, and complex mixtures of the anionic species [27]. The kinetics and extension of the corrosion reactions are influenced by the physicochemical characteristics of the resulting corrosion products, such as, composition morphology, structure, compactness, adherence to the underlying metal substrate [27-29]. Furthermore, weather conditions including the duration and frequency of wet-dry cycles, rain, temperature and wind regimes, and the presence of typical pollutants in the atmosphere, such as chlorides and sulphates, may modify the characteristics of the corrosion products [27].

The pH of aqueous solutions that contact Zn have an impact on its corrosion rate [30]. The Eh-pH diagram of Zn at 25°C is shown in **Figure 2.13**. Eh-pH diagrams show the equilibrium potential (Eh), with respect to the standard hydrogen electrode (SHE), between a metal and its various oxidized species as a function of pH [28]. Eh-pH diagrams are used in corrosion engineering to study the dissolution and passivation behaviour of different metals in aqueous environments [28]. It can be observed from **Figure 2.13** that within a pH range of approximately 8.5 to 11.0, Zn corrosion products, mainly $Zn(OH)_2$, form a passive protective barrier on the surface of Zn [28]. Zn would therefore be expected to exhibit a low corrosion rate when exposed to environments within this pH range [30]. Outside of this pH range, Zn is expected to corrode readily, forming $Zn^{2+}$ ions below pH 8.5 and $ZnO_2^{2-}$ ions above a pH of 11.0. A higher corrosion rate is predicted for Zn exposed to these pH ranges [30].

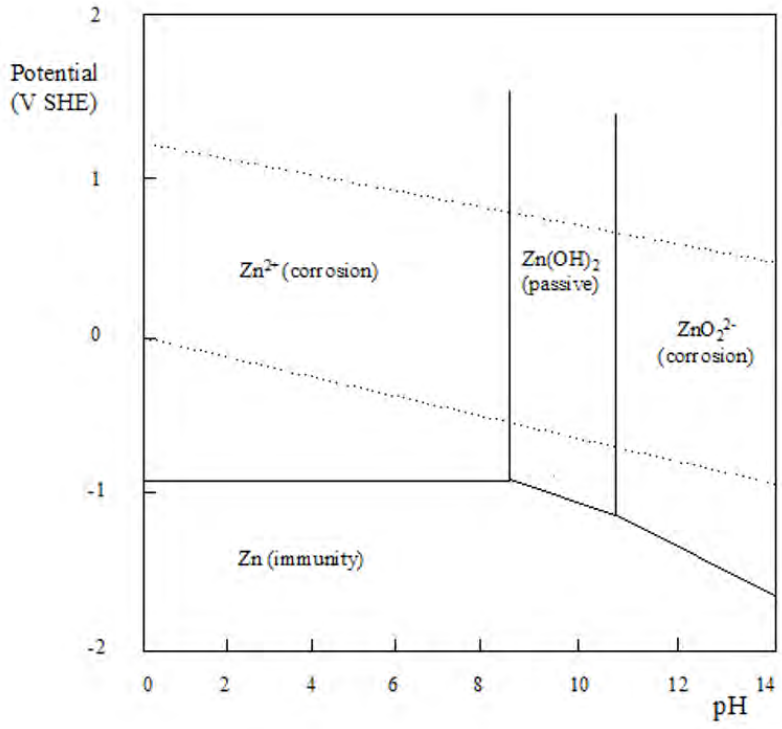


**Figure 2.13: Eh-pH diagram for Zn at 25°C [28, 29]**

While hot dip Zn coatings are adequate in protecting steel in most environments, field and laboratory tests have both shown that Zn coatings do not perform well in harsh environments represented by industrial and marine settings, as may be observed from the graph in **Figure 2.14** [30]. Marine and industrial environments are classified as harsh environments due to the presence of highly corrosive pollutants including chloride salts, sulphur dioxide and hydrogen sulphide which accelerate the rate of corrosion of both Zn and the underlying steel when it eventually becomes exposed to corrosion attack [30].

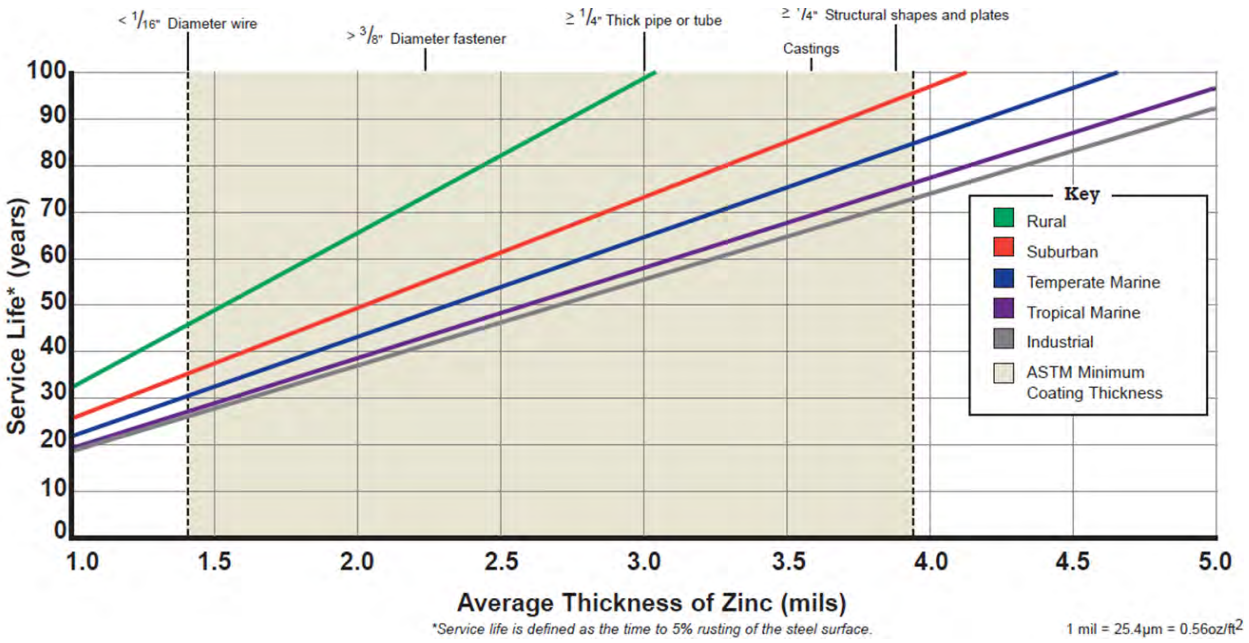


**Figure 2.14: Service life chart for hot-dip galvanized coatings** [30].

## 2.7 Review of Hot Dip Zn-Al Alloy Coatings

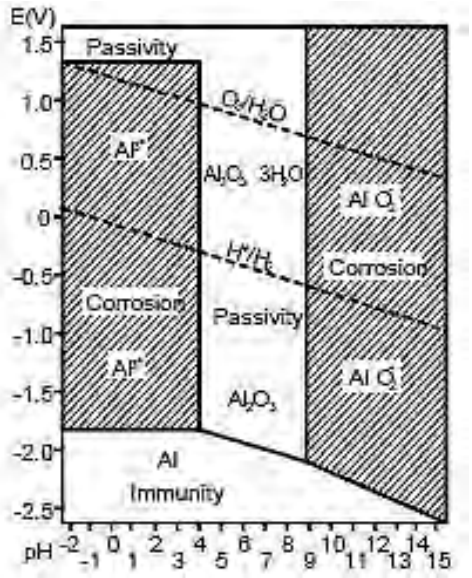


**Figure 2.15: Eh-pH diagram for Al at 25°C** [29]

Al owes its superior corrosion resistance to the natural formation of a thin but very stable oxide film [29]. The Eh-pH diagram of Al, in Figure **2.15**, indicates that in neutral aqueous solutions (4 < pH < 9) Al passivates to form $Al_2O_3$ an oxide film that protects the metal from further corrosion [29]. However, in acidic conditions (4 < pH) Al corrodes to form $Al^{3+}$ ions, while $AlO^-_2$ ions are formed during corrosion when Al is exposed to alkaline conditions (pH > 9) [29].

The use of Al in small amounts (≈0.20 wt%) in the molten Zn bath prevents formation of brittle Fe-Zn intermetallic phases which vastly improves the ductility of hot dip Zn coatings, as previously discussed in **Section 2.6.2** [18,31]. High additions of Al lead to the formation of Zn-Al alloy coatings with superior corrosion performance compared to Zn in marine and industrial environments [18,31]. The increased corrosion performance of Zn-Al alloys results from the passivation of Al to form inert corrosion products on the surface of the coating combined with the galvanic protection provided by Zn [17].

Zn-5Al and Zn-55Al coatings are two commercially produced Zn-Al alloy coatings applied onto steel by the hot dip process [32]. The Zn-55Al alloy coating is best suited for applications such as roofing and automotive parts where a combination of corrosion resistance and high heat reflectivity are advantageous [32]. The Zn-5Al alloy coating is ideally suited for use on deep-drawn parts and wire owing to its good formability in addition to superior corrosion performance [32]. A summary of performance of Zn, Zn-5Al and Zn-55Al coatings on sheet steel based various attributes is shown in **Table 2.7**.

**Table 2.7: Performance of Zn, Zn-5Al and Zn-55Al Hot Dip Coatings on Steel Sheet**

| | Zn | Zn-5Al | Zn-55Al |
|---|---|---|---|
| Formability | 3 | 5 | 3 |
| Corrosion Resistance (bare) | 3 | 4 | 5 |
| Sacrificial protection | 5 | 5 | 3 |
| Corrosion Resistance (formed) | 3 | 5 | 3 |
| Paint Adhesion | 4 | 5 | 4 |
| Weldability | 4 | 4 | 2 |
| Heat Resistance / Reflectivity | 3 | 3 | 4 |

**Note: 6 = best, 1 = worst**

### 2.7.1 The Hot Dip Zn-5Al Alloy Coating

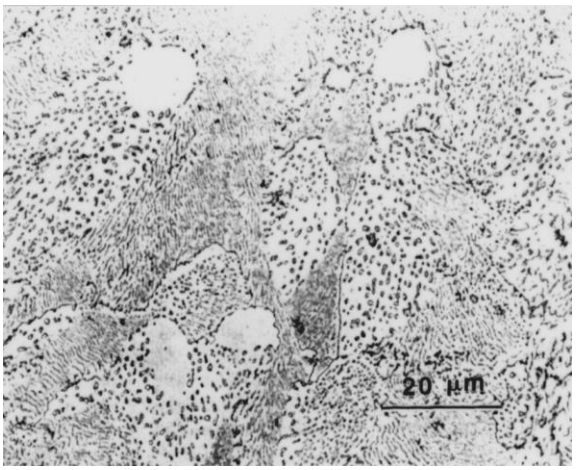


**Figure 2.16: Micrograph of the Zn-5Al alloy coating showing planar view of the two phase microstructure [17].**

Zn-5Al is an eutectic alloy that exhibits a complex microstructure [18,31,33]. Additions of up to 0.10% mischmetal containing lanthanum and cerium have been reported to increase the fluidity and wettability of the Zn-5Al molten bath, therefore contributing towards a more uniform coating thickness [34-36]. Studies have also revealed that the corrosion performance of Zn-5Al coatings with mischmetal additions exhibited improved corrosion performance in comparison to the Zn-5Al coating without mischmetal additions [33]. Magnesium may also be incorporated into the Zn-5Al alloy in small amounts (up to 0.5 wt%) as a substitute for mischmetal which also has the effect of enhancing the corrosion performance of the alloy [17,32]. The Zn-5Al alloy displays superior corrosion resistance, formability, paintability and cathode edge protection [17,31].

### 2.7.2 The Zn-5Al Hot Dip Process

The Zn-5Al alloy coating is applied via the double dip process outlined schematically in **Figure 2.17** [4]. Properly annealed, cleaned, and fluxed steel articles are coated conventionally in a molten Zn bath. The Zn galvanised steel article then enters a second bath containing the molten Zn-5Al alloy. The double dip process is used because the molten Zn-5Al alloy is not compatible with flux systems normally used in hot dip galvanizing [4,24]. Transformation of the brittle Fe-Zn intermetallic layers into an Al-Fe-Zn intermetallic layer occurs when the Zn coated object is transferred from the first molten Zn bath into the Zn-5Al bath [4].

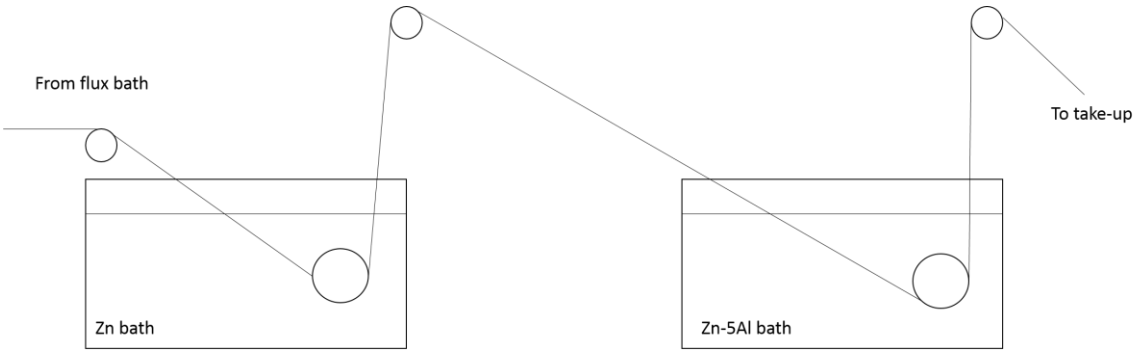


**Figure 2.17: Schematic representation of Zn-5Al double dip process line [4].**

### 2.7.3 Review of Composition of Zn-5Al Alloy Bath

The typical composition of elements making up the Zn-5Al alloy bath are specified by the ASTM B 750-12 standard as shown in **Table 2.8** [37]**.** Zn-5Al alloy ingots for hot dip coatings may contain Sb, Cu, and Mg in amounts of up to 0.002%, 0.1%, and 0.1 %, respectively. Al may be specified up to 12% depending on application of the coated steel [37]. Pb and Cd, and to a lesser extent Sn and Sb, are known to cause intergranular corrosion in Zn-Al alloys [37]. Therefore it is important that the composition of these elements are maintained below the limits specified in **Table 2.8**.

**Table 2.8: Composition of elements in typical hot dip Zn-5Al alloy coating bath from ASTM B 750-12 standard** [37]

| Element | Composition (%) |
|---|---|
| Al | 4.2 – 6.2 |
| Ce + La total | 0.03 – 0.10 |
| Fe | 0.075 (max) |
| Si | 0.015 (max) |
| Pb, | 0.005 (max) |
| Cd, | 0.005 (max) |
| Sn, | 0.002 (max) |
| Others (except Sb, Cu, Mg, Ti, Zr) | 0.04 (max) |
| Zn | Remainder |

### 2.7.4 Solidification of the Zn-5Al Alloy during Slow Cooling

A summary of the phase transformations during the solidification of the Zn-5Al alloy have been illustrated in **Figure 2.18**. Above the eutectic temperature (381°C), the Zn-5Al alloy exists as a liquid. During slow cooling through the eutectic temperature, the liquid solidifies into a two phase solid solution consisting of Zn-rich aluminium solid solution (β) and Zn (η) phases arranged in lamellar morphology [18,38]. The early stages of solidification involve the nucleation of pro-eutectic Zn (η) particles, consisting of approximately 1 wt% Al [34]. These particles then serve as heterogeneous nucleation sites for the solidification of the eutectic microstructure [18,39]. The microstructure remains

stable as the alloy is slow cooled down to the eutectoid temperature (277°C). Below the eutectoid temperature, the Zn-rich aluminium solid solution (β) phase decomposes into the Zn (η) phase and an Al-rich solution solid phase (α) [18,40,41]. This transformation is related to the decrease in solubility of Zn in the fcc Al-solid solution as temperature decreases [26]. The Al-rich (α) and Zn (η) phases continue to exhibit the regular lamellar morphology and remain stable as the alloy is slow cooled down to room temperature [34,35]. **Table 2.9** summarizes the phase transformations that occur during the solidification of the Zn-5Al alloy under conditions of slow cooling [18,40].

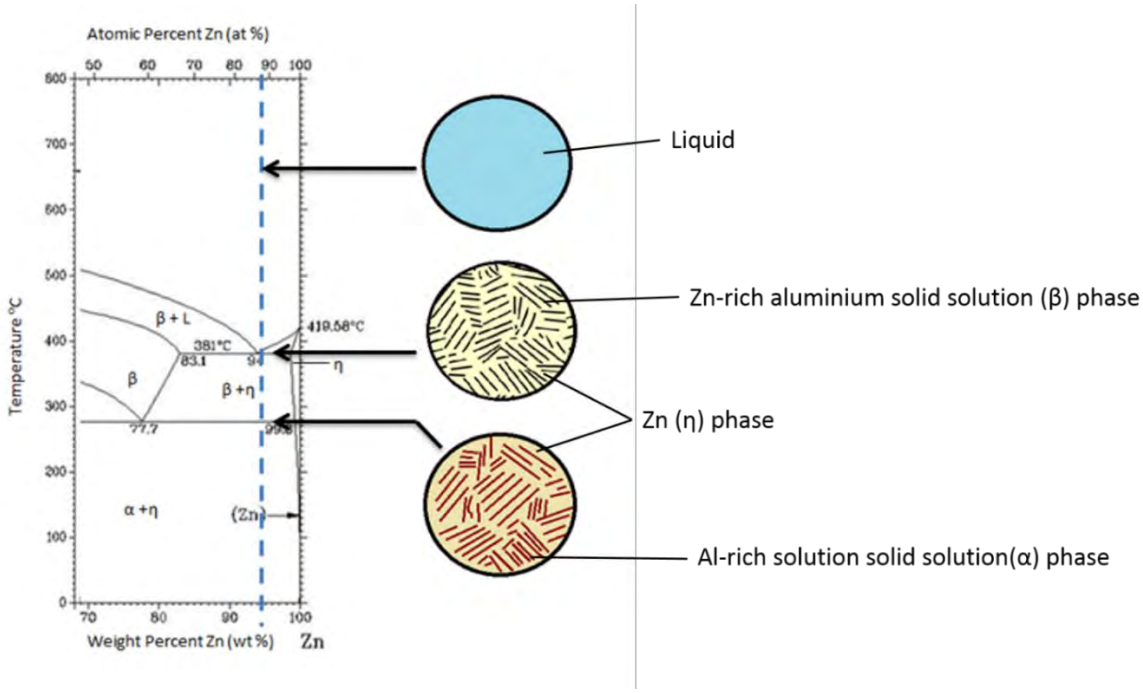


**Figure 2.18: Phase Changes during Solidification of Zn–5Al Alloy Coating [36].**

**Table 2.9: Phase transformations in the Zn–Al system [17]**

| Phase Transformation | Zn Composition (wt%) | Temperature (°C) | Transformation Type |
|---|---|---|---|
| L ↔ β + η | 95.0 | 381 | Eutectic |
| B ↔ α + η | 77.7 | 277 | Eutectoid |
| α + β | 61.3 | 351.5 | Critical |
| L + η | 100 | 419.58 | Congruent |
| L (Al) | 0 | 660.45 | Congruent |

### 2.7.5 Impact of Cooling Rate on Microstructural Evolution in Zn-5Al Alloy

A study of the microstructural changes in Zn-5Al alloy galvanizing as a function of processing parameters revealed that in situations where fast cooling of the molten alloy occurred, the eutectic microstructure was finer, with decreased inter-lamellar spacing. The primary Zn (η) dendrites were smaller size and fewer in number in the fast cooled, or quenched, condition compared to when the alloy underwent slow cooling [31]. Researchers also observed that fast cooling led to a change in the

eutectic morphology to include rod structures [31]. In terms of corrosion performance, the fast cooled Zn-5Al alloy coating displayed better cut edge corrosion performance but diminished surface corrosion compared to the slow cooled coating [31].

### 2.7.6 The Zn-55Al Alloy Coating

The Zn-55Al alloy coating is composed of 55wt% Al, 43.4wt% Zn and 1.6wt% Si [42,43]. The addition of Si prevents an exothermic reaction at the coating/steel substrate interface [17]. The Zn-55Al alloy coating layer consists of an Fe-Al-Zn alloy intermetallic layer and an overlay layer composed of Al-rich dendrites , Zn-rich interdendritic areas and a fine dispersion of Si particles (**Figure 2.19**) [17,38]. The composition of Al, Zn, and Si in the Al-rich dendrites and Zn-rich interdentritic regions are shown in **Table 2.10**.

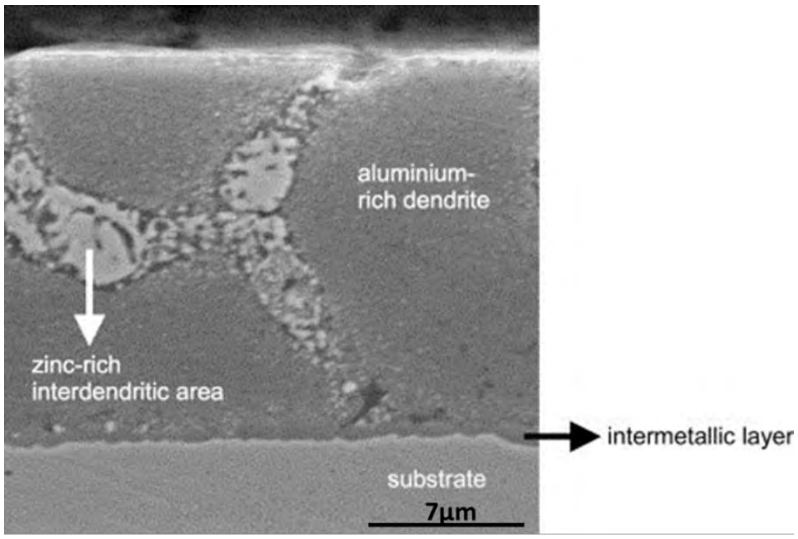


**Figure 2.19: Micrograph of cross section through Zn-55Al alloy coating** [38].

**Table 2.10: Phase composition in Zn-55Al alloy coating** [38]

| Phase | Elemental Composition | | |
|---|---|---|---|
| | Al | Zn | Si |
| Al-rich dendrites | 64.5 | 35.3 | 0.2 |
| Zn-rich interdendritic regions | 20.4 | 78.9 | 0.7 |

### 2.7.7 Microstructural Evolution in Zn-55Al Coating during Slow Cooling

Microstructural evolution in the Zn-55Al alloy coating during slow cooling was studied with the aid of the Zn-Al binary equilibrium phase diagram (**Figure 2.20**). The formation of Al-rich dendrites containing 22wt% Zn begins at a temperature of 570°C (point 1). The composition of the solid phase to the liquid phase is 50:50 during continued slow cooling down to 530°C (point 2). Complete solidification of the alloy occurs with complete homogenisation of the composition at 490°C (point 3). The solid reaches the immiscibility gap region between the temperature ranges of 320°C – 277°C

where the Al solid solution consists of Al-rich (αAl) phase and Zn-rich (βAl) fcc Al solid solution phases. At 300°C (point 4), the composition of Zn in the Al-rich (αAl) and Zn-rich phase (βAl) phases is 38wt% Zn and 75wt% Zn respectively. Further cooling through 277°C, the monotectoid reaction isotherm, results in the conversion of Zn-rich (βAl) to give Al-rich (αAl) + Zn (η). At a temperature of 200°C αAl phase contains 13wt% Zn and Zn (η) contains approximately 100wt% Zn, with the 63.2% and 36.8% compositions of αAl and Zn (η) respectively [38].

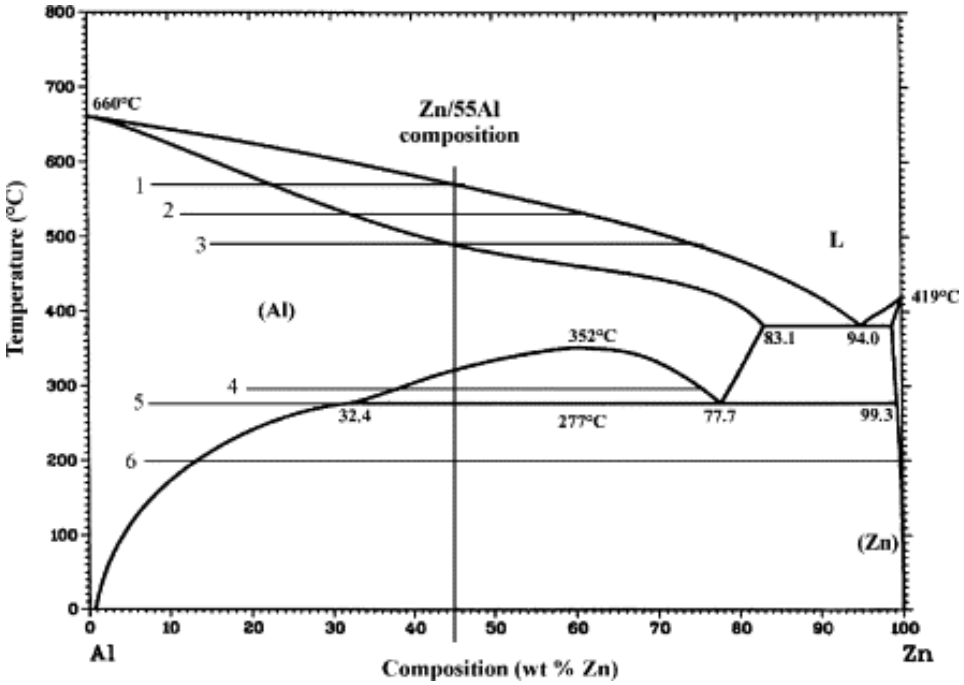


**Figure 2.20: Zn-Al binary equilibrium diagram with indication of six points during slow cooling in a straight line that locates the Zn-55Al** [38].

## 2.8 Review of Environmental Exposure Tests and Salt Spray Tests to Assess Corrosion Performance of Zn and Zn-Al Coated Steel in Specific Studies

Coated steel sheets present investigators with various options for corrosion assessment. In a study on corrosion protection assessment of 17 Zn and Al sacrificial coating systems as a function of exposure time in a marine environment, Schmidt et al. used a combination of visual and electrochemical measurements [44]. The visual observations provided a clear record of corrosion damage on the surface, while open circuit potentials taken throughout the exposure period revealed information on the coating/electrolyte interface [44]. A second electrochemical measurement, electrochemical impedance spectroscopy (EIS) provided values for comparison with regards to coating protections performance as a function of exposure time. Schmidt et al.'s findings revealed that visual observations during atmospheric exposure, open circuit versus time during atmospheric exposure, and EIS as a function of atmospheric exposure time provided complementary results for the coating systems analysed[44].

Yan carried out a comparative investigation of hot dip Zn-25Al (144.9g/m$^2$), Zn-55Al-Si (120.7 g/m$^2$) and Zn (396.6 g/m$^2$) coatings on steel wire with emphasis to their corrosion performance in seawater over a 2-year exposure period [32]. Corrosion performance was evaluated using tensile tests, electrochemical tests, corrosion rate calculations and examination of the corrosion products on the specimens [32]. Yan observed that in tidal and immersion environments, Zn-25Al alloy coating was several times more durable than Zn coating of double thickness as shown in **Figures 2.21 and 2.22 respectively** [32]. At long exposure times, corrosion rate for the Zn-25Al alloy coating remained indistinguishable from that for the Zn-55Al-Si coating of similar thickness in tidal zone, and was two to three times lower than the latter in immersion zone [32]. The decrease in tensile strength, exhibited in **Figure 2.23**, suggested that galvanized and Zn-55Al-Si coated steel suffered intense pitting corrosion in immersion zone [32]. Corrosion rate calculations were based on weight loss data, however corrosion rate could have also been determined from polarization methods as employed by Budruk et al. in a study of corrosion behaviour of Mg-Cu and Mg-Mo composites in 3.5% NaCl [32,45].

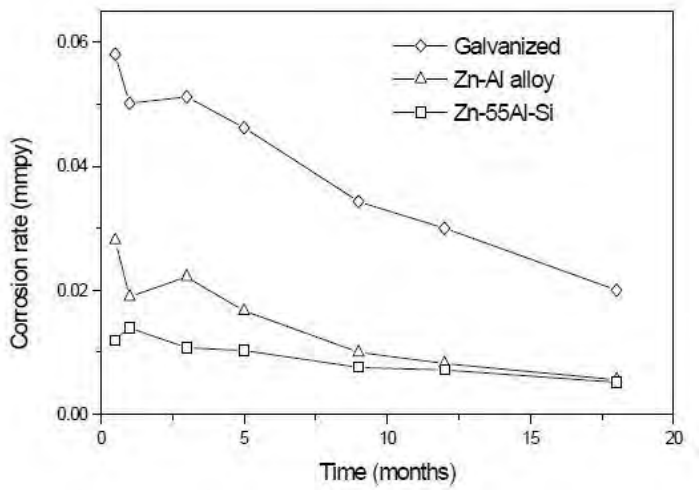


**Figure 2.21: Corrosion rate as a function of time for hot dip coatings in tidal zone [32].**

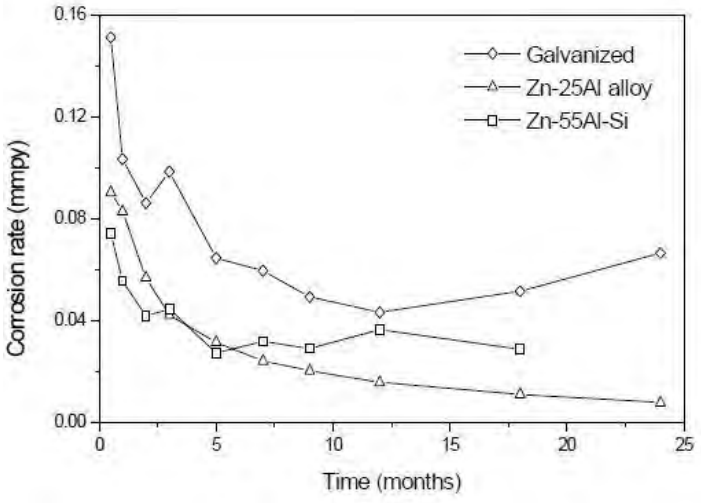


**Figure 2.22: Corrosion rate as a function of time for hot dip coatings in immersion zone.[32].**

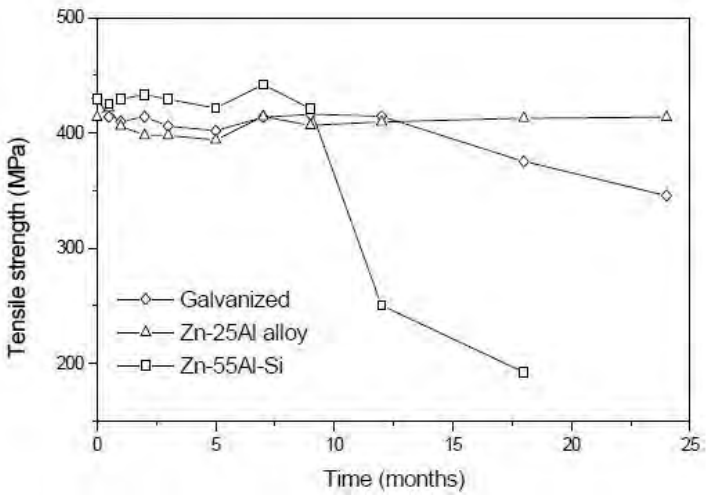


**Figure 2.23: Tensile strength as a function of time for hot dip coatings after removal from seawater [32].**

The electrochemical tests carried out by Yan showed that all the coatings effectively provided cathodic protection to the substrate metal; the galvanic potentials were equal to – 1,050, – 1,025 and – 880 mV (SCE) for Zn, Zn-25Al alloy and Zn-55Al-Si coatings, respectively, which are adequate to keep the steel inside the immunity region [28].

Yan concluded that the superior performance of the Zn-25Al alloy coating was due to its optimal combination of uniform corrosion resistance and pitting corrosion resistance. The inferior corrosion performance, by comparison, of the Zn coating was attributed to its larger dissolution rate, while the failure of the Zn-55Al-Si coating was most probably related to its higher susceptibility to pitting corrosion in seawater.

The use of salt spray tests in evaluating the corrosion performance of Zn (300 g/m$^2$), Zn-10%Al (300 g/m$^2$), and Zn-11%Al-1~3%Mg (200 g/m$^2$) coated steel wire was carried out by Sugimaru et al [46]. The main objective of their study was to investigate whether the addition of Mg to Zn-Al alloy coatings translated into improved corrosion performance [46].

**Table 2.11: Salt spray testing condition [42]**

| | |
|---|---|
| Concentration of salt | 4.8 - 5.15% |
| pH | 6.8 - 6.9 |
| Spraying quantity | 1.7 - 1.8 l/min |
| Temperature | 35°C |

Sugimaru et al's experimental methods involved using specimens approximately 120 mm long that were sealed at the cut ends such that the specimen length to be examined was 100 mm [46]. Specimens were weighed an electronic balance down to 1 mg [46]. Wire specimens were then exposed to continuous salt spray testing for 3,000 hrs under conditions shown in Table 2.11 [46]. At the end of the salt spray test, corrosion products were removed from the surface of the specimens by immersing the specimens in a 300g/l $CrO_3$ aqueous solution at room temperature (25$^0$C) for 5

minutes [46]. Residual corrosion products were removed by rinsing the specimens under running water [46]. Following this, the dried specimens were reweighed and weight decrement was determined by the difference between the weight of the specimens before and after the salt spray test [46].

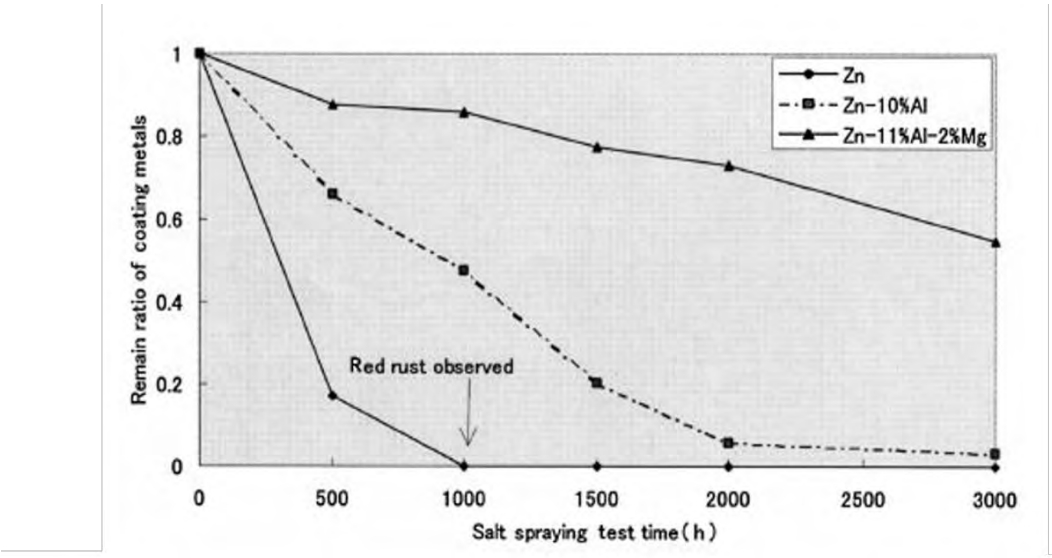


**Figure 2.24: Remain ratio of coatings after salt spray test exposure [46].**

**Figure 2.24** shows graphs representing the ratio of the remainder of the coating (= coating weight minus corrosion loss) to the original coating weight for Zn (300 g/m$^2$), Zn-10%Al (300 g/m$^2$), and Zn-11%Al-2%Mg (200 g/m$^2$) steel wire after the salt spray test [46]. The Zn (300 g/m$^2$) coating completely transformed to corrosion products within 1,000 hrs of the salt spray test while the Zn-10%Al (300 g/m$^2$) coating was mostly transformed to corrosion products after 2,000 hrs [46]. However, by the end of the 3,000 hrs salt spray test only 40% of the Zn-11%Al-2%Mg (200 g/m$^2$) coating had been converted into corrosion products, thus proving the beneficial effect on corrosion performance of Mg additions in to Zn-Al alloy coatings [46].

Sugimaru et al's study also reveals the importance of cooling rate on microstructural evolution in Zn-Al alloy coatings [46]. **Figure 2.25** shows secondary-electron images taken using an electron probe micro-analyzer of Zn-10%Al (300 g/m$^2$) and Zn-11%Al-3%Mg (200 g/m$^2$) coated steel wire under conditions of water cooling and air cooling [46]. Under water cooled conditions, in the Zn-10%Al (300 g/m$^2$) coating, crystals in α-phase (black regions) rich in Al initially grow as columnar crystals. However, under air cooled conditions they grow as granular crystals. In both instances, the remaining solid solution is consists of Zn and α-phase at the eutectic temperature, with transformation of the α-phase into a structure where Zn and Al are separated at the eutectoid temperature [46].

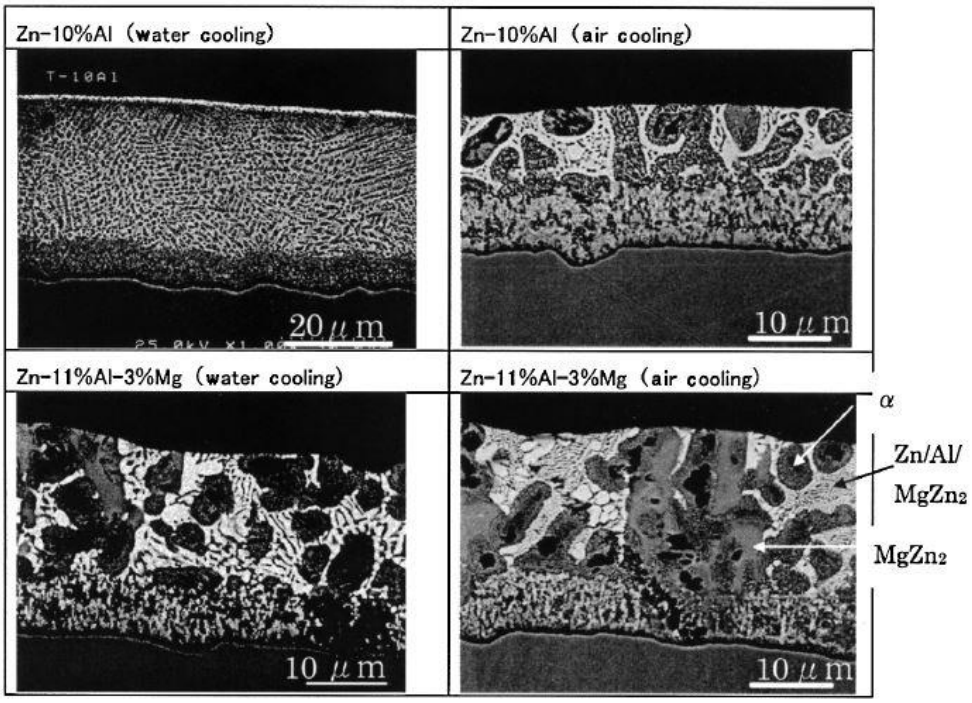


**Figure 2.25: Cross-sectional structure of coated wires captured using an electron probe micro-analyser (in secondary-electron imaging mode) [46].**

The Zn-11%Al-3%Mg (200 g/m$^2$) coating exhibits a 3 phase microstructure: the darkest layer is a course α-phase layer rich in Al, the grey regions consist of a Zn-Mg binary product, presumably $MgZn_2$, while the lightest regions represent a ternary eutectic composition ($Zn/Al/MgZn_2$) [46]. Under conditions of water cooling, the α-phase layer is granular and is smaller in relation to when it is air-cooled [46].

The microstructure of the coatings produced has an impact on corrosion performance of the coatings as shown in **Figure 2.26** [46]. The Zn-10%Al (300 g/m$^2$) coating performed nearly 3 times better against corrosion in instances where it was air cooled in comparison to when it was water cooled [46]. The performance of the Zn-11%Al-1%Mg (200 g/m$^2$) and Zn-11%Al-3%Mg (200 g/m$^2$) air cooled coatings were indistinguishable from each, however they both outperformed the Zn-10%Al (300 g/m$^2$) air cooled coating [46].

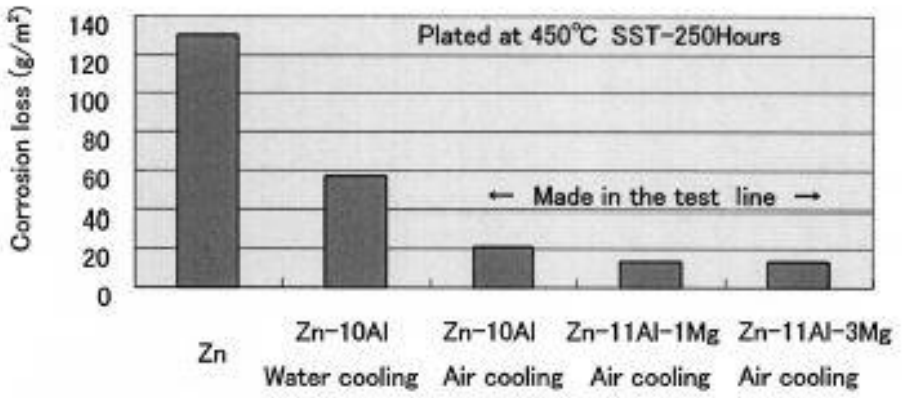


**Figure 2.26: Corrosion loss of Zn-Al alloy coatings on steel wire [46].**

# 3. Experimental Approach

Corrosion performance of Zn and select Zn-Al alloy coatings on various steel wire structures was evaluated by using accelerated laboratory corrosion tests and an environmental exposure test. Two separate accelerated laboratory corrosion tests were run; the aggressive ASTM B117 test and the moderate VW PV 1210 test. The environmental exposure test was carried out over a 16-month period by installing specimens at select catch fences along Chapman's Peak Drive. The general testing methods for the accelerated laboratory corrosion tests and the environmental exposure test are described in this section.

## 3.1 Material Description

**Table 3.1: Description of samples used in this study**

| Structure | Coating Type | Coating Mass Distribution (g/m²) | Wire Diameter (mm) |
|---|---|---|---|
| Wire | Zn Class A | 235 | 3 |
| | Zn Class B | 135 | 3 |
| | Zn-5Al | 150 | 3 |
| | Zn-5Al-xMg | 150 | 3 |
| | Zn-10Al | 300 | 3 |
| Bundles | | | |
| 12-strand bundle | Zn Class A | 235 | 3 |
| | Zn Class B | 235 | 3 |
| | Zn-5Al | 150 | 3 |
| | Zn-5Al-xMg | 150 | 3 |
| | Zn-10Al | 300 | 3 |
| Rope | | | |
| 8mm dia. rope | Zn | 70 | 0.9 |
| | Zn-5Al | 70 | 0.9 |
| 16mm dia. rope | Zn | 80 | 1.1 |
| | Zn-5Al | 80 | 1.1 |
| 22mm dia. rope | Zn | 90 | 1.3 |
| | Zn-5Al | 90 | 1.3 |

A total of 16 samples were supplied by a global wire manufacturer. Samples were classified according to structure, the type of coating applied, coating thickness and wire diameter (**Table 3.1**). In terms of structure, samples were provided in the form of individual wires, wire bundles and wire rope. For simplicity, the structure will be referred to as wire, bundles and rope respectively. The bundles were available in 12-strand wire arrangements. The rope came in three different diameter sizes of 8mm, 16mm and 22mm where the unit wires making up these ropes had diameters of 0.9mm, 1.1mm and 1.3mm respectively. The wires making up the bundles and ropes were individually coated with Zn and Zn-Al alloys before the bundles and ropes were formed.

## 3.2 Accelerated Corrosion Tests

### 3.2.1 Test Coupon Preparation for Accelerated Corrosion Tests

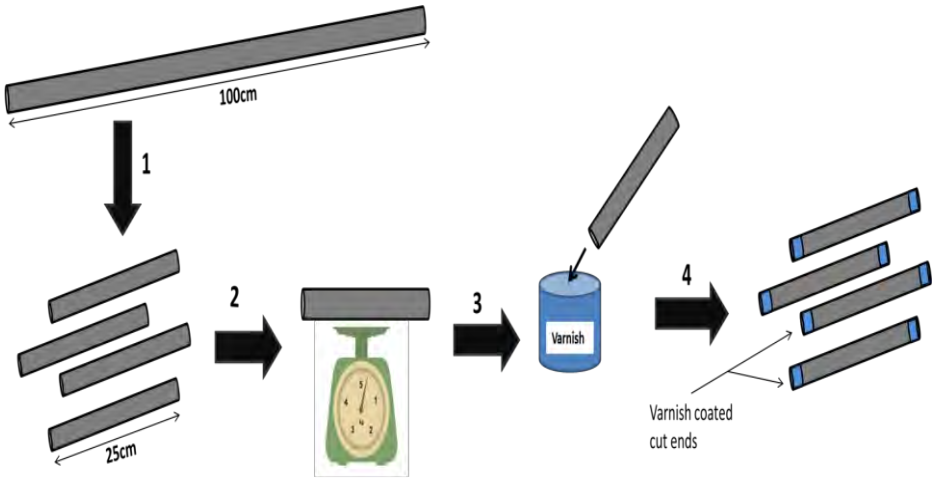


**Figure 3.1: Flow diagram showing the main steps in the preparation of wire specimens for accelerated corrosion tests**

The main steps involved in the preparation of wire coupons for laboratory corrosion tests have been illustrated (**Figure 3.1**). The process can be summarized as follows:

1. The original 100cm long wire samples were cut into specimens measuring 25cm in length. Specimens were rinsed with water and dried using a blow dryer.
2. The clean specimens were weighed and their mass recorded. The recorded mass of specimens was later used in corrosion rate calculations.
3. The cut ends of each specimen were dipped 0.5cm deep into varnish, which is a resin containing liquid coating material that dries into a hard, transparent film. This had the beneficial effect of sealing steel exposed at the cut ends where the protective metallic coating was not present.
4. The varnish was allowed to dry night overnight, after which specimens were ready for corrosion experiments.

Bundle and rope specimens were prepared in a similar manner to the wire specimens. However, a shorter specimen length of 20cm was used for bundles and ropes, as opposed to the 25cm specimen length used for wires. The wire specimens were made longer as they were later sectioned and mounted for microscopic examination of the impact of corrosion on the microstructure of the specimens. The bundle and rope specimens were only used for qualitative assessment of corrosion performance which involved an observation of how corrosion products on the test coupon surfaces evolved during the course of the experiment.

### 3.2.2 Importance of Sealing Steel Exposed at Cut Ends of Test Coupons

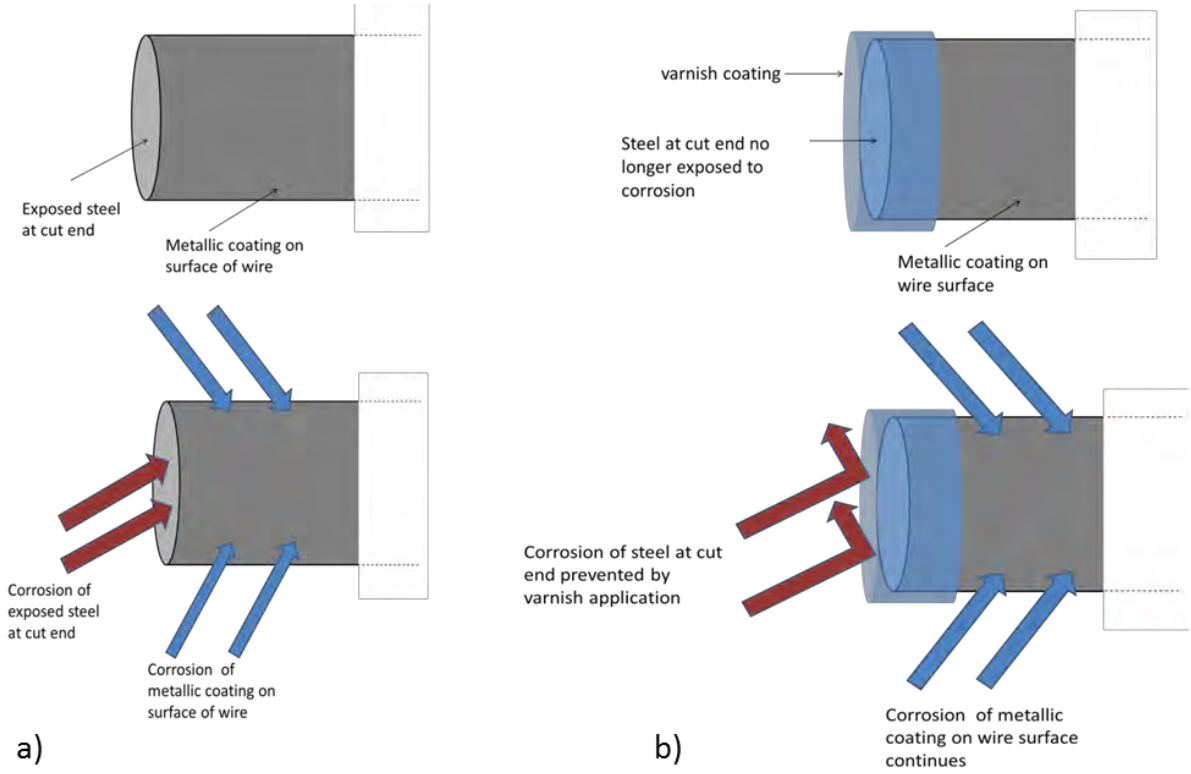


**Figure 3.2: The progression of corrosion on wire coupon with (a) exposed cut ends and (b) varnish protected cut ends.**

The exposed steel at the cut ends of specimens would have readily corroded during accelerated corrosion testing had the steel not been sealed off (**Figure 3.2a**). Corrosion of steel in this instance would prevent an effective assessment of the corrosion performance of the Zn and Zn-Al alloy metallic coatings from being conducted. This situation was prevented by coating the exposed steel with varnish (**Figure 3.2b**). Varnish coating ensured that any corrosion of steel observed during both accelerated corrosion tests and the environmental exposure test would have been due to the failure of the Zn and Zn-Al alloy metallic coatings. The presence of red/brown corrosion products of steel would therefore serve as a clear indication that the metallic coatings would have been breached as a result of corrosion, thus exposing the underlying steel to corrosion attack.

### 3.2.3 Salt Spray Tests

Salt spray tests are controlled and reproducible accelerated laboratory corrosion tests used to examine the corrosion performance of metals, metallic coatings and organic coatings in a given test chamber [47,48]. Salt spray tests can either be continuous or cyclic. In the continuous salt spray test, specimens are constantly exposed to one environment throughout a given testing period [40]. The major limitation of continuous salt spray tests is that they do not accurately represent natural environmental conditions and so they cannot be reliably used to predict the performance of protective metallic coatings in natural environments [47,48]. Continuous corrosion tests are often

carried out in tandem with long-term environmental exposure tests. Correlation and extrapolation of corrosion performance based on continuous corrosion tests can be considered only if there is corroboration with the long-term environmental exposure tests [41].

Two different salt spray tests were run in this study; the VW PV 1210 test and the ASTM B117 test (**Figure 3.4**) described in **Appendices A** and **B** respectively. The ASTM B117 is a continuous exposure test in which samples were exposed to a fine salt mist throughout the testing period. The VW PV 1210 test schedule is a cyclic exposure test in which samples were exposed to various environmental conditions in a repetitive cycle. The VW PV 1210 may be described as a moderate salt spray test since test samples were not constantly exposed to the corrosive salt mist. On the other hand, the ASTM B117 test may be described as an aggressive test due to the constant exposure of samples to salt mist. A comparison of the key differences between these tests was carried out and summarized (**Table 3.2**).

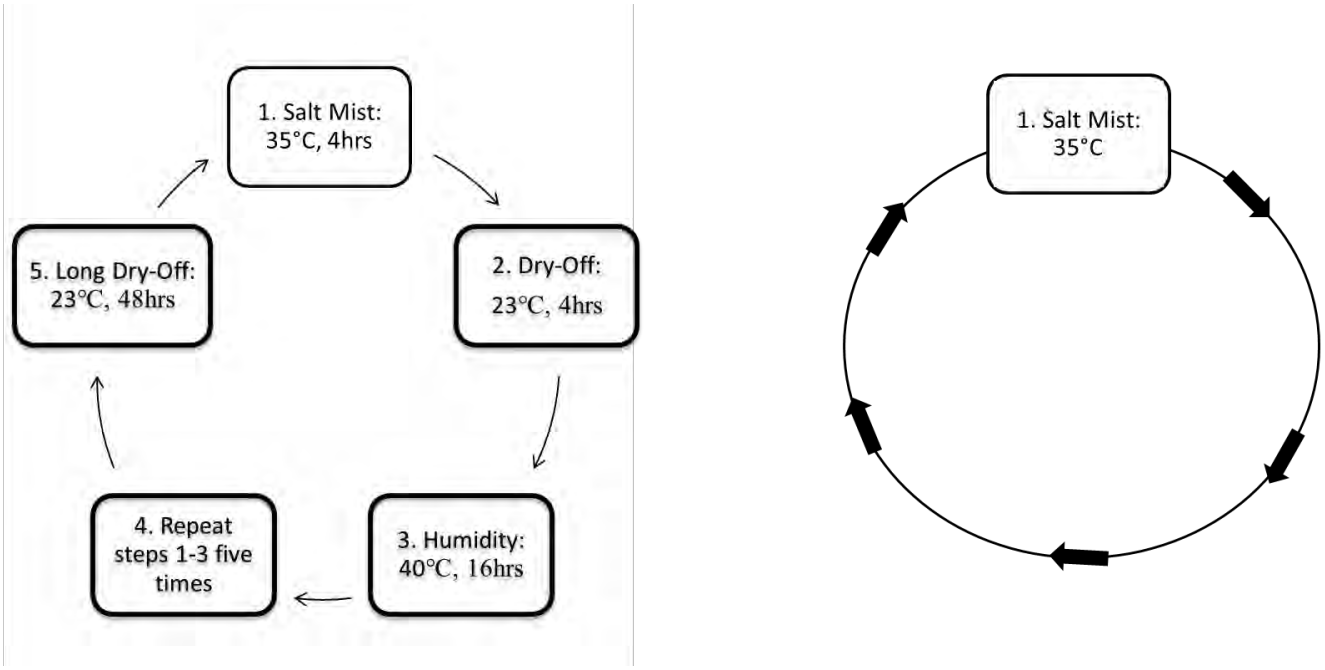


**(a) VW PV 1210 test** **(b) ASTM B117 test**

**Figure 3.4: Description of laboratory corrosion test schedules run using the Q-Fog 1100 cyclic corrosion tester [47,48].**

**Table 3.2: Differences between VW PV 1210 and ASTM B117 salt spray test**

| VW PV 1210 cyclic corrosion test | ASTM B117 test |
|---|---|
| Coupons exposed to 4 separate environmental atmospheres; salt mist, high humidity, short dry period, long dry period | Coupons exposed to 1 environmental condition; salt mist |
| Long drying periods allow corrosion products to solidify and accumulate to form a thick layer on coating surface | Absence of drying period prevents corrosion products from forming a thick layer on coating surface |
| Time of wetness of coupons is 60% relative to the time of wetness of coupons in ASTM B117 test procedure | Coupon surface remains wet throughout the test |
| Coupons exposed to salt mist (which contains chloride ions) 12% of the time relative to ASTM B117 | Coupons constantly exposed to salt mist |

### 3.2.4 Q-Fog Cyclic Corrosion Tester

The ASTM B117 and VW PV 1210 salt spray tests were carried out in a Q-Fog 1100 cyclic corrosion tester (**Figure 3.5**). The corrosive media used in this study was substitute ocean water prepared as outlined in the ASTM D1141 standard shown in **Appendix C** [49]. Substitute ocean water was stored in the solution reservoir (A) while test coupons were installed within the chamber's interior compartment (B). The ASTM B117 and VW PV 1210 test schedules were programmed using the control panel (C). The Q-Fog 1100 cyclic corrosion tester exposes test coupons to four main environmental conditions; fog, dry-off, humidity and dwell [50].

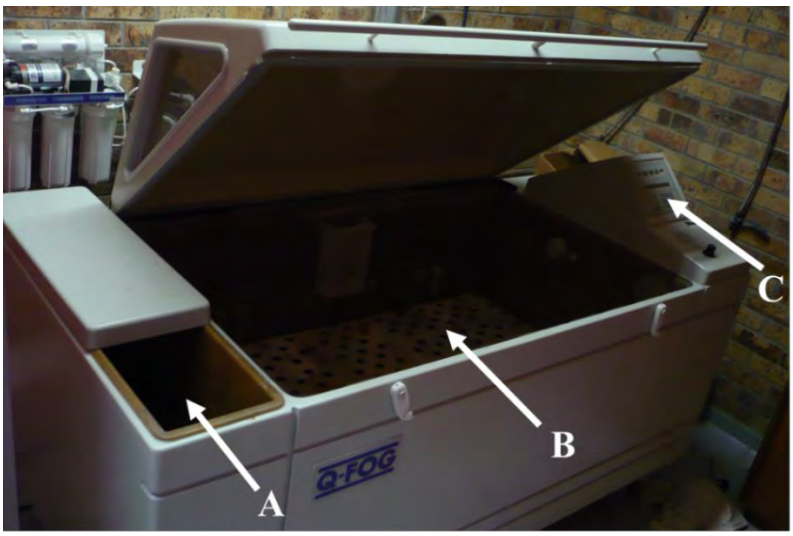


**Figure 3.5: Q-Fog 1100 cyclic corrosion tester showing (A) solution reservoir, (B) internal chamber and (C) control panel.**

### 3.2.4.1 Fog Environment

During this function, a fine mist of corrosive fog is sprayed evenly throughout the chamber (**Figure 3.6).** The process begins with a spray pump drawing the substitute ocean solution from the reservoir to the spray nozzle. While this is taking place, compressed air, saturated with water vapour, is also directed to the spray nozzle in order to atomize the substitute ocean solution [50]. This is then introduced into the internal chamber as a fine mist. Temperature is maintained at a preset value by heaters at the base of the chamber [50].

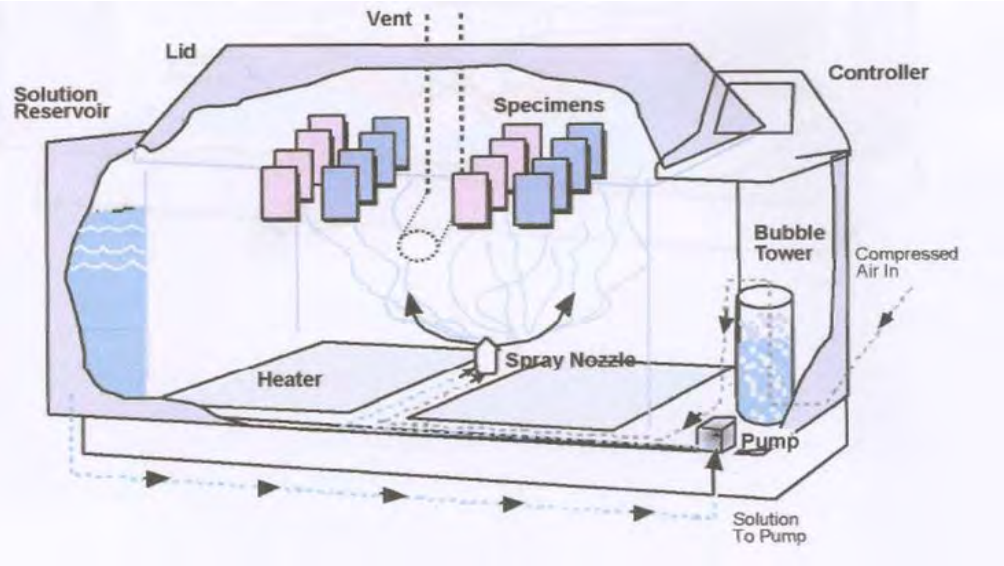


**Figure 3.6: Schematic of Q-fog cyclic corrosion tester operating the fog environment [50].**

### 3.2.4.2 Dry-Off Environment

During the Dry-Off function, the purge blower is activated in order to bring room air into the chamber. The air heater is automatically activated when the preset air temperature for dry-off is higher than ambient temperature. This ensures that airflow from the blower is at the required temperature when introduced into the chamber [50].

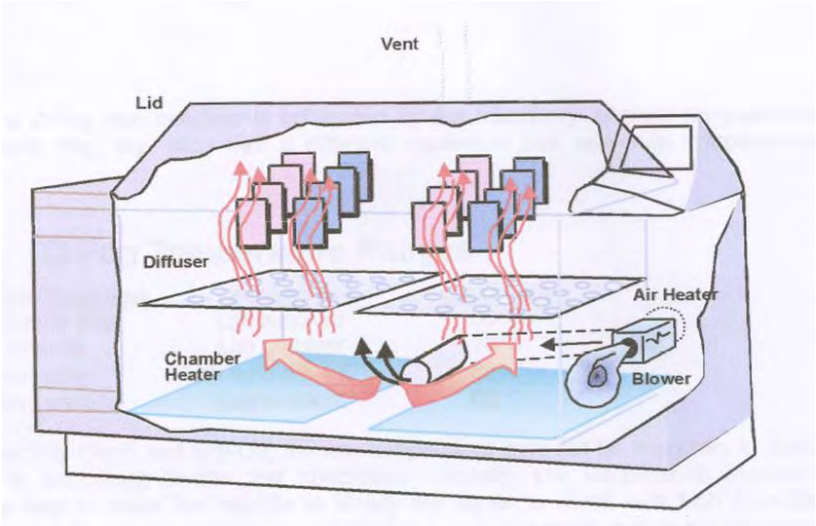


**Figure 3.7: Schematic of Q-fog cyclic corrosion tester operating the dry-off environment** [50].

### 3.2.4.3 Humidity Environment

A 100% relative humidity environment is maintained by water heated in the vapour generator, creating steam which is then introduced into the chamber (**Figure 3.7**).

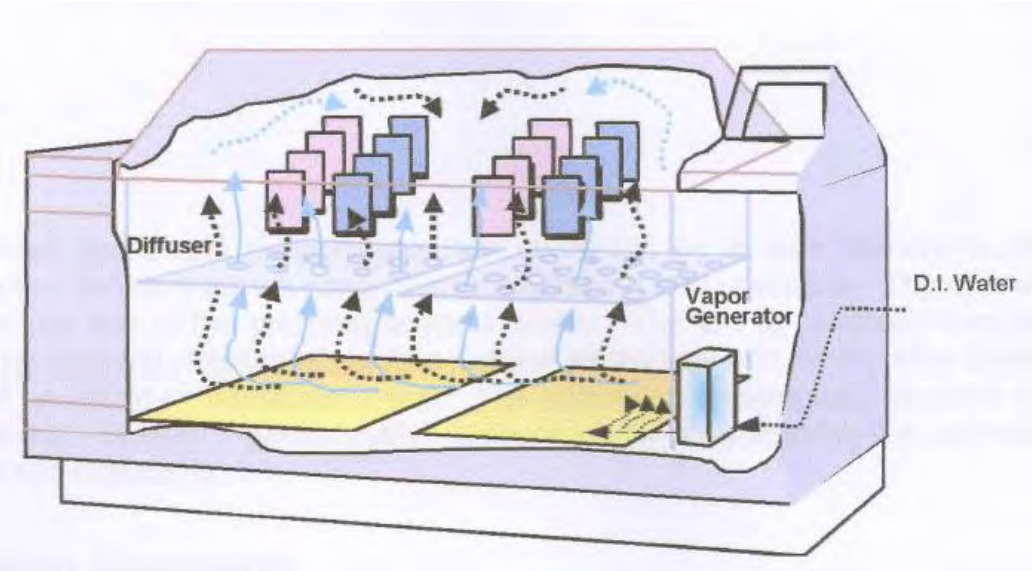


**Figure 3.8: Schematic of Q-fog cyclic corrosion tester operating the humidity environment** [50].

## 3.2.5 Test Coupon Set-up inside Q-Fog Cyclic Corrosion Tester

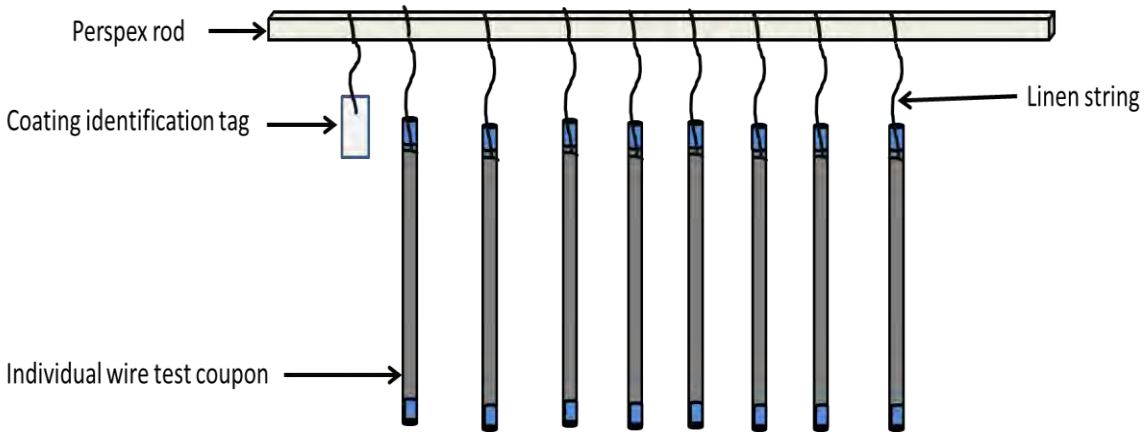


**Figure 3.9: Illustration of wire specimens set-up for salt spray tests.**

Specimens were suspended from Perspex rods using linen string (**Figure 3.9**). Fully labelled tags were used to distinguish between the various specimens. A total of 8 specimens were used for each of the 16 samples supplied. This meant that at the beginning of both the ASTM B117 and VW PV 1210 salt spray tests the Q-fog 1000 cyclic corrosion tester had 128 specimens installed within its chamber (**Figure 3.10**).

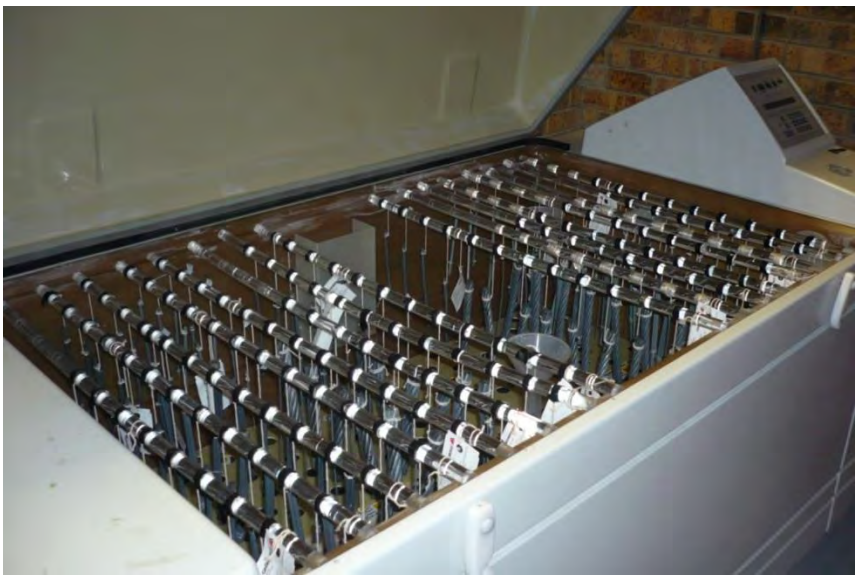

**Figure 3.10: Specimens set-up inside Q-Fog 1100 cyclic corrosion tester at the beginning of the ASTM B117 test.**

## 3.3 Evaluation of Corrosion Performance by Qualitative Methods

The texture and colour of corrosion products formed on test coupons during the salt spray tests were examined at set time intervals and recorded. The time taken for 5% of the surface area of specimens to be covered in red/brown corrosion products was determined and recorded. This was performed by calculating the total surface area of test coupons and then establishing 5% of this value. The time taken for 5% of a specimen to be covered in a red/brown corrosion product is taken as the standard failure condition for protective coatings during salt spray tests [48]. The red/brown corrosion products represent corrosion of steel. The presence these oxides indicate that the protective Zn and Zn-Al alloy coatings would have been breached, and thus exposing the underlying steel wire to corrosion attack.

### 3.3.1 Corrosion Grids

**Appendix D** shows corrosion grids used to determine the percentage of red/brown corrosion products on the surfaces of the specimens. Each unit cell on a corrosion grid represents 5% of the total surface area of the specimen. Corrosion grids were superimposed on to the test coupons in order to estimate the percentage of their surface area covered in red/brown corrosion products.

### 3.3.2 Determination of Surface Area of Specimens

The formula for calculating the surface area of cylindrical objects such as wires, bundles and rope is given in equation [1] below:

**Surface area of wires and cables** = **2πrh** [1]

Where:

r = radius

h = active specimen length

The active length of test coupons (h) is obtained by subtracting the specimen length coated with varnish (2l), at cut ends, from the overall specimen length (L) (**Figure 3.11**). The active length (h) value is used in surface area calculations, as opposed to the overall specimen length (L). The length of specimen coated in varnish (2l) is protected from corrosion during salt spray tests and thus it is excluded from in surface area calculations.

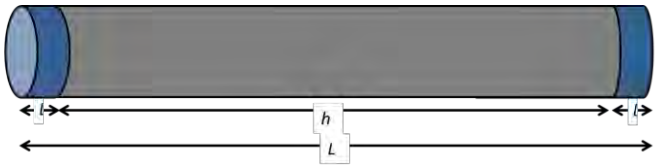


*Active test coupon length (h) = Overall test coupon length (L) – Test coupon length coated with varnish (2l)*

**Figure 3.11: Schematic of individual wire coupon showing how the active specimen length is determined.**

### 3.3.3 Surface Area Determination for Bundle and Rope Specimens

The diameter was measured with calipers at 4 different orientations as illustrated in **Figure 3.12**. The diameter readings were recorded as $D_1$, $D_2$, $D_3$ and $D_3$. The average of these values, $D_{ave}$, was used as the diameter of the bundle specimens (**Figure 3.12**).

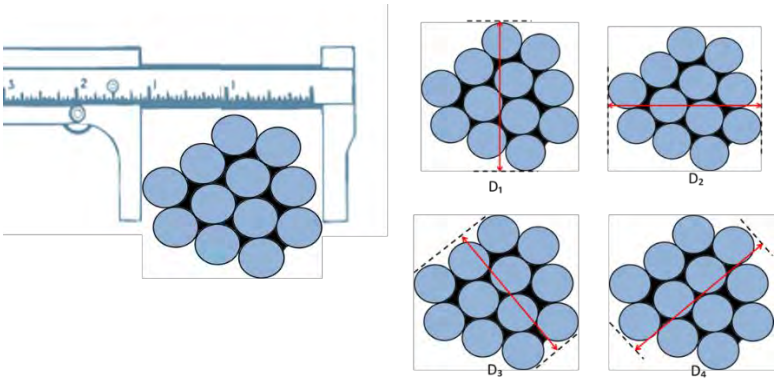


**Figure 3.12: Determination of diameter for bundle specimens. $D_1$, $D_2$, $D_3$ and $D_4$ are values of the specimen's diameter measured from different orientations. The dashed lines indicate the position where the calipers were positioned.**

An illustration of a rope specimen has been shown (**Figure 3.13**). The diameter of the ropes used in this study were provided, however confirmatory measurements were nevertheless taken.

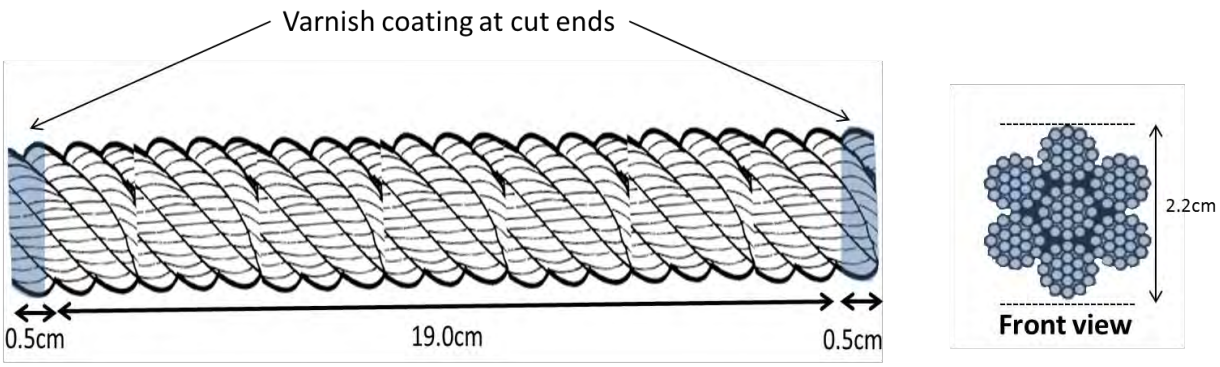


**Figure 3.13: Illustration of 22mm diameter wire rope specimen**

The diameter of a rope is given by the diameter of a circumscribed circle that encloses all the strands (**Figure 3.14a**) [51]. The correct way of measuring wire rope diameter has been illustrated (**Figure 3.14b**).

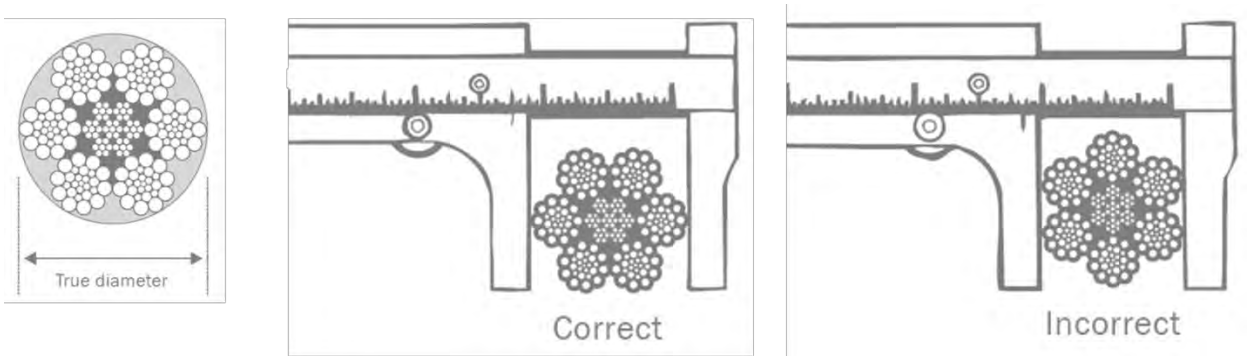


**(a)** **(b)** **(c)**

**Figure 3.14: Determination of diameter of rope specimens showing (a) the true diameter of a rope, (b) the correct way of measuring rope diameter, and (c) the incorrect was of measuring rope diameter.**

## 3.4 Evaluation of Corrosion Performance by Quantitative Methods

The corrosion rates of Zn and Zn-Al coatings on wire specimens were determined using the equation below:

$$\textbf{Corrosion rate (mm/yr)} = \frac{K \times W}{A \times T \times D} \qquad [2]$$

Where:

K = corrosion constant,
T = time of exposure in hours to the nearest 0.01h,
A = surface area in cm² to nearest 0.01cm²,

W= mass loss in g, to the nearest 1mg,
D = density in g/cm³.

The calculation of mass loss due to corrosion, which has been described in **Section 3.21**, is represented by equation 3.

**Mass loss (W) = Initial mass (I) – Final mass (F)** **[3]**

The corrosion rate and cumulative mass loss of metallic coatings exposed to the salt spray tests were represented graphically. Corrosion rate, in this study, represented a measure of uniform corrosion which was only applicable to wire specimens. The construction of the bundles and ropes makes them highly vulnerable to crevice corrosion, thus preventing an accurate study of uniform corrosion from being performed on these specimens [12].

### 3.4.1 Wire Specimen Cleaning Procedure after Corrosion Tests

Specimens were extracted from the Q-fog 1000 cyclic corrosion tester at predetermined time intervals and cleaned. The cleaning process involved removing varnish coating from the cut ends of specimens and rinsing corrosion products off their surface. Specimens were finally dried, reweighed, and their mass recorded.

Corrosion products were cleaned off the surface of wire specimens by ultrasonic immersion in a 10% vol. solution of SurTec 414 Neutral Activator (**Figure 3.15**) [52]. SurTec 414 is a yellowish-clear, surfactant free liquid that removes rust and oxidic films from metallic surfaces at neutral pH-value [52]. Additionally, ultrasonic immersion in a 10% aqueous solution of di-ammonium hydrogen citrate ($C_6H_{14}N_2O_7$) was carried out in instances where corrosion products were not entirely removed by use of SurTec 414. $C_6H_{14}N_2O_7$ is mildly acidic (pH 5.2) that removes corrosion products without etching away steel [53]. It was observed that cleaning specimens ultrasonically with SurTec414 followed by $C_6H_{14}N_2O_7$ gave the best results as opposed to using these cleaning approaches singly. Effective removal of corrosion product allowed accurate metallic coating mass loss values resulting from corrosion damage to be determined.

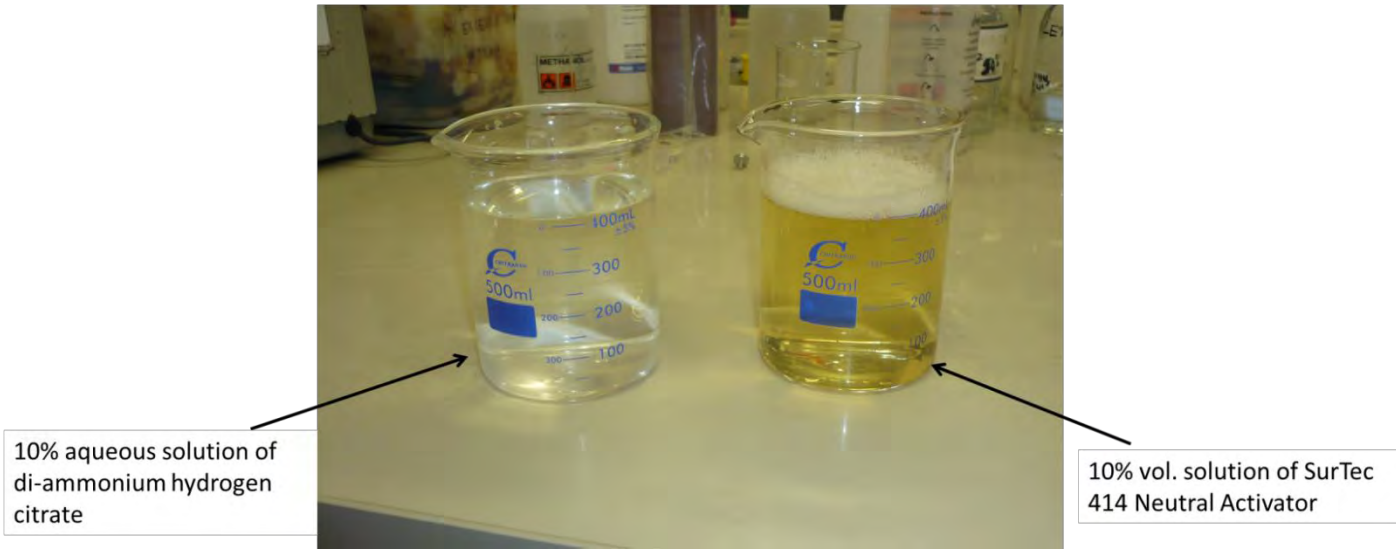


**Figure 3.15: Solutions of 10% di-ammonium hydrogen citrate and 10% vol. solution of SurTec 414 Neutral Activator used to clean corrosion products from wire specimens following their extraction from the Q-fog cyclic corrosion tester.**

### 3.4.2 Specimen Preparation for Microstructural Examination

Wire specimens were prepared for microstructural investigation by first cutting them into small sections of 2.0cm in length using an IsoMet low speed saw, followed by hot compression mounting in PolyFast resin. PolyFast is a phenolic resin consisting of carbon filler which promotes edge retention and examination in SEM.

Specimens were mounted in a vertical, or upright, orientation for cross sectional investigation of the microstructure of the steel wire and metallic coating (**Figure 3.16**).

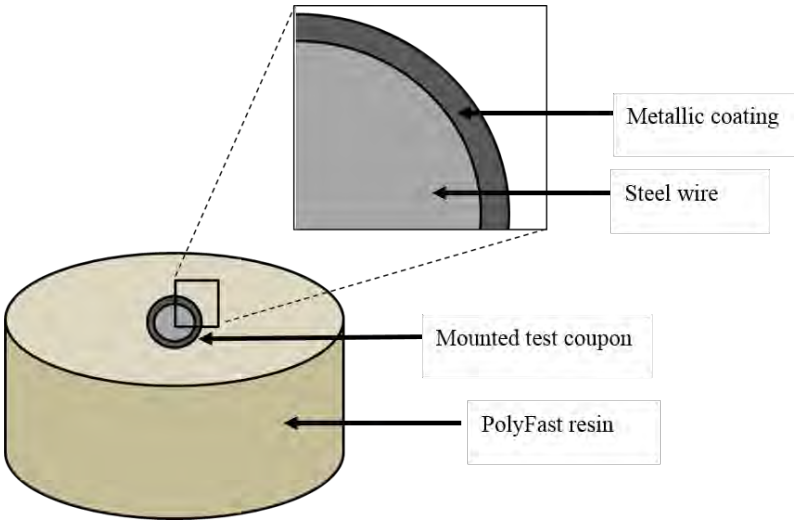


**Figure 3.16: Illustration of wire specimen mounted in PolyFast resin.**

### 3.4.3. Metallographic Preparation of Mounted Specimens

**Table 3.4: Summary of grinding steps followed in metallographic preparation of specimens for microscopic investigation [54].**

| Preparation Method<br>Grinding | | | |
|---|---|---|---|
| | Step | PG | FG 1 |
| | Surface | SiC-paper, #320 | MD-Largo |
| | Suspension | | DiaPro Allegro-Largo |
| | Lubricant | Water | |
| | rpm | 300 | 150 |
| F | Force [N] | 30 per sample | 30 per sample |
| | Time | As needed | 4 min. |

Mounted specimens were ground and polished automatically using Struers TegraPol-11 grinding/polishing machine. This approach gave more reliable and reproducible results over manual grinding and polishing.

Mounted specimens were first ground using 320 grit silicon carbide paper (SiC-paper, #320) with water as a lubricant. This was succeeded by grinding on a special fine grinding disc (MD-Largo) onto which a special diamond suspension, DiaPro Allegro-Largo, was applied. MD-Largo gives great edge retention which enhances the observation of metallic coatings at magnifications of X 1000 [54]. A summary of the various settings for grinding with SiC-paper and MD-Largo pads respectively are summarized in **Table 3.4**.

Polishing was carried out by following steps described in **Table 3.5**. Silk pads were used to ensure that specimens remained flat and that no scratches were introduced during polishing. On account of Zn's reaction with water,which may led to staining, waterfree diamond suspensions and lubricants were used for polishing, while ethanol denatured isopropyl alcohol was used for all cleaning steps during polishing. The effect of the reaction between water and Zn is not significant during grinding [54].

**Table 3.5: Summary of polishing steps followed in metallographic preparation of mounted specimens for microscopic investigation** [54]

| Polishing | | | | |
|---|---|---|---|---|
| | Step | DP 1 | DP 2 | OP |
| | Surface | MD-Dac | MD-Dur | OP-Chem |
| | Suspension | DP-Susp. A, 3 µm | DP-Susp. A, 1 µm | |
| | Lubricant | DP-Yellow | DP-Yellow | Ethanol* |
| | rpm | 150 | 150 | 150 |
| F | Force [N] | 25 per sample | 20 per sample | 15 per sample |
| | Time | 4-6 min. | 4-6 min. | 15-20 sec. |
| *Comments* | | **Ethanol denatured with isopropyl alcohol* | | |

### 3.4.4 Light Microscopy

Optical light micrographs were acquired using a Leica MZ8 stereomicroscope and a Reichert MeF3A microscope. The Leica MZ8 stereomicroscope was specifically used to obtain low magnification images of the surface of unmounted specimens before and after the salt spray tests were performed in order to observe changes occurring to the coatings as a result of corrosion. Medium magnification images of the microstructure of metallic coatings before and after salt spray testing were obtained using the Reichert MeF3A microscope in bright-field mode.

### 3.4.5 Scanning Electron Microscopy

The Nova NanoSEM 430 operating at 20 kV was used to carry out high magnification and high resolution observation of the microstructure of various Zn and Zn-Al coatings for mounted and polished test coupons prior to, and after corrosion testing. Elemental composition analyses of the phases present in Zn-Al coatings were performed using Energy Dispersive Spectroscopy (EDS). Backscattered electron images in the SEM display compositional contrast that results from the different atomic number elements and their distribution. EDS allows identification of those particular elements and their relative proportions. Best EDS analysis results are obtained under conditions where the sample surface is flat without contamination, is in a horizontal orientation, and where the area of analysis is homogenous [55].

## 3.5 Environmental Exposure Tests

Environmental exposure tests differ from accelerated laboratory corrosion tests in that specimens are exposed to the actual environment in which they are used in service. Therefore, the results from these experiments are more meaningful in terms of studying the actual corrosion performance of metallic coatings [40]. The major drawback with field exposure tests is that they are time consuming and thus not always practical to perform.

### 3.5.1 Selection of Location for Environmental Exposure Test

Chapman's Peak Drive is a 9km road which runs along the Atlantic Seaboard coastline, and connects Hout Bay to Noordhoek. Chapman's Peak Drive was an ideal location for the environmental exposure tests due to the catch fences, or rock fall protection barriers, installed to protect motorists from rock falls. The catch fences were located within a kilometre from the shoreline, an environment where high corrosion activity would be expected due to its salinity and wet conditions. **Figure 3.17** shows catch fences installed along Chapman's Peak Drive. The catch fences are composed of the wire, bundle and rope material used in this study, as shown in **Figure 3.18**. Ropes anchor and support the catch fences while the bundles, formed into ring structures, and wire nets are the primary components of catch fences [56].


**Figure 3.17: Catch fences installed along Chapman's Peak Drive to protect motorists from rock falls**

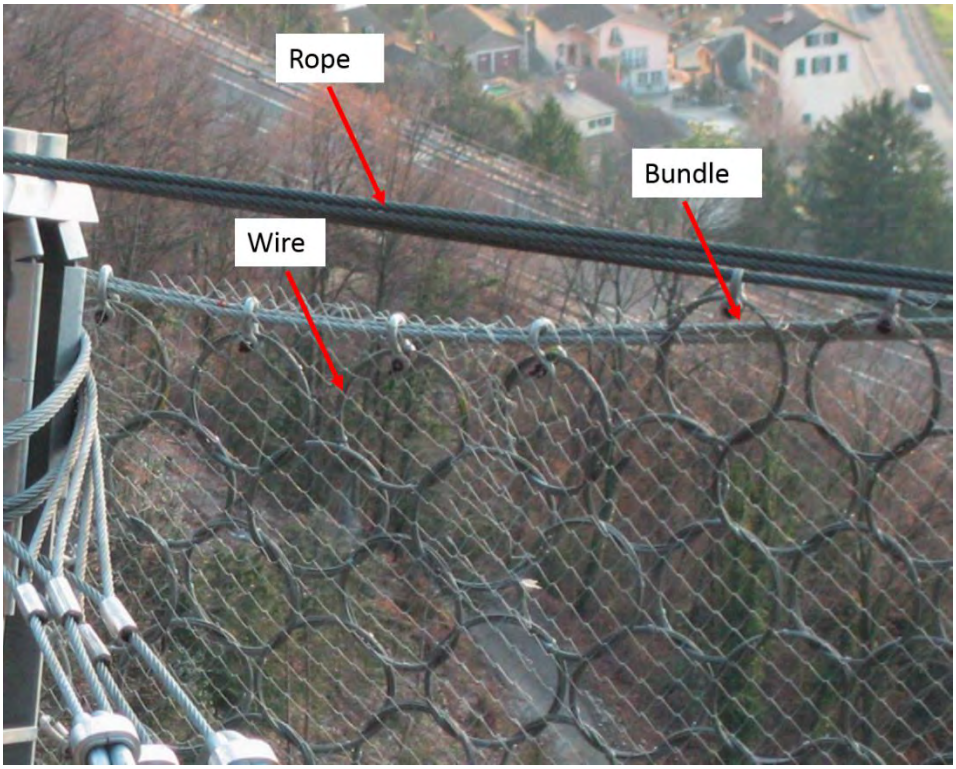


**Figure 3.18: Section of catch fence showing rope, bundle and wire components**

### 3.5.2 Specimen Preparation for Environmental Exposure Test

Specimens were prepared for the environmental exposure test based on guidelines described in **Section 3.2.1**. The major difference in preparation was that the specimens used in the environmental exposure test were not weighed since mass loss investigation were not performed. Only an examination of the colour and texture of corrosion products was carried out. Another difference in specimen preparation between the laboratory and environmental exposure tests was the lengths of specimens used. The lengths of the bundles and rope coupons were 70cm and 100cm respectively. Long specimen lengths were used in the field test so that corrosion occurring over a larger surface area could be observed. The length of the bundles were shorter than the rope as the quantity of the material was limited.

### 3.5.3 Description of Specimen Installation Sites along Chapman's Peak Drive

Specimens were suspended from three catch fences along Chapman's Peak Drive using 5mm diameter elastic cord string. The three catch fences, namely catch fences 2, 23C and 38, where specimens were suspended from were chosen primarily on the basis of their ease of accessibility and the fact that they represent slightly different exposure to weather conditions.

### 3.5.3.1 Catch Fence 2

| Structure | Coating Type | Coating Mass Distribution (g/m²) | Wire Diameter (mm) |
|---|---|---|---|
| Bundles | | | |
| 12-strand bundle | Zn Class A | 235 | 3 |
| | Zn Class B | 235 | 3 |
| | Zn-5Al | 150 | 3 |
| | Zn-5Al-xMg | 150 | 3 |
| | Zn-10Al | 300 | 3 |
| Rope | | | |
| 8mm dia. rope | Zn | 70 | 0.9 |
| | Zn-5Al | 70 | 0.9 |
| 22mm dia. rope | Zn | 90 | 1.3 |
| | Zn-5Al | 90 | 1.3 |

**Figure 3.19: Image showing position of catch fence 2 (indicated by arrow). The accompanying table describes the specimens installed at catch fence 2 for the environmental exposure test.**

Catch fence 2 is located at the base of the mountain along road level. Test specimens installed at catch fence 2 were in constant shade based on the location of catch fence 2.

### 3.5.3.2 Catch Fence 23C

| Structure | Coating Type | Coating Mass Distribution (g/m²) | Wire Diameter (mm) |
|---|---|---|---|
| Rope | | | |
| 8mm dia. rope | Zn | 70 | 0.9 |
| | Zn-5Al | 70 | 0.9 |
| 22mm dia. rope | Zn | 90 | 1.3 |
| | Zn-5Al | 90 | 1.3 |

**Figure 3.20: Image showing position of catch fence 23C (indicated by arrow). The accompanying table describes the specimens installed at catch fence 23C for the environmental exposure test.**

Catch fence 23C is also situated at road level similar to catch fence 2. However, specimens were fully exposed to weather elements at this location unlike at catch fence 2 where the mountain served as barrier to some weather elements, such as direct sunlight exposure. The limited space for Catch Fence 23C only allowed for rope specimens to be installed there.

#### 3.5.3.3 Catch Fence 38

| Structure | Coating Type | Coating Mass Distribution (g/m²) | Wire Diameter (mm) |
|---|---|---|---|
| Bundles | | | |
| 12-strand bundle | Zn Class A | 235 | 3 |
| | Zn Class B | 235 | 3 |
| | Zn-5Al | 150 | 3 |
| | Zn-5Al-xMg | 150 | 3 |
| | Zn-10Al | 300 | 3 |
| Rope | | | |
| 8mm dia. rope | Zn | 70 | 0.9 |
| | Zn-5Al | 70 | 0.9 |
| 22mm dia. rope | Zn | 90 | 1.3 |
| | Zn-5Al | 90 | 1.3 |

**Figure 3.21: Image showing position of catch fence 38 (indicated by arrow). The accompanying table describes the specimens installed at catch fence 38 for the environmental exposure test.**

Catch fence 38 is located approximately 40 metres above road level. The catch fence is situated between a crevice in the mountain. The neighbouring terrain slopes downward towards road level creating a channel through which rain water flows downhill.

### 3.5.4 Method of Corrosion Performance Assessment

Trips were made to Chapman's Peak Drive once every 4 months in order to examine the specimens installed at the various catch fences. Specimens were removed from the catch fences at the end of the 16 month testing period and taken to the laboratory where an examination of the corrosion products was carried out.

# 4. Results and Discussion of Corrosion in Rope System

## 4.1 Development of Corrosion Products on Specimens during Accelerated Laboratory Tests

Specimens exposed to the ASTM B117 and VW PV 1210 salt spray tests were examined daily for red/brown corrosion products. Where red/brown corrosion products were present, corrosion grids were used to approximate the amount of these corrosion products covering the surface of specimens. The time taken for red/brown corrosion products to cover 5% of a specimen's surface area was recorded. Development of red/brown corrosion products on the specimens represented corrosion attack of the underlying steel. Steel corroded in regions of specimens where the protective Zn and Zn-Al alloy coatings had been disrupted by corrosion to the extent that the coatings were unable to effectively provide barrier and galvanic corrosion protection to the underlying steel.

## 4.2 Comparison of ASTM B117 and VW PV 1210 Salt Spray Test Results

The development of corrosion products on the surface of the Zn and Zn-5Al alloy hot dip coated rope specimens during the ASTM B117 and VW PV 1210 salt spray tests are exhibited in **Figures 4.1-4.6.**

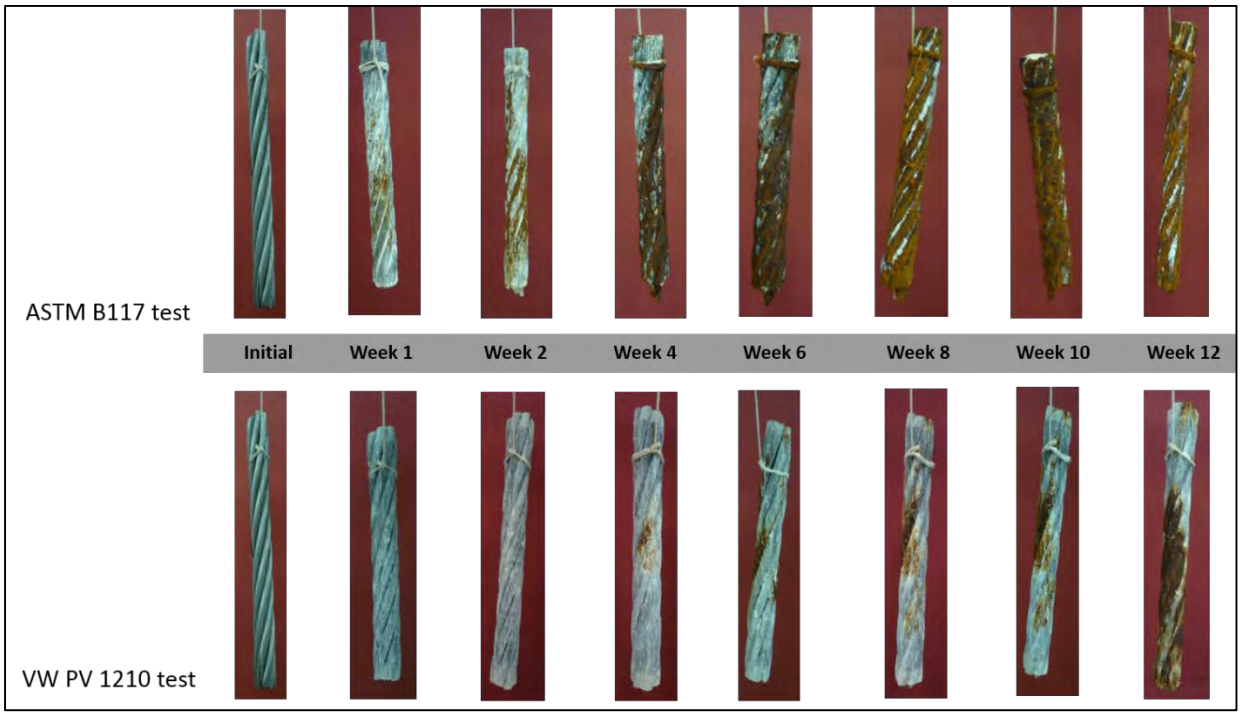


**Figure 4.1: Development of corrosion products on Zn (90g/m$^2$) Class B coated wire in 22mm diameter rope during ASTM B117 and VW PV 1210 salt spray tests.**

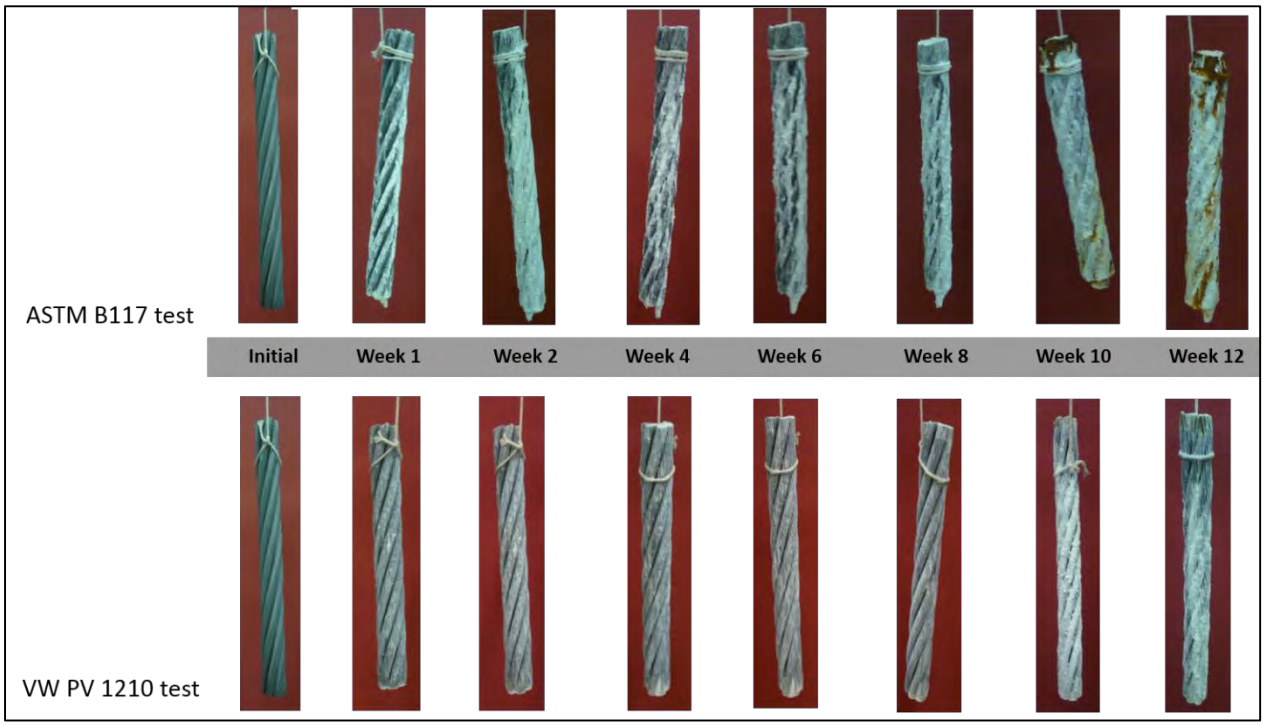


**Figure 4.2: Development of corrosion products on Zn-5Al (90g/m$^2$) Class B coated wire in 22mm diameter rope during ASTM B117 and VW PV 1210 salt spray tests.**


**Figure 4.3: Development of corrosion products on Zn (80g/m$^2$) Class B coated wires in 16mm diameter rope during ASTM B117 and VW PV 1210 salt spray tests.**

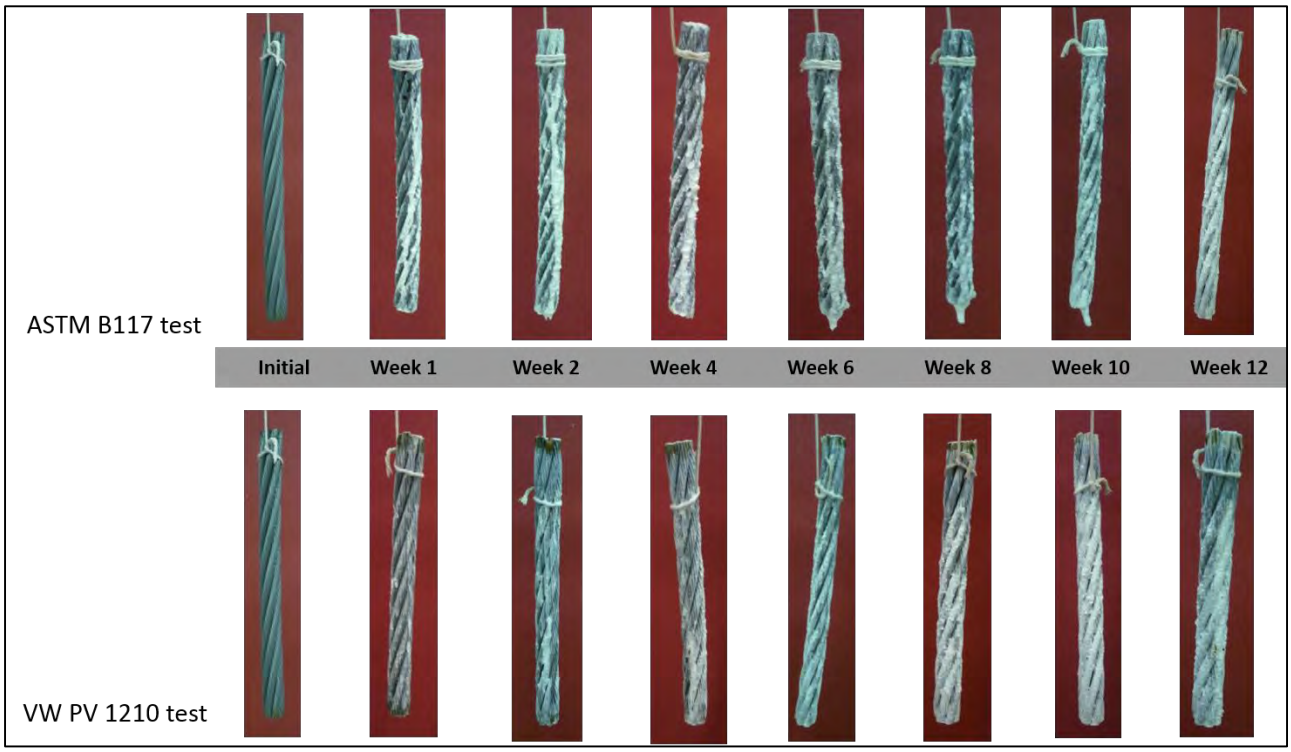


**Figure 4.4: Development of corrosion products on Zn-5Al (80g/m$^2$) Class B coated wires in 16mm diameter rope during ASTM B117 and VW PV 1210 salt spray tests.**


**Figure 4.5: Development of corrosion products on Zn (70g/m$^2$) Class B coated wires in 8mm diameter wire rope during ASTM B117 and VW PV 1210 salt spray tests.**


**Figure 4.6: Development of corrosion products on Zn-5Al (70g/m$^2$) Class B coated wires in 8mm diameter wire rope during ASTM B117 and VW PV 1210 salt spray tests.**

The time taken for red/brown corrosion product appearance on 5% of a specimen's surface area is illustrated graphically in **Figure 4.7**. This is representative of the expected relative service life of metallic coatings on steel [40].

Results of the salt spray tests shown in **Figures 4.1 - 4.7** revealed that the Zn-5Al coatings outperform Zn in both the ASTM B117 test and the VW PV 1210 test. The substitution ocean water used in laboratory corrosion tests was maintained between pH 6.5 – 7.5. The Eh-pH diagrams of Zn and Al shown in **Figure 2.13** and **Figure 2.15** predict that within this pH range Zn will corrode readily to produce soluble compounds consisting of $Zn^{2+}$ ions, while Al corrodes to form $Al_2O_3$ , an inert product that adheres to the surface of the metal to prevent further attack to the underlying substrate [**ref3**]. The Zn component of the Zn-5Al alloy coating corrodes preferentially until such a time as the outer surface becomes Al rich [30,32]. This happens as the level of Al rises at the exposed surface owing to the depletion of Zn [26]. The rate of attack will decrease significantly because the atmosphere 'sees' only Al. Al is more resistant to atmospheric corrosion than Zn because of its highly insulating oxide film that is formed [30,32].

The coatings exhibited better corrosion performance in the VW PV 1210 test relative to the ASTM B117. The ASTM B117 test exposed specimens to a more corrosive environment in comparison to the VW PV 1210 test for reasons summarized in **Table 3.3** in **Section 3.2.3**. Two of the most important environmental factors which impact the corrosion rate of steel, Zn and Zn-Al coatings are the level of airborne pollutants and time of wetness. The main pollutants in this study were chlorides contained in the substitution ocean water used to generate the salt mist. Time of wetness, defined as the length of time during which the coatings were covered by a film of water, was greater in the ASTM B117 test where specimens were continuously exposed to a salt mist throughout the entire testing period [30]. The VW PV 1210 test exposed specimens to periods of salt mist, dry-off and humid conditions in a cyclic manner, as illustrated in **Figure 3** in **Section 3.2.3**. As a result, the specimens exposed to the ASTM B117 were susceptible to a higher rate of corrosion than specimens in VW PV 1210 test.

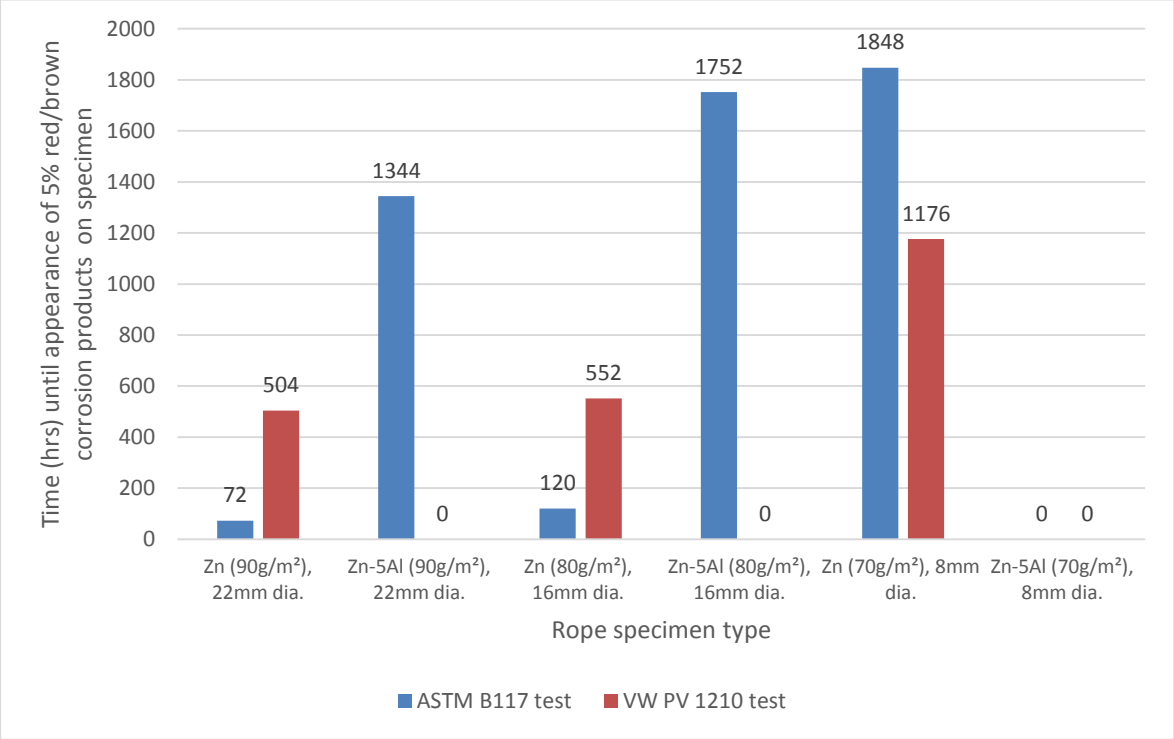


**Figure 4.7: Time taken for red/brown corrosion product appearance on 5% of specimen surface area during ASTM B117 and VW PV1210 corrosion tests.**

The trend observed from results of the salt spray tests summarized in **Figure 4.7** is that the time elapsed until appearance of red/brown corrosion products on 5% surface area of rope specimen increased as coating mass distribution and rope diameter decreased. This is contrary to guidelines in coating standards and results of various studies which indicate that corrosion performance of coatings should improve as coating mass distribution increases [26,50,51]. A possible explanation for these results relates to the construction of rope and its impact on localized corrosion activity [49]. The complexity, as well as the number of wires in the rope specimens, increased with rope diameter from 8mm to 22mm, as shown in **Table 4.1**. The greater number of wires in the larger ropes created a significant system of crevices where corrosion activity is predicted to be prevalent [49]. Crevice corrosion is highly likely to occur in the rope at the following locations:

i) valleys between the strands that made up the rope

ii) naturally occurring crevices existing between wires

iii) on wires where surface disruptions exist.

**Table 4.1: Description of Rope Specimens**

| | **22mm dia. rope** | **16mm dia. rope** | **8mm dia. Rope** |
|---|---|---|---|
| **Diameter of outer wires (mm)** | 1.3 | 1.1 | 0.9 |
| **Coating mass distribution on outer wires (g/m$^2$)** | 90 | 80 | 70 |
| **Total no. of wires in rope** | 216 | 114 | 42 |
| **Wire arrangement** | 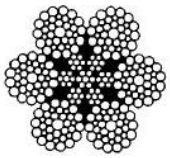 | 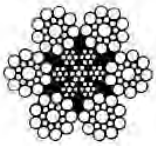 | 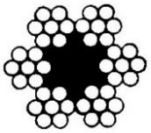 |

# 5. Results and Discussion of Corrosion Performance of Hot Dip Zn and Zn-Al Alloy Coatings on Wire

## 5.1 Corrosion Rates and Cumulative Coating Mass Loss Results

Wire specimens with various hot dip Zn and Zn-Al alloy coatings, as described in **Section 3.1**, were exposed to the ASTM B117 and VW PV 1210 salt spray tests. Specimens were removed from the Q-fog 1000 cyclic corrosion tester at time intervals of 336 hrs (2 weeks), 672 hrs (4 weeks), 1,008 hrs (6 weeks), 1,344 hrs (8 weeks), 1,680 hrs (10 weeks) and 2,016 hrs (12 weeks) respectively. Upon collection, test coupons were cleaned by methods outlined in **Section 3.4.1**. Specimens were weighed to determine the mass of coatings lost as a result of corrosion damage during the salt spray tests.

The corrosion rates (mm/yr) of hot dip Zn and Zn-Al alloy coatings on wire exposed to the ASTM B117 and VW PV 1210 salt spray tests were determined by the method described in **Section 3.4**. Corrosion rates (mm/yr) and cumulative coating mass losses (mg) are illustrated in **Figures 5.1 – 5:12.** In all instances, the corrosion rates and cumulative coating mass losses of the metallic coatings were significantly higher in the more aggressive ASTM B117 test in comparison to the VW PV 1210 test. The corrosion rates of coatings exposed to the ASTM B117 test peaked between 1,000 – 1,500 hrs of testing, after which corrosion rates gradually decreased. The cumulative mass losses also peaked between 1,000 – 1,500 hrs of testing before levelling off. No distinct trends were observed for coatings exposed to the VW PV 1210 test. The levelling off of corrosion rates and cumulative mass loss relate to the formation of a barrier layer of corrosion products on the Zn and Zn-Al alloy coatings which shield the coatings, and therefore the underlying steel, from further corrosion attack [7].

## 5.2 Corrosion Performance of Hot Dip Zn Coatings on Wire

### 5.2.1 Results of the ASTM B117 Test

The corrosion rates (mm/yr) and cumulative coating mass losses (mg) for Zn Class A (235 g/m$^2$) and Zn Class B (135 g/m$^2$) coatings on wire specimens in the ASTM B117 test are illustrated in **Figures 5.1 – 5.4**. Results show that corrosion rates of the coatings increase initially before decreasing with respect to testing time. Specimens were covered with white corrosion products but a few spots of red/brown corrosion products appeared representing substrate steel corrosion. The thickness of corrosion products, as well as the surface area of specimens covered by these products, also increased with respect to testing time. Therefore the Zn coatings and underlying steel were increasing shielded from further corrosion attack by the secondary barrier formed by corrosion products on the surface of the specimens as the test progressed. As a result, the cumulative coating

mass loss for both Zn Class A (235 g/m$^2$) and Zn Class B (135 g/m$^2$) coatings decreased as shown in **Figures 5.2** and **Figures 5.4** respectively.

The initial and peak corrosion rates for the Zn Class A (235 g/m$^2$) coating were recorded as approximately 0.125 mm/yr and 0.145 mm/yr respectively as shown in **Figure 5.1**. Both values fall below the initial and peak corrosion rates of the Zn Class B (135 g/m$^2$) coating recorded as approximately 0.165 mm/yr and 0.22 mm/yr respectively as shown in **Figure 5.3**. On the basis of these results, it is predicted that in harsh marine environments, represented by the ASTM B117 test in this study, the Zn Class A (235 g/m$^2$) coating will slightly outperform the Zn Class B (135 g/m$^2$) on wire.

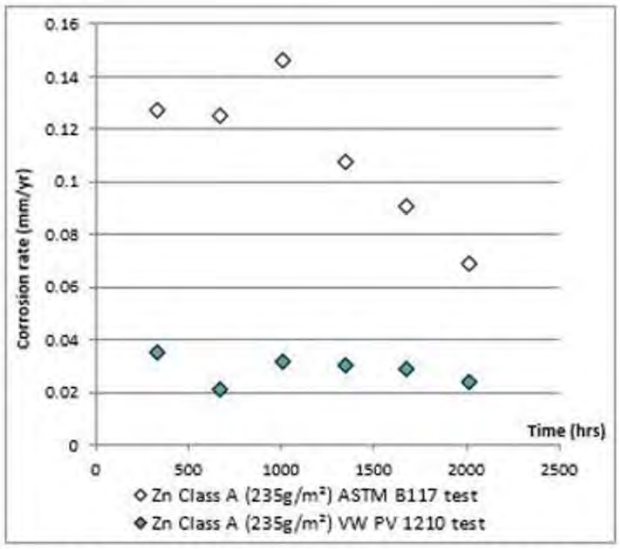


Figure 5.1: Comparison of corrosion rates of Zn Class A (235g/m²) coated wire in ASTM B117 and VW PV 1210 salt spray tests over a 2,016hrs (12 week) testing period.

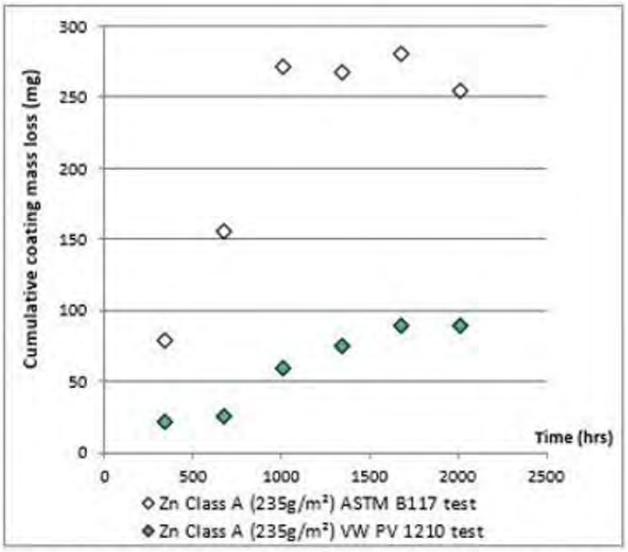


Figure 5.2: Cumulative mass loss of Zn Class A (235g/m²) coated wire in ASTM B117 and VW PV 1210 salt spray tests over a 2,016hrs (12 week) testing period.

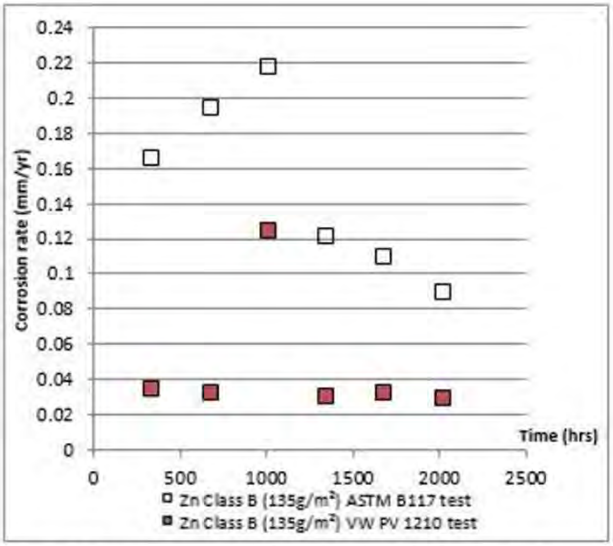


Figure 5.3: Comparison of corrosion rates of Zn Class B (135g/m²) coated wire in ASTM B117 and VW PV 1210 salt spray tests over a 2,016hrs (12 week) testing period.

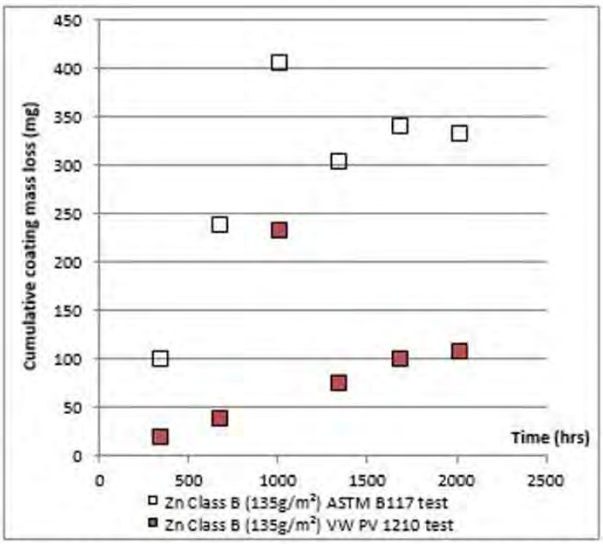


Figure 5.4: Cumulative mass loss of Zn Class B (135g/m²) coated wire in ASTM B117 and VW PV 1210 salt spray tests over a 2,016hrs (12 week) testing period.

### 5.2.2 Results of the VW PV 1210 Test

The corrosion rates (mm/yr) and cumulative coating mass loss (mg) for Zn Class A (235 g/m$^2$) and Zn Class B (135 g/m$^2$) coatings on wire specimens in the VW PV 1210 test are also illustrated in **Figures 5.1 – 5.4**. The coatings exhibited indistinguishable corrosion rates in the VW PV 1210 test. Initial and final corrosion rates of approximately 0.04 mm/yr and 0.03 mm/yr respectively were recorded for both coatings as shown in **Figure 5.1** and **Figure 5.3**. An outlier result was recorded for Zn Class B (135 g/m$^2$) after 1,008 hrs (6 weeks) of testing which had a corrosion rate of approximately 0.12 mm/yr. The increased coating mass loss may have been caused by damage to the coating during the cleaning process after the test. Alternatively, the coating of that particular specimen may have had surface disruptions or breaks which would have exposed underlying steel to corrosion. As a result, the galvanic corrosion activity of Zn would have been greater leading to a higher rate of Zn loss by corrosion. In terms of performance, it can be predicted on the basis of these results that in less aggressive environments, represented by the VW PV 1210 test in this study, Zn Class A (235 g/m$^2$) and Zn Class B (135 g/m$^2$) coatings will perform similarly on wire.

Although similar corrosion performance, represented by corrosion rate, is predicted for the Zn coatings, it is not expected that the Zn coatings will have similar lifespans. The Zn Class B (135 g/m$^2$) coating has a lower coating mass distribution in comparison to the Zn Class A (235 g/m$^2$) coating. Coating mass distribution impacts the lifespan of metallic coatings in corrosive environments; the general principle is that the greater the coating mass distribution, the longer the lifespan of the coating [26]. Therefore, a shorter lifespan is predicted for the Zn Class B (135 g/m$^2$).

## 5.3 Corrosion Performance of Various Hot Dip Zn-Al Alloy Coatings on Wire

### 5.3.1 Results of the ASTM B117 Test

Corrosion rates (mm/yr) and cumulative coating mass loss (mg) for Zn-5Al (150 g/m$^2$), Zn-5Al-xMg (150 g/m$^2$), and Zn-10Al (300 g/m$^2$) coatings on wire specimens in the ASTM B117 test are shown in **Figures 5.5 – 5.10**. The Zn-5Al (150 g/m$^2$) coating recorded initial and peak corrosion rates of approximately 0.080 mm/yr and 0.110 mm/yr respectively as shown in **Figure 5.5**. These values were higher than the initial and peak corrosion rates for the Zn-5Al-xMg (150 g/m$^2$) coating recorded as approximately 0.05mm/yr and 0.0725 mm/yr respectively illustrated in **Figure 5.6**. In both instances the corrosion rate decreased with respect to testing time as corrosion products formed a barrier layer on the surface of the specimens as the test progressed, which subsequently shielded the coatings from further attack.

The primary difference in composition of the Zn-5Al (150 g/m$^2$) and Zn-5Al-xMg (150 g/m$^2$) coatings is the addition of Mg in the latter. The coatings were applied onto the wire by the same method and the coating mass distributions were identical. Thus improved corrosion performance of the Zn-5Al-xMg (150 g/m$^2$) coating over the Zn-5Al (150 g/m$^2$) may only be attributed to the Mg presence in the alloy which is believed to stabilise the secondary barrier formed by corrosion products on the

surface of the specimens [57]. On the basis of the results of the ASTM B117 test, it can therefore be predicted that Mg additions improve the corrosion performance of the Zn-5Al coating in harsh marine environments.

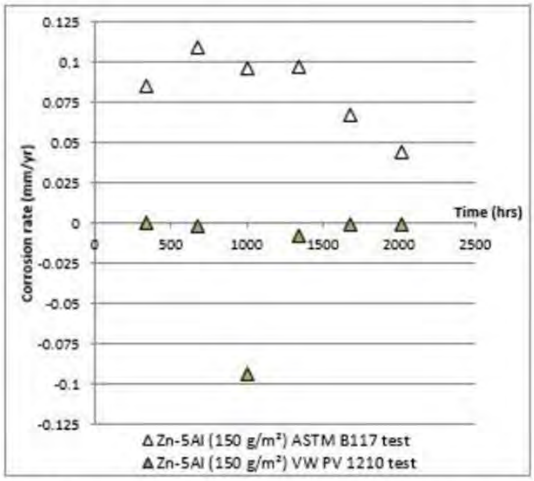


Figure 5.5: Comparison of corrosion rates of Zn-5Al (150g/m²) coated wire in ASTM B117 and VW PV 1210 salt spray tests over a 2,016hrs (12 week) testing period.

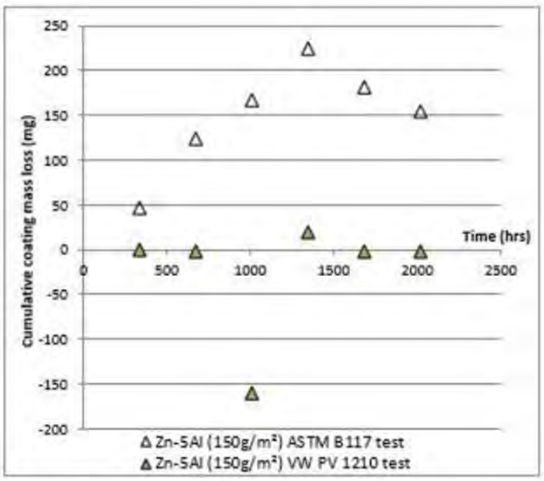


Figure 5.6: Cumulative mass loss of Zn-5Al (150g/m²) coated wire in ASTM B117 and VW PV 1210 salt spray tests over a 2,016hrs (12 week) testing period.

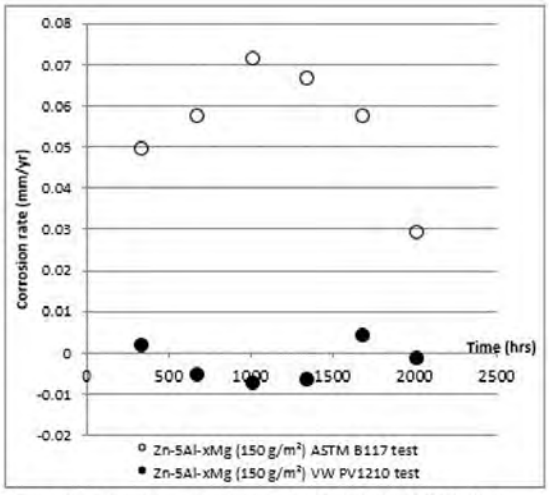


Figure 5.7: Comparison of corrosion rates of Zn-5Al -xMg (150g/m²) coated wire in ASTM B117 and VW PV 1210 salt spray tests over a 2,016hrs (12 week) testing period.

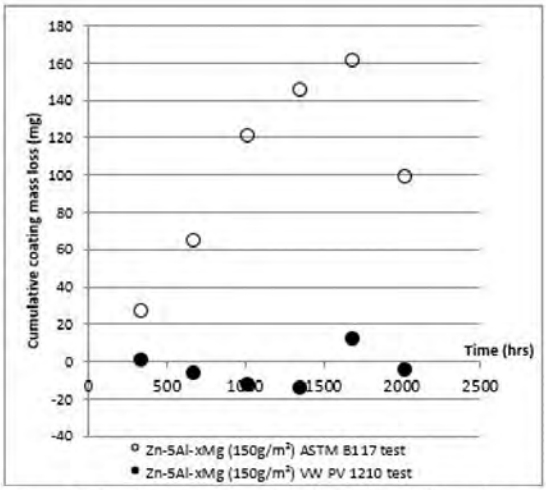


Figure 5.8: Cumulative mass loss of Zn-5Al-xMg (150g/m²) coated wire in ASTM B117 and VW PV 1210 salt spray tests over a 2,016hrs (12 week) testing period.

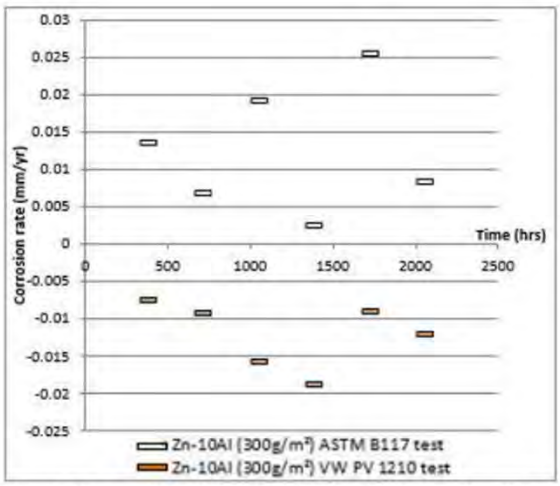


Figure 5.9: Comparison of corrosion rates of Zn-10Al (300g/m²) coated wire in ASTM B117 and VW PV 1210 salt spray tests over a 2,016hrs (12 week) testing period.

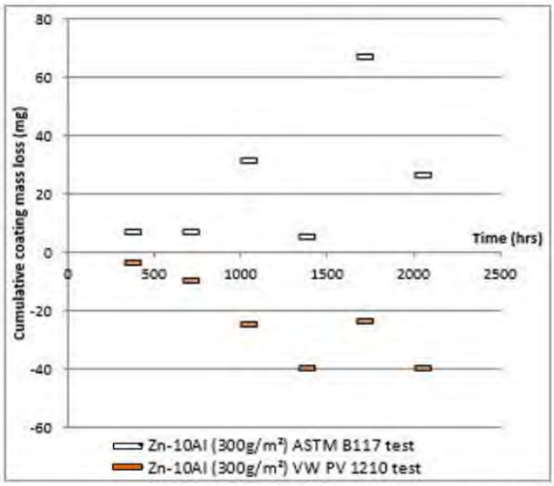


Figure 5.10: Cumulative mass loss of Zn-10Al (300g/m²) coated wire in ASTM B117 and VW PV 1210 salt spray tests over a 2,016hrs (12 week) testing period.

No clear trends concerning corrosion rates were observed for the Zn-10Al (300g/m$^2$) coating during the ASTM B1117 test. Corrosion rates fluctuated between 0.015 mm/yr and 0.025 mm/yr during the testing period as shown in **Figure 4.10**.

The Zn-10Al (300 g/m$^2$) coating consists of double the amount of Al relative to the Zn-5Al (150 g/m$^2$) and Zn-5Al-xMg (150 g/m$^2$) coatings. The increased Al content accounts for the improved corrosion performance [18,42]. The relative service lifespan of the Zn-10Al (300 g/m$^2$) is predicted to be longer than the Zn-5Al (150 g/m$^2$) and Zn-5Al-xMg (150 g/m$^2$) coatings based on the greater coating mass distribution[30].

### 5.3.2 Results of the VW PV1210 Test

Corrosion rates (mm/yr) and cumulative coating mass loss (mg) for Zn-5Al (150 g/m$^2$), Zn-5Al-xMg (150 g/m$^2$), and Zn-10Al (300 g/m$^2$) coatings on wire specimens in the VW PV 1210 test are shown in **Figures 5.5 – 5.10.**

The various Zn-Al alloy coatings exhibited negative corrosion rates during the VW PV 1210 test as shown in **Figures 5.5, 5.7** and **5.9** for Zn-5Al (150 g/m$^2$), Zn-5Al-xMg (150 g/m$^2$), and Zn-10Al (300 g/m$^2$) coatings respectively. A gain in mass was recorded when coupons were weighed after corrosion products had been removed from their surfaces following their removal from the Q-fog 1000 cyclic corrosion tester. As a result, when equation [3] was used to determine coating mass loss during VW PV 1210 test negative values for mass loss were obtained since the final masses of the Zn-Al alloy coated specimens were greater than their initial masses prior to the commencement of the VW PV 1210 test. The negative cumulative coating mass losses are shown in **Figures 5.6, 5.8** and **5.10** for Zn-5Al (150 g/m$^2$), Zn-5Al-xMg (150 g/m$^2$), and Zn-10Al (300 g/m$^2$) coatings respectively.

Although accurate corrosion rates for Zn-Al alloy coatings on wire could not be determined, the results point towards similar corrosion performance of these Zn-Al alloy coatings on wire in moderate environments represented by the VW PV 1210 test.

$$\textbf{Mass loss (W) = Initial mass – Final mass} \qquad \textbf{[3]}$$

## 5.4 Comparison of Corrosion Performance of Zn and Zn-Al Alloy Coatings in Salt Spray Tests

### 5.4.1 Comparison of Corrosion Performance during ASTM B117 Test

**Figure 5.11** and **Figure 5.12** show the corrosion rates and cumulative coating mass loss for all the Zn and Zn-Al alloy coatings used in this study during exposure to the ASTM B117 test. As predicted, the Zn-Al alloy coatings significantly outperformed the Zn coatings. Al additions lead to improved barrier corrosion performance [17,42]. A general trend observed is that corrosion rate decreased with testing time for all coatings except for the Zn-10Al (300g/m$^2$), which was stable throughout the test in comparison to the other coatings. The observed decrease in corrosion rates is related to a

levelling off in the cumulative mass loss during the latter parts of the test as seen in **Figure 5.12**. The explanation for this is that corrosion products accumulated on the surface of the coatings forming a barrier layer that effectively shielded the coatings for further attack.

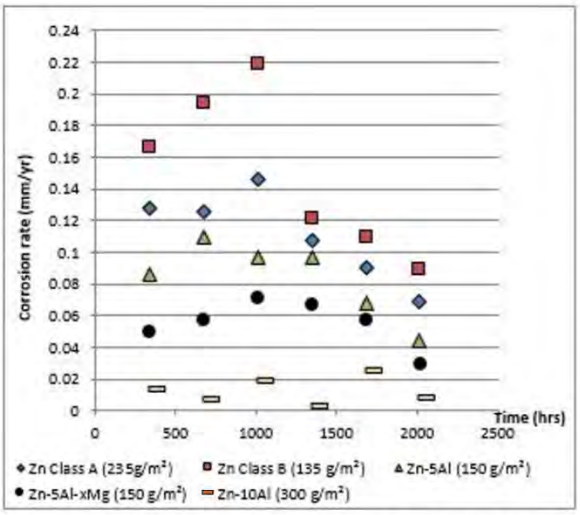


**Figure 5.11: Corrosion rates of various Zn and Zn-Al alloy coatings on wire during 2,016hr (12 week) ASTM B117 test**

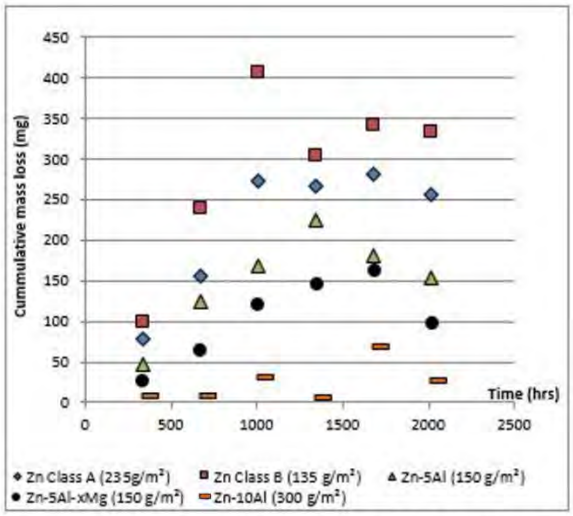


**Figure 5.12: Cumulative coating mass loss of Zn and Zn-Al alloy coatings on wire during 2,016hr (12 week) ASTM B117 test**

### 5.4.2 Comparison of Corrosion Performance during VW PV 1210 Test

**Figure 5.13** and **Figure 5.14** show the corrosion rates and cumulative coating mass loss for the Zn and Zn-Al alloy coatings used in this study during exposure to the VW PV 1210 test. The corrosion rates were fairly constant throughout the testing period, which is different from corrosion rates in the ASTM B117 test which decreased as the test progressed. Results reveal that the corrosion performance of Zn Class B (135g/m$^2$) and Zn Class A (235g/m$^2$) coatings on steel wire was similar, disregarding a couple of outlying readings. The corrosion performance of Zn-Al alloy coatings was also very similar in the VW PV 1210 test. Once again, Zn-Al alloy coatings were observed to exhibit superior corrosion performance in comparison to the Zn coatings.

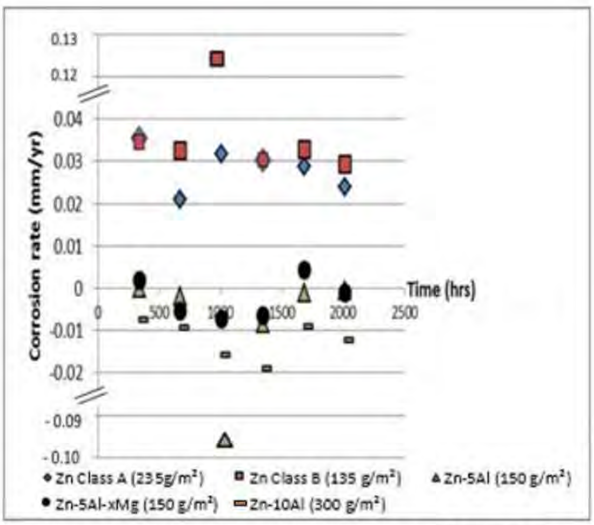


**Figure 5.13: Corrosion rates of various Zn and Zn-Al alloy coatings on wire during 2,016hr (12 week) VW PV 1210 test**

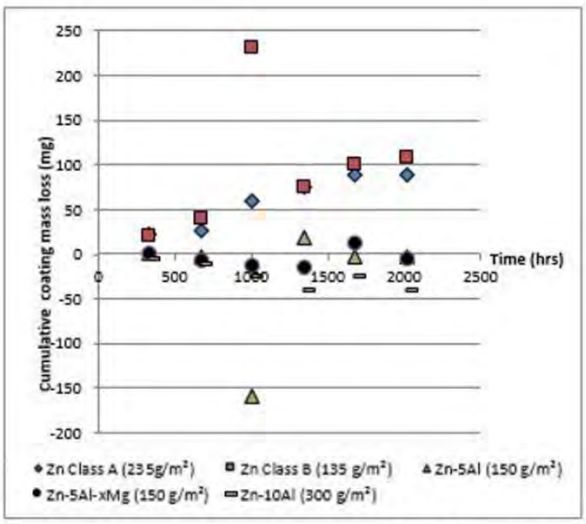


**Figure 5.14: Cumulative coating mass loss of Zn and Zn-Al alloy coatings on wire during 2,016hr (12 week) VW PV 1210 test**

# 6. Results of Microscopic Examination of Wire Specimens

## 6.1 Low Magnification Examination of Coating Surface

A Leica MZ8 stereomicroscope was used generate low magnification images of the surface of the coated wire specimens:

a) before salt spray testing, in order to show the original state of the Zn and Zn-Al alloy coatings on wire before exposure to salt spray tests
b) at the end of ASTM B117 test, in order to show the nature and distribution of corrosion products on the surface of the specimens
c) when corrosion products had been removed from specimens exposed to ASTM B117 test, thus revealing extent of corrosion damage of the coatings
d) at the end of VW PV 1210 test, in order to show the nature and distribution of corrosion products on the surface of the specimens
e) when corrosion products had been removed from specimens exposed to VW PV 1210 test, thus revealing extent of corrosion damage of the coatings

Image (a) in **Figures 6.1 - 6.5** shows the surface of the Zn and Zn-Al coatings on wire prior to salt spray exposure. The coatings on the specimens were bright in appearance, smooth in texture and neither exhibited evidence of disruptions or breaks in the coatings nor signs of corrosion. A comparison of images (b) and (d) in **Figures 6.1 - 6.5** show that corrosion products were thicker and distributed over a larger surface area of the specimens following exposure to the VW PV 1210 test, relative to the ASTM B117. The thicker corrosion product layer formed in the VW PV 1210 test resulted in a better secondary barrier layer against corrosion. As a result, lower cumulative mass loss (mg) and corrosion rates (mm/yr) observed for specimens exposed to the VW PV 1210 test as described in **Section 5**. The barrier layer of Zn corrosion products formed is fairly soluble [26]. It is therefore more likely to be dissolved during the ASTM B117 test where specimens are exposed to a salt mist throughout the entire testing period. However, specimens exposed to the VW PV 1210 test benefited from periods of drying whereby the corrosion product barrier layer was allowed to solidify and thus developed into a more effective secondary barrier against corrosion [26].

Images (c) and (e) in **Figures 6.1 - 6.5** reveal that Zn and Zn-Al alloy coated specimens consisted of roughened, darkened and pitted coating surfaces as a result of corrosion damage when examined after removal of corrosion products [15,20].

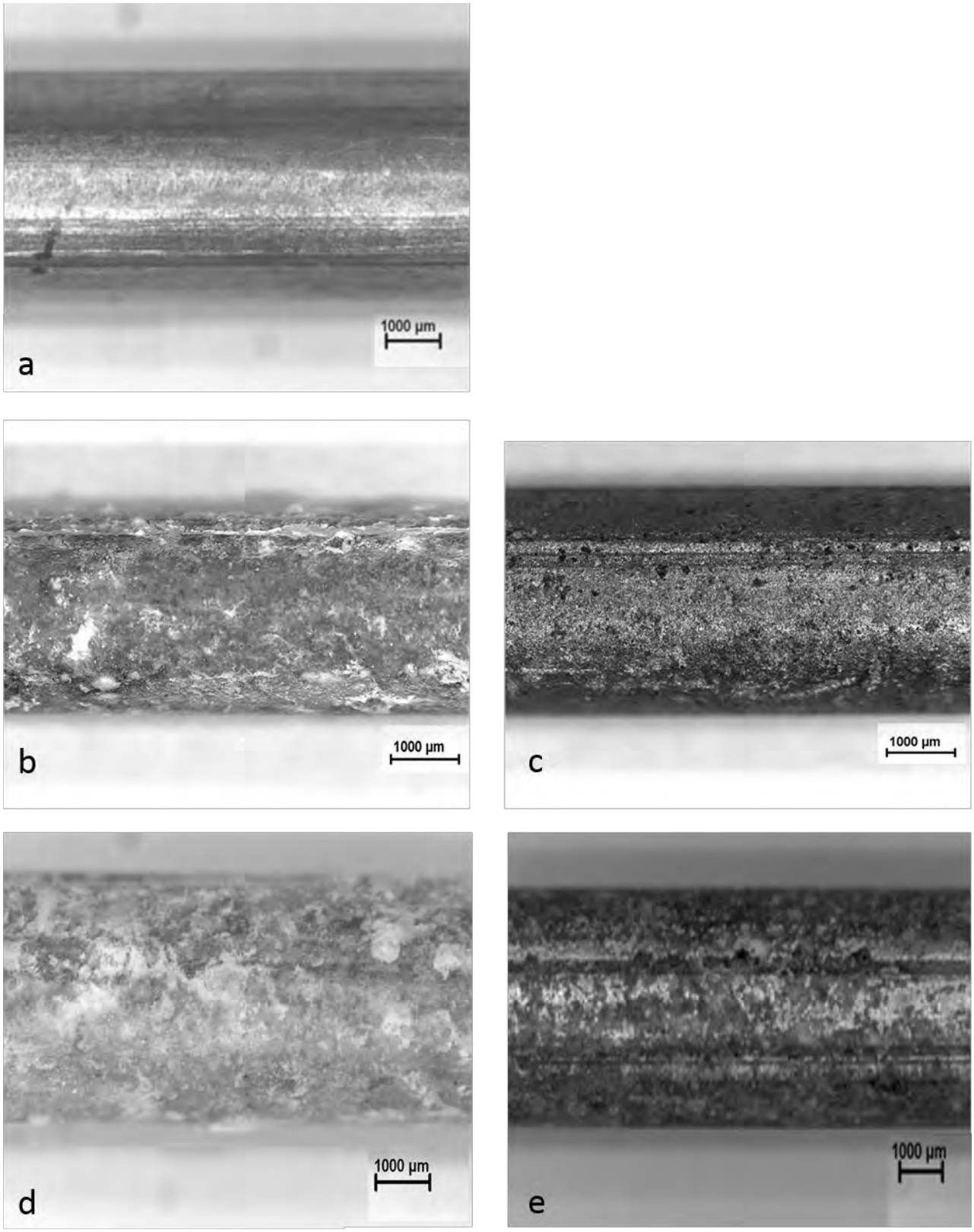


**Figure 6.1: Zn Class A (235g/m$^2$) wire specimen (a) prior to salt spray test exposure, (b) with corrosion products after ASTM B117 test , (c) corrosion products removed after ASTM B117 test, (d) with corrosion products after VW PV 1210 test, (e) corrosion products removed after VW PV 1210 test.**

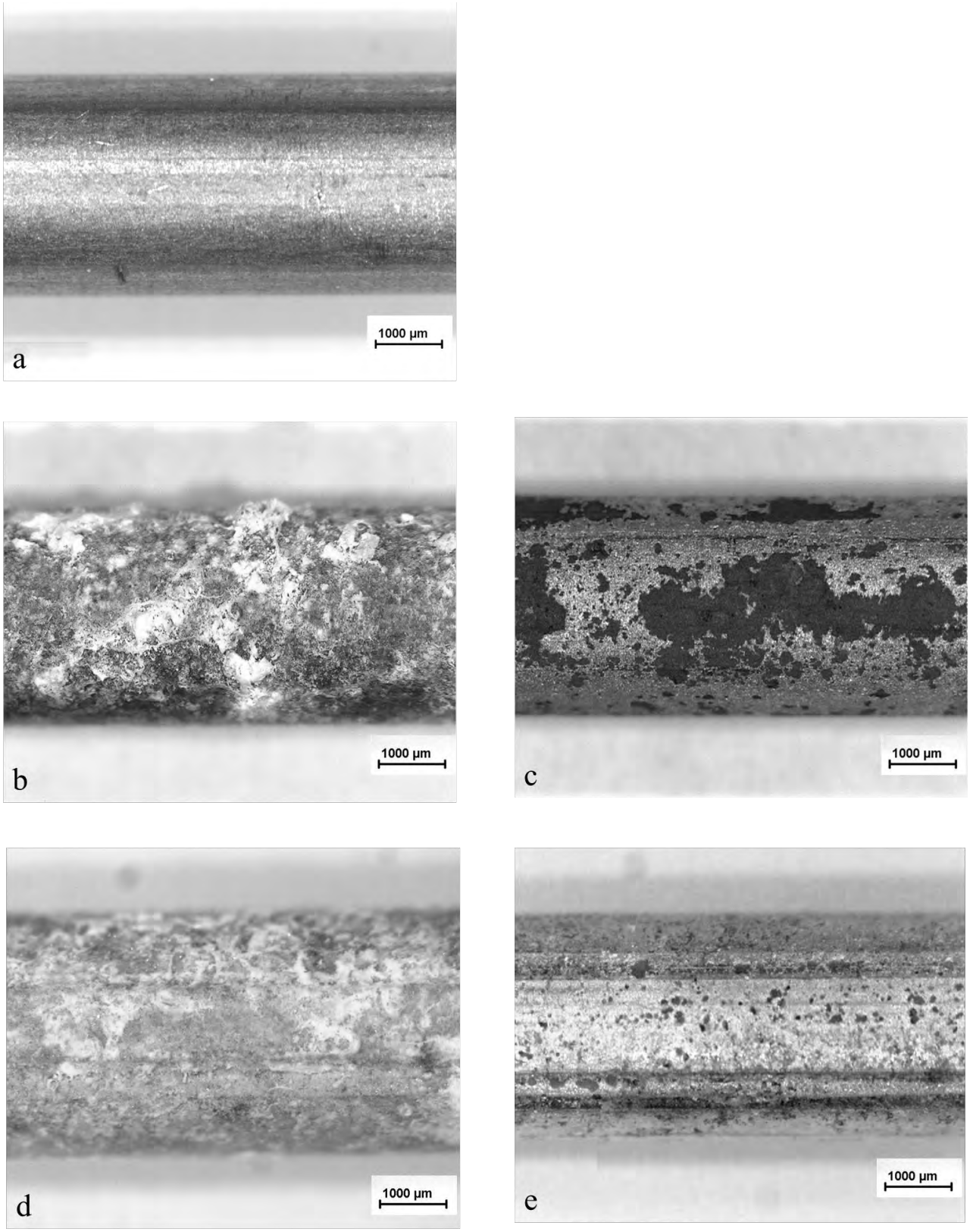


**Figure 6.2: Zn Class B (135g/m$^2$) wire specimen (a) prior to salt spray test exposure, (b) with corrosion products after ASTM B117 test , (c) corrosion products removed after ASTM B117 test, (d) with corrosion products after VW PV 1210 test, (e) corrosion products removed after VW PV 1210 test.**

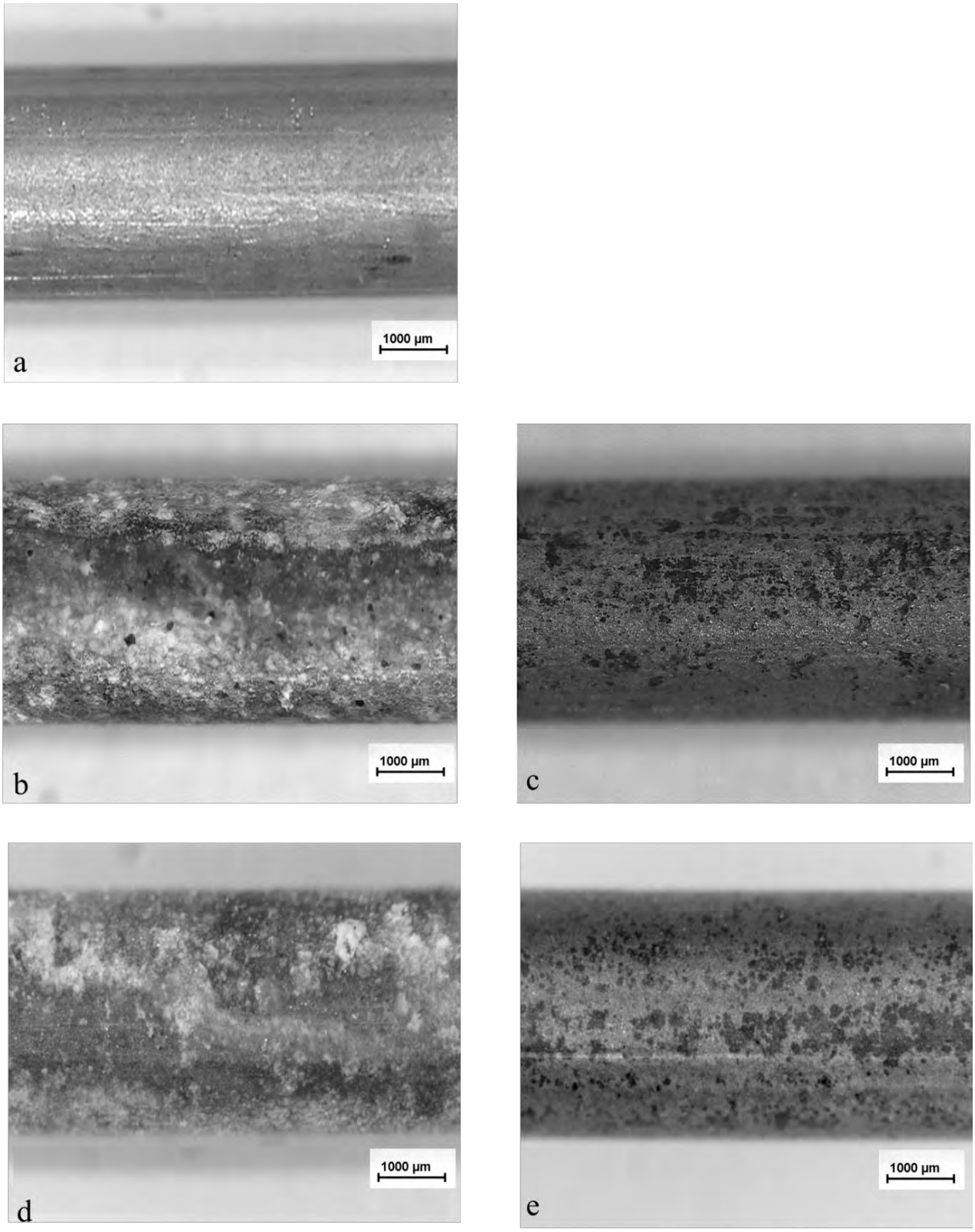


**Figure 6.3: Zn-5Al (150g/m$^2$) wire specimen (a) prior to salt spray test exposure, (b) with corrosion products after ASTM B117 test , (c) corrosion products removed after ASTM B117 test, (d) with corrosion products after VW PV 1210 test, (e) corrosion products removed after VW PV 1210 test.**

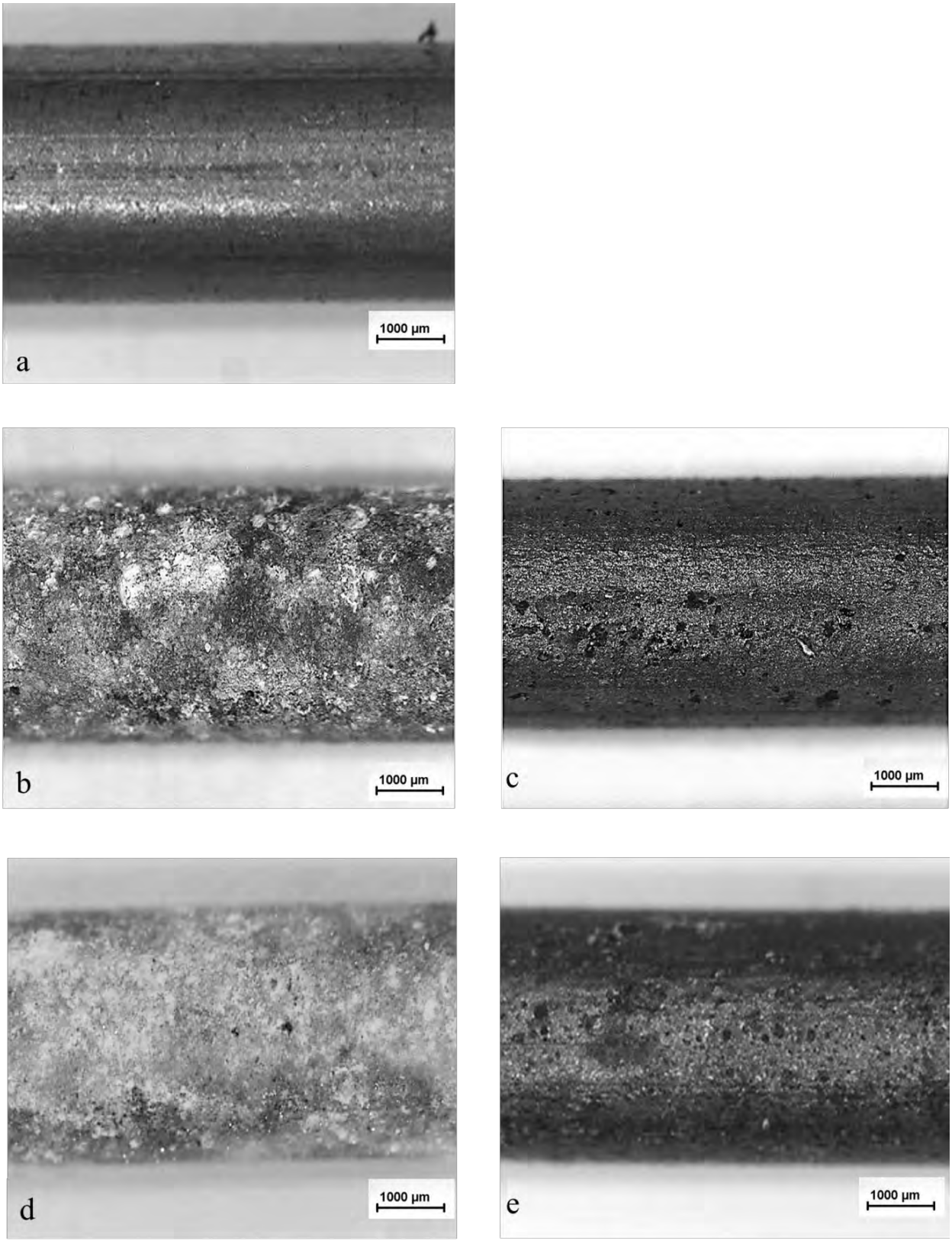


**Figure 6.4: Zn-5Al-xMg (150g/m$^2$) wire specimen (a) prior to salt spray test exposure, (b) with corrosion products after ASTM B117 test , (c) corrosion products removed after ASTM B117 test, (d) with corrosion products after VW PV 1210 test, (e) corrosion products removed after VW PV 1210 test.**

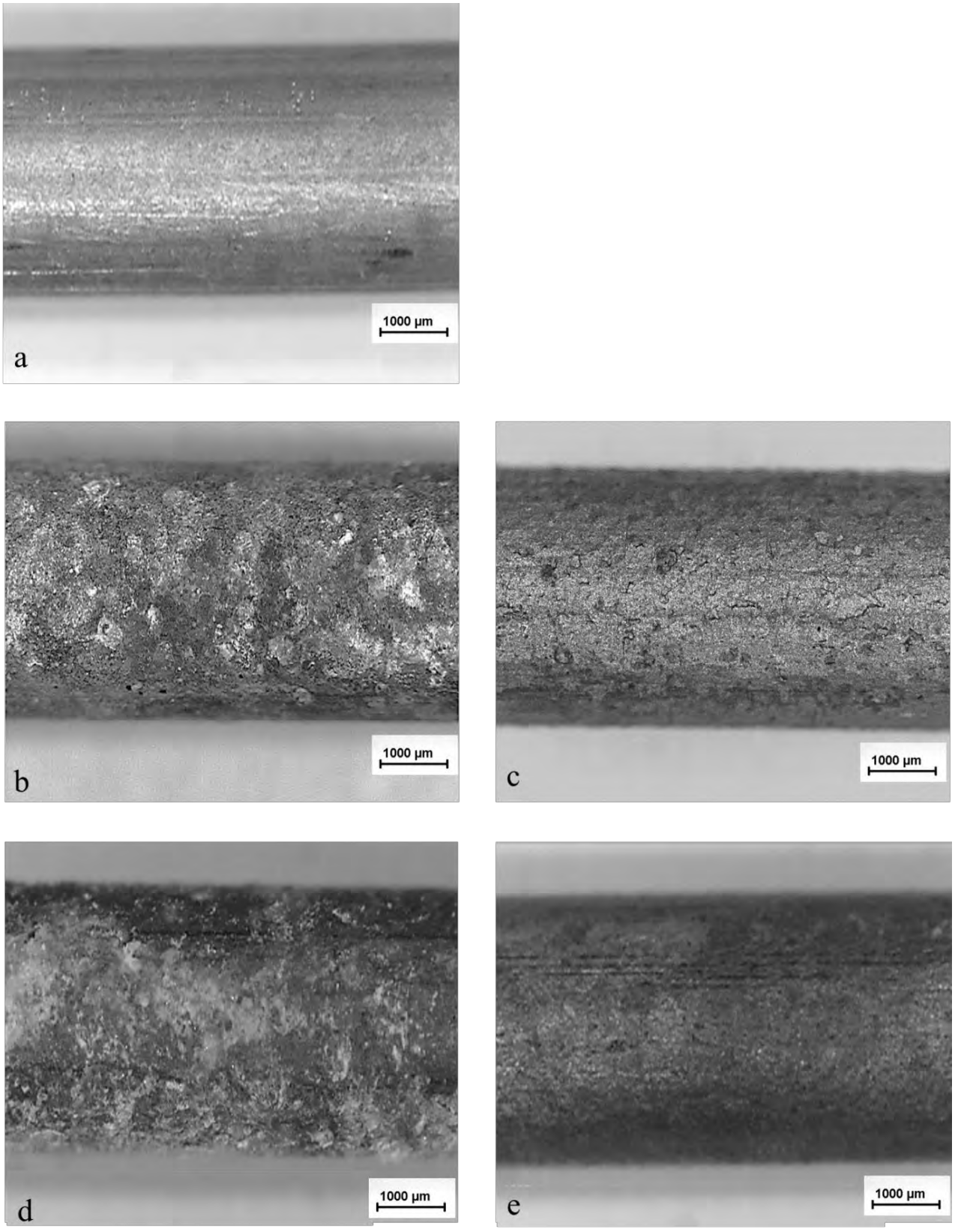


**Figure 6.5: Zn-10Al (300g/m$^2$) wire specimen (a) prior to salt spray test exposure, (b) with corrosion products after ASTM B117 test , (c) corrosion products removed after ASTM B117 test, (d) with corrosion products after VW PV 1210 test, (e) corrosion products removed after VW PV 1210 test.**

## 6.2 Low Magnification Examination of Cross Section through Coatings

Zn and Zn-Al alloy coated wires were prepared for light and electron microscopy by methods described in **Section 3.4.2**. Light micrographs revealing cross sections of wire coated with Zn and Zn-Al alloy coatings before and after the ASTM B117 test are shown in **Figures 6.6 – 6.11**. Light micrographs of specimens exposed to the VW PV 1210 test are not shown in this section because the mechanism by which the Zn and Zn-Al alloys coatings corrode will be similar in both tests. Results of the ASTM B117 have been presented since the highest corrosion rates were observed when specimens were exposed to this test in the study.

### 6.2.1 Examination of Zn Coated Wire

The process of corrosion left the Zn Class A (235 g/m$^2$) and Zn Class B (235 g/m$^2$) coatings highly pitted as can observed in **Figures 6.6(b)** and **6.7(b)** respectively. Pits arose due to localized corrosion taking place on the surface of the coatings [9]. In the case of the Zn Class B (135 g/m$^2$) coating, a pit is observed to have penetrated the coating layer thus exposing underlying steel. However the steel is not expected to corrode unless the area of steel exposed by the pit exceeds the area over which the electrochemical protective reaction can be maintained [15].

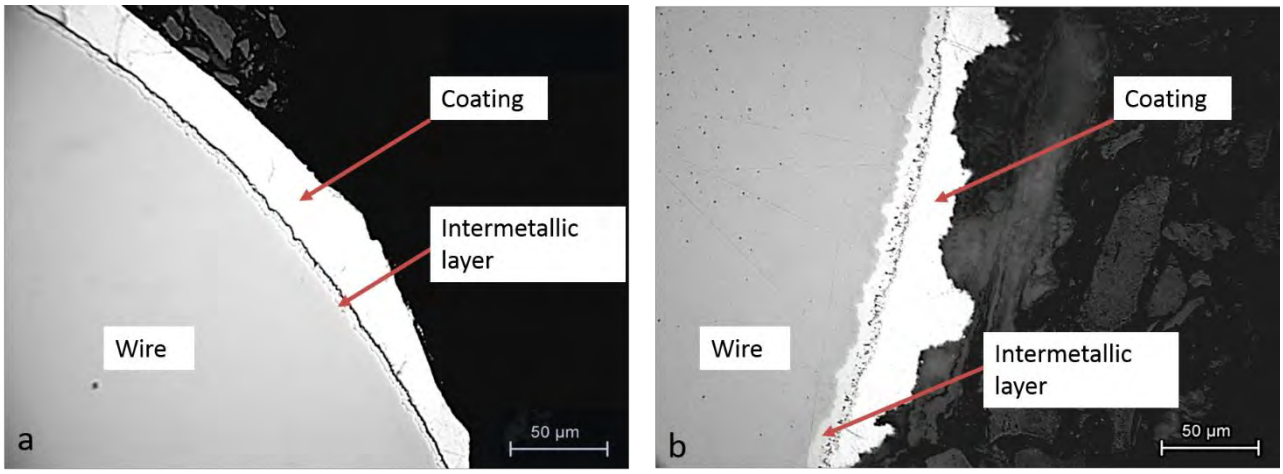


**Figure 6.6: Light micrograph revealing cross section through wire with Zn Class A (235g/m$^2$) coating before (a) and after (b) ASTM B117 test.**

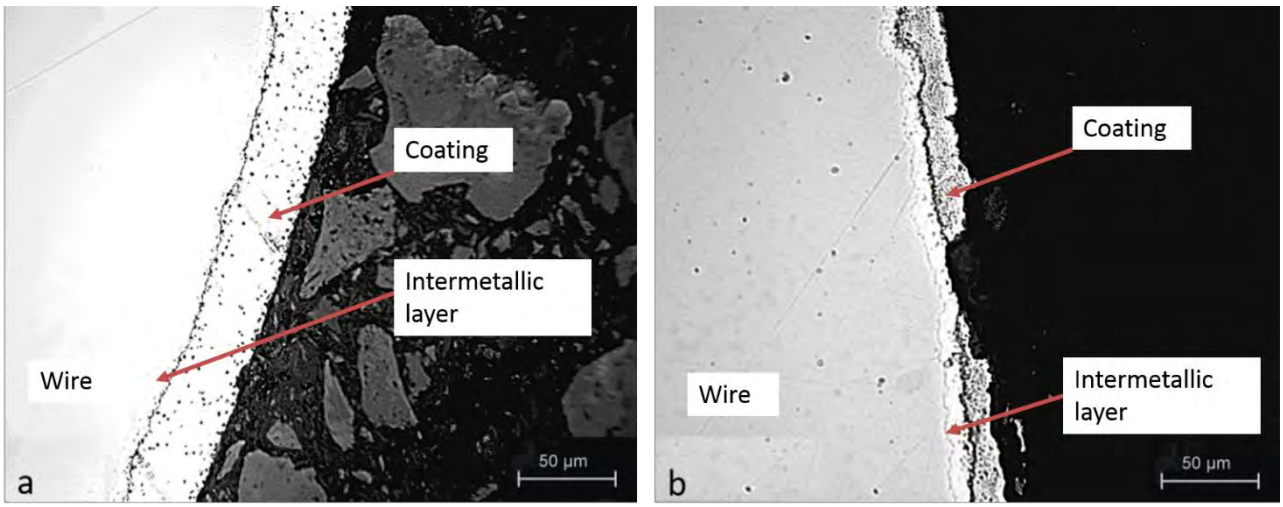


**Figure 6.7: Light micrograph revealing cross section through wire with Zn Class B (235g/m$^2$) coating before (a) and after (b) ASTM B117 test.**

### 6.2.2 Examination of Zn-Al Alloy Coated Wire

**Figures 6.8 – 6.10** show light micrographs of Zn-5Al (150 g/m$^2$), Zn-5Al-xMg (150 g/m$^2$) and Zn-10Al (300 g/m$^2$) coated wire respectively. All the Zn-Al alloy coatings displayed extensive crevices when observed after the exposure to the ASTM B117 test. Despite this extensive cracking, the coatings remained as continuous barrier layers shielding the underlying steel from the corrosive environment. This is in contrast to the Zn coatings that had numerous pits which in some cases exposed the underlying steel to the corrosive environment of the ASTM B117.

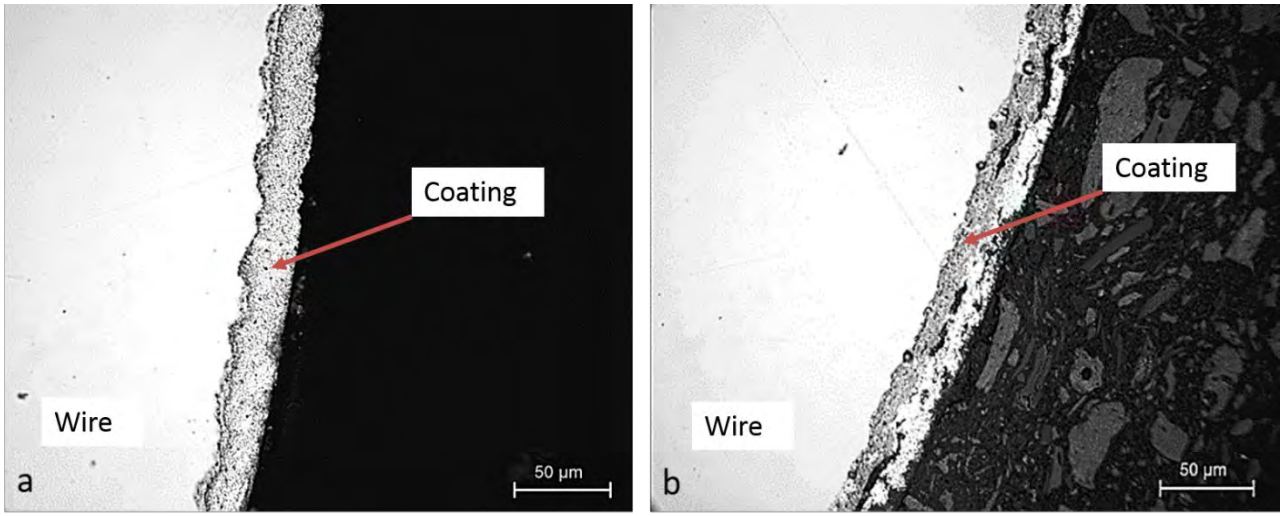


**Figure 6.8: Light micrograph revealing cross section through wire with Zn-5Al (150g/m$^2$) coating before (a) and after (b) ASTM B117 test.**

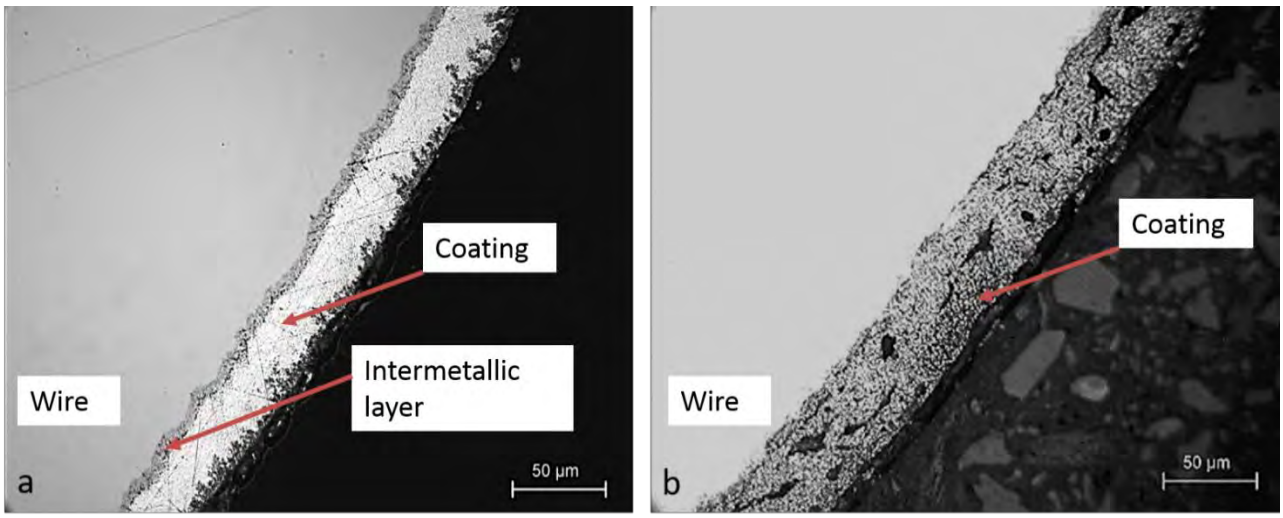


**Figure 6.9: Light micrograph revealing cross section through wire with Zn-5Al-xMg (150g/m$^2$) coating before (a) and after (b) ASTM B117 test.**

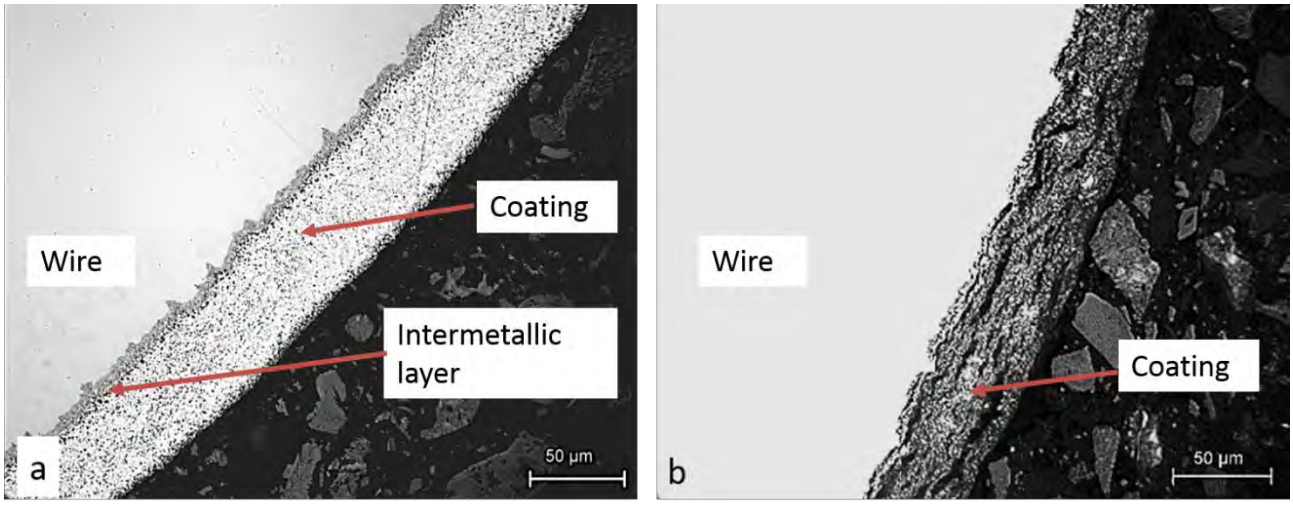


**Figure 6.10: Light micrograph revealing cross section through wire with Zn-10Al (300g/m$^2$) coating before (a) and after (b) ASTM B117 test.**

## 6.3 High Magnification Zn-Al Alloy Coating Microstructure Analysis

High magnification images of wire with the various Zn-Al alloy coatings exposed to both the ASTM B117 and VW PV 1210 tests were captured using a Nova NanoSEM 430 microscope in order to observe the microstructure of the coatings in detail. **Figures 6.11 – 6.13** show SEM (BSE) images for the Zn-5Al (150 g/m$^2$), Zn-5Al-xMg (150g/m$^2$) and Zn-10Al (300g/m$^2$) coatings revealing a two phase microstructure represented by light and dark regions within the coating. EDS was carried out in order to determine the relative composition of Zn and Al within these regions. Five dark regions and five light regions were randomly selected for EDS readings. EDS results, displayed adjacent to their respective coatings, revealed that the light regions had a greater composition of Zn relative to the dark regions. However, it must be noted that the overlapping interaction volumes of the two phases prevented acquisition of highly accurate EDS analysis results [55].

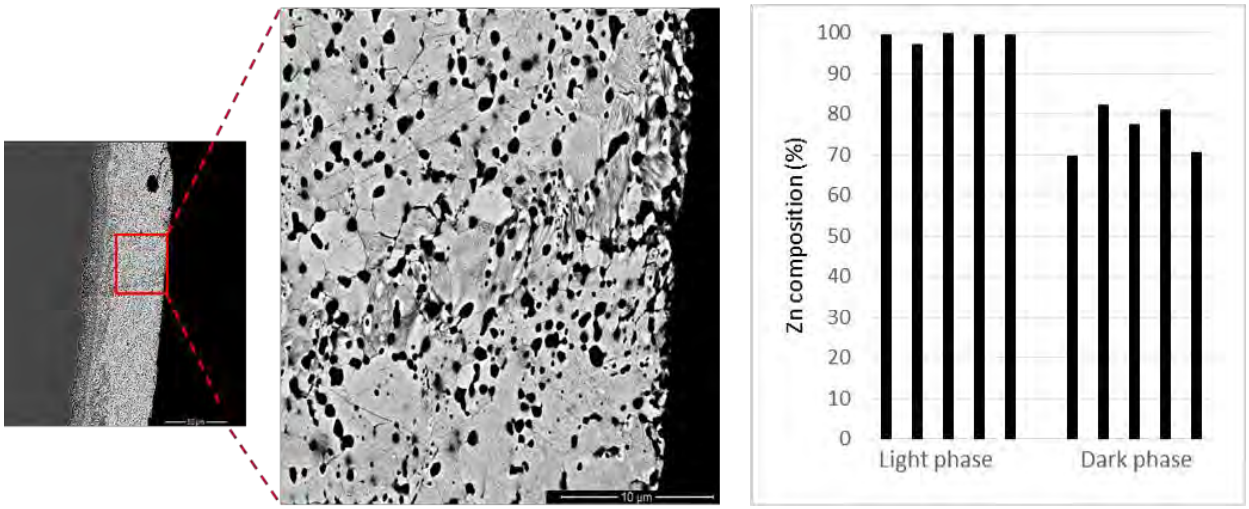


**Figure 6.11: SEM (BSE) image of cross section through Zn-5Al alloy coating revealing a two phase microstructure of light (higher Zn composition) and dark (lower Zn composition) regions.**

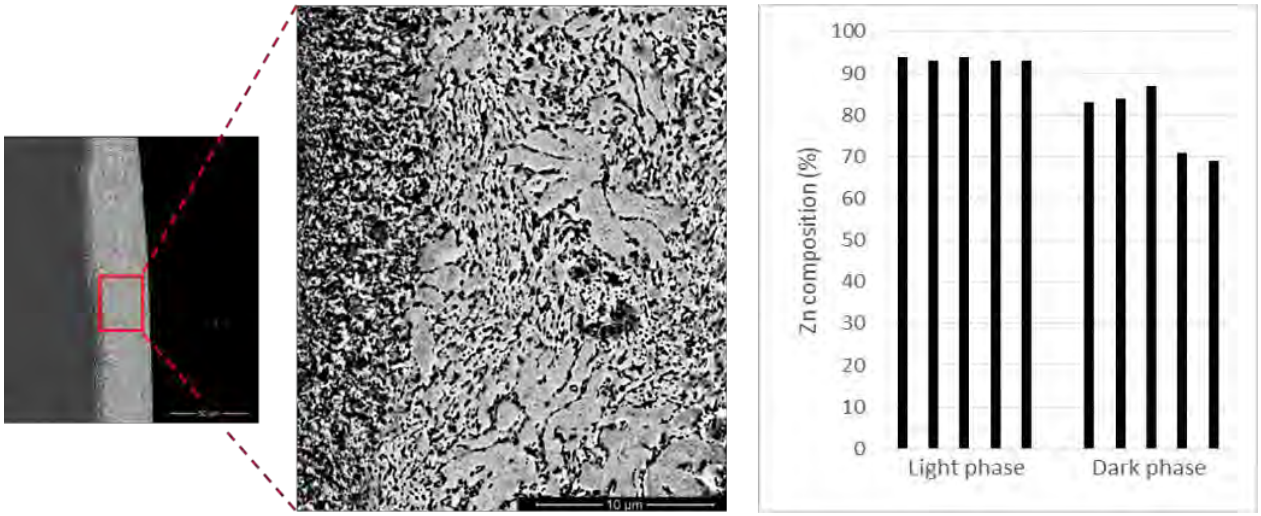


**Figure 6.12: SEM (BSE) image of cross section through Zn-5Al-xMg alloy coating revealing a two phase microstructure of light (higher Zn composition) and dark (lower Zn composition) regions.**

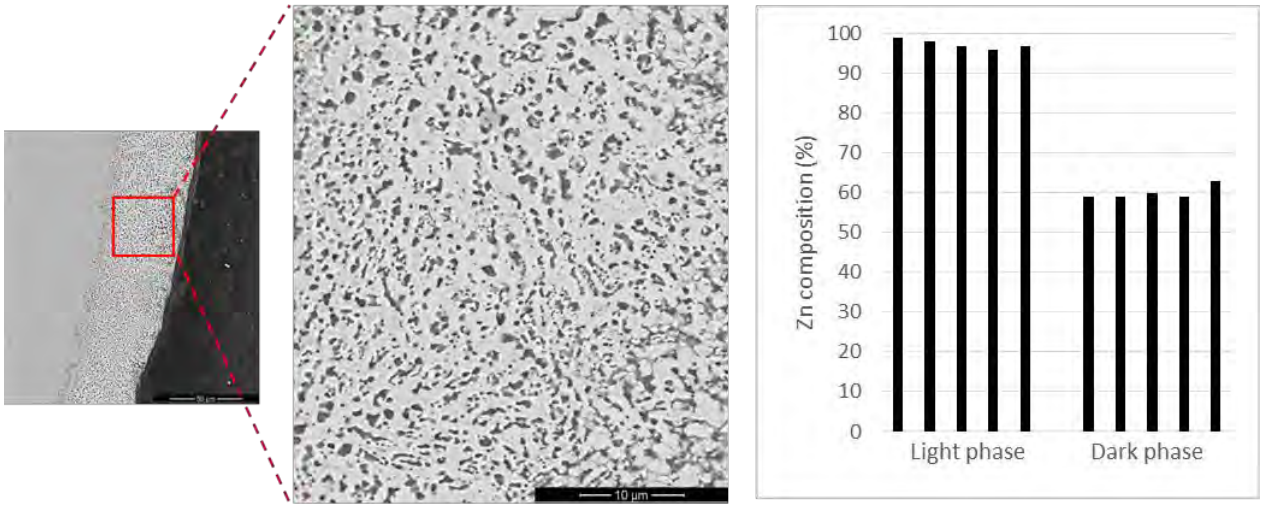


**Figure 6.13: SEM (BSE) image of cross section through Zn-10Al alloy coating revealing a two phase microstructure of light (higher Zn composition) and dark (lower Zn composition) regions.**

The light and dark regions in the Zn-5Al and Zn-5Al-xMg alloy coatings represent the Zn (η) phase and Zn-rich aluminium solid solution (β) phase respectively on the basis of the composition of Zn in these phases [18,58]. The lower composition of Zn in the dark phase in the Zn-10Al coating suggests that it is the Al-rich solution solid (α) phase. The Zn-5Al and Zn-Al-xMg alloy coatings do not exhibit the microstructure reported in literature characterized by dendritic (Zn) primary crystals in a fine pearlitic eutectic matrix [50]. The different morphology is probably a consequence of the cooling rate of the coating during solidification which is known to greatly influence microstructure of Zn-5Al alloys [17].

The high magnification images of the Zn-5Al, Zn-5Al-xMg and Zn-10Al coatings taken after the salt spray tests are shown in **Figures 6.14 – 6.16**. Corrosion products were observed within the coatings in all cases, thus supporting findings of a study on corrosion performance of hop dipped Zn based coatings in 3.5% NaCl solution using electrochemical impedance spectroscopy. The study revealed that the potential difference that exists between Zn (η) phase and the Zn-rich aluminium solid solution (β) phase of a Zn-5Al coating in 3.5% NaCl solution creates a micro-galvanic couple between the two phases. The Zn (η) phase had a lower negative free corrosion potential and thus corroded preferentially which led to the accumulation of corrosion products in these regions [50]. The cracking observed in the Zn-Al alloy coatings is probably due to the force of the internal corrosion products creating stress within the coating as these corrosion products expand.

The accumulation of corrosion products within the Zn-Al alloy coatings may also explain the negative corrosion rates observed for these coatings during the VW PV 1210, as reported in **Section 5.3.2**. Although corrosion was observed on the coatings when the coatings were examined, corrosion rates and cumulative coating mass loss values suggested that no corrosion activity had taken place. Washing the specimens after the test would have removed corrosion products on the surface of the coatings, but not corrosion products within the coatings. For this reason, calculating corrosion rates for Zn-Al alloy coatings on the basis of coating mass loss may not be very accurate.

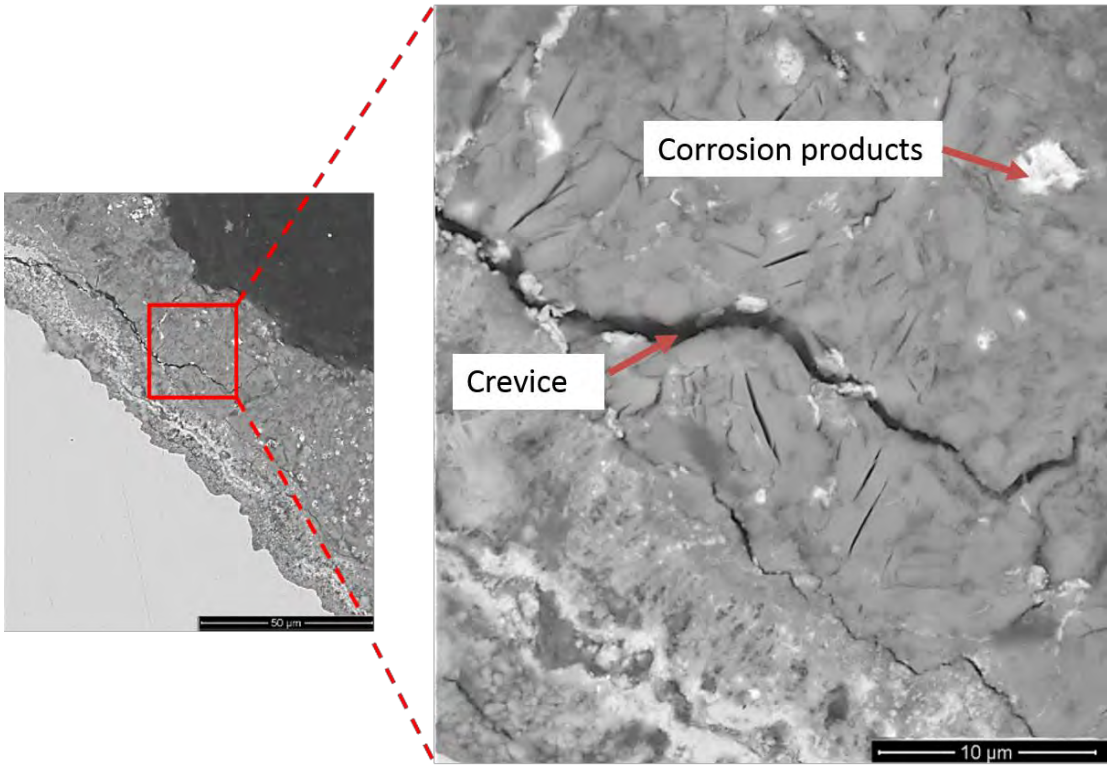


a)

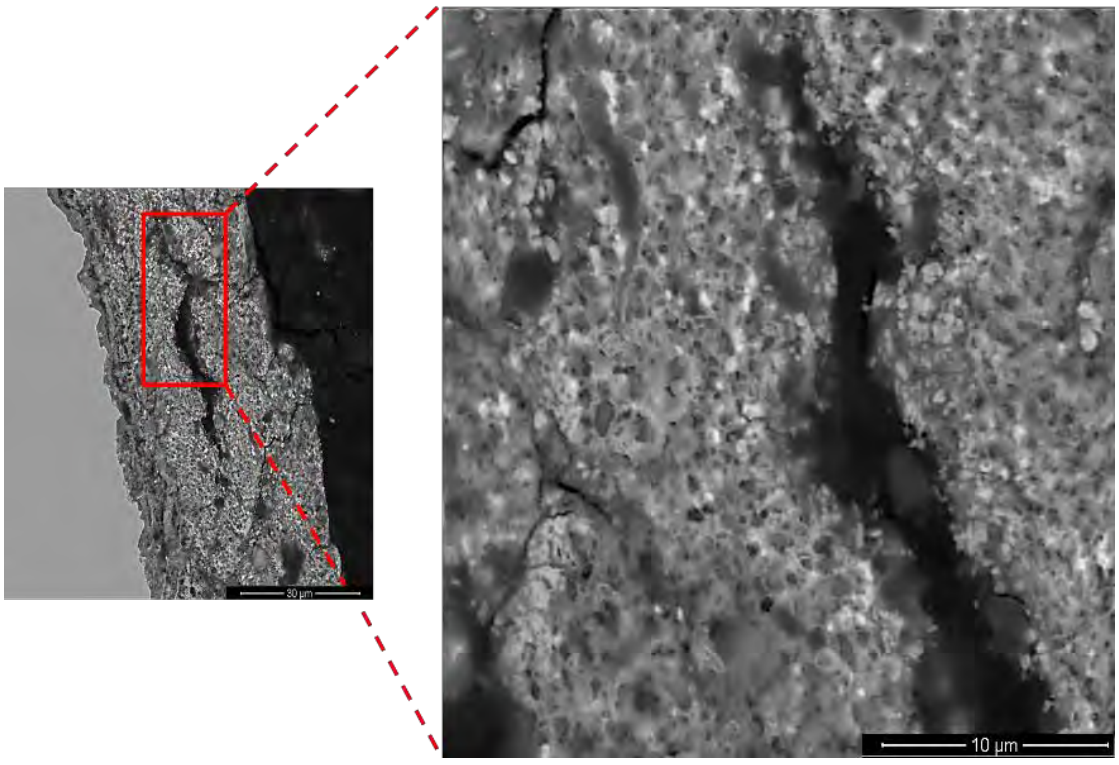


b)

**Figure 6.14: SEM (BSE) images revealing crevices and corrosion products within Zn-5Al (150 g/m$^2$) coating at the conclusion of; a) ASTM B117 test and b) VW PV 1210 test.**

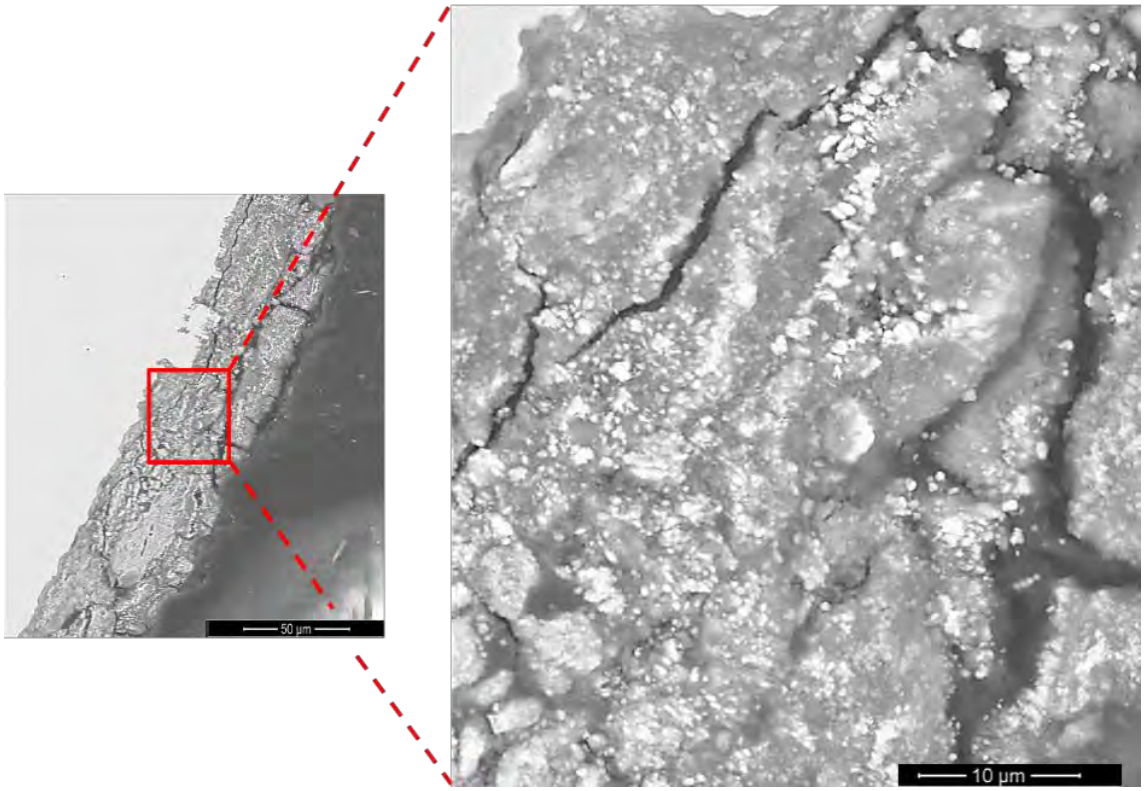


a)

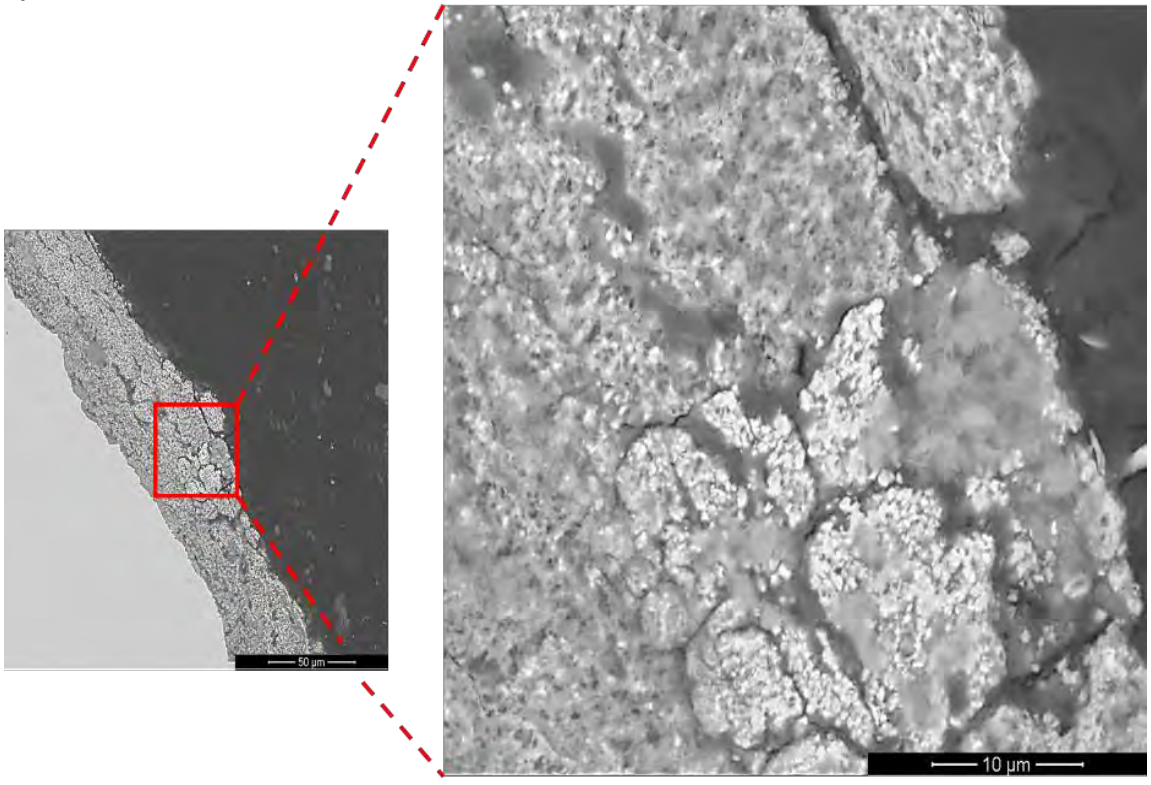


b)

**Figure 6.15: SEM (BSE) images revealing crevices and corrosion products within Zn-5Al-xMg (150 g/m$^2$) coating at the conclusion of; a) ASTM B117 test and b) VW PV 1210 test.**

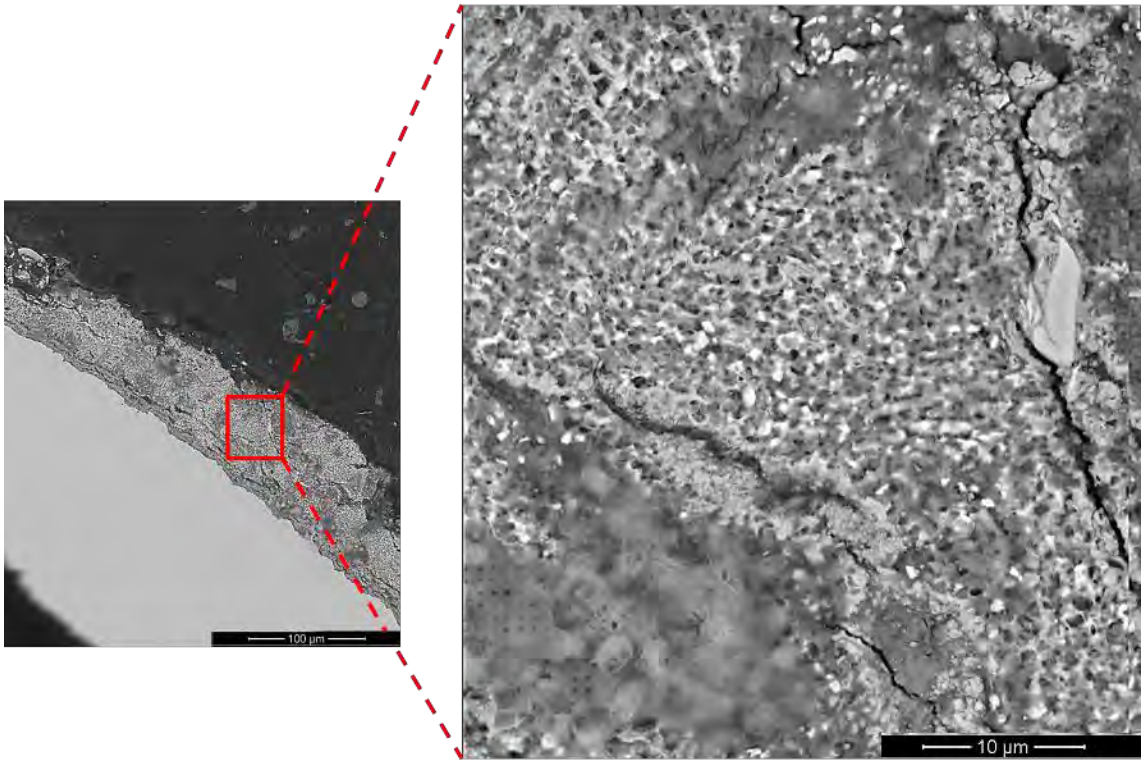


a)

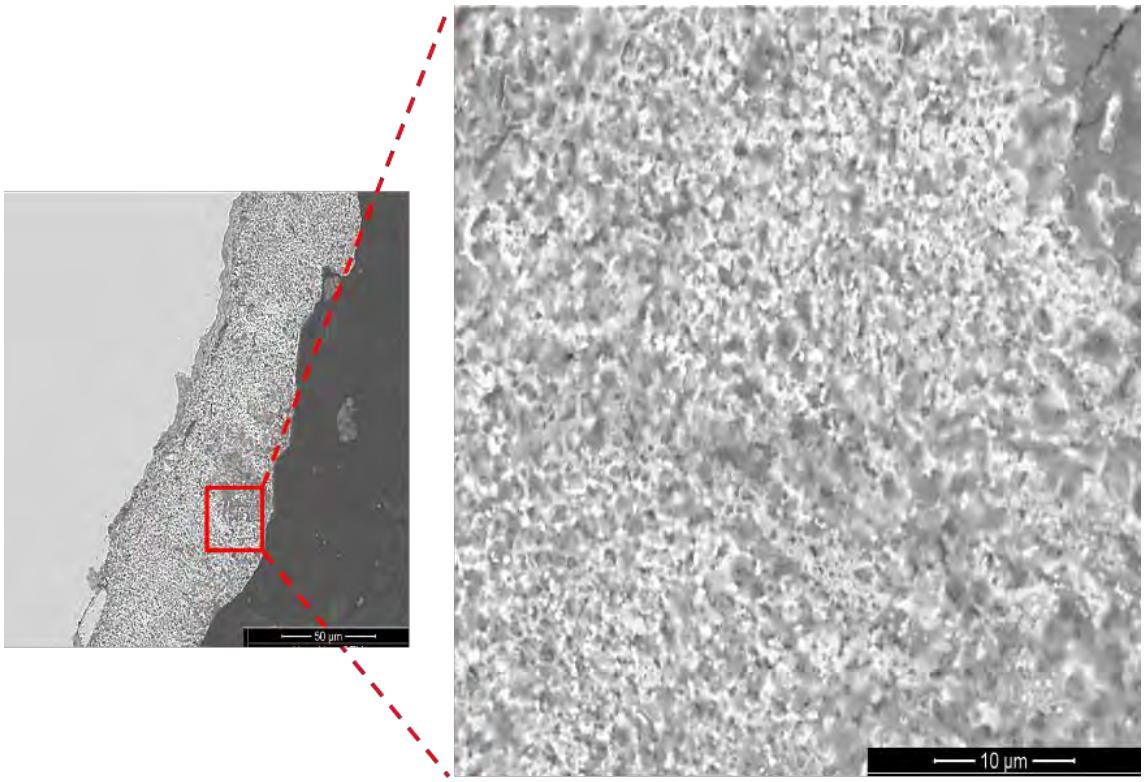


b)

**Figure 6.16: SEM (BSE) images revealing crevices and corrosion products within Zn-10Al (300 g/m$^2$) coating at the conclusion of; a) ASTM B117 test and b) VW PV 1210 test.**

# 7. Corrosion Performance of Wire in Bundle Configuration

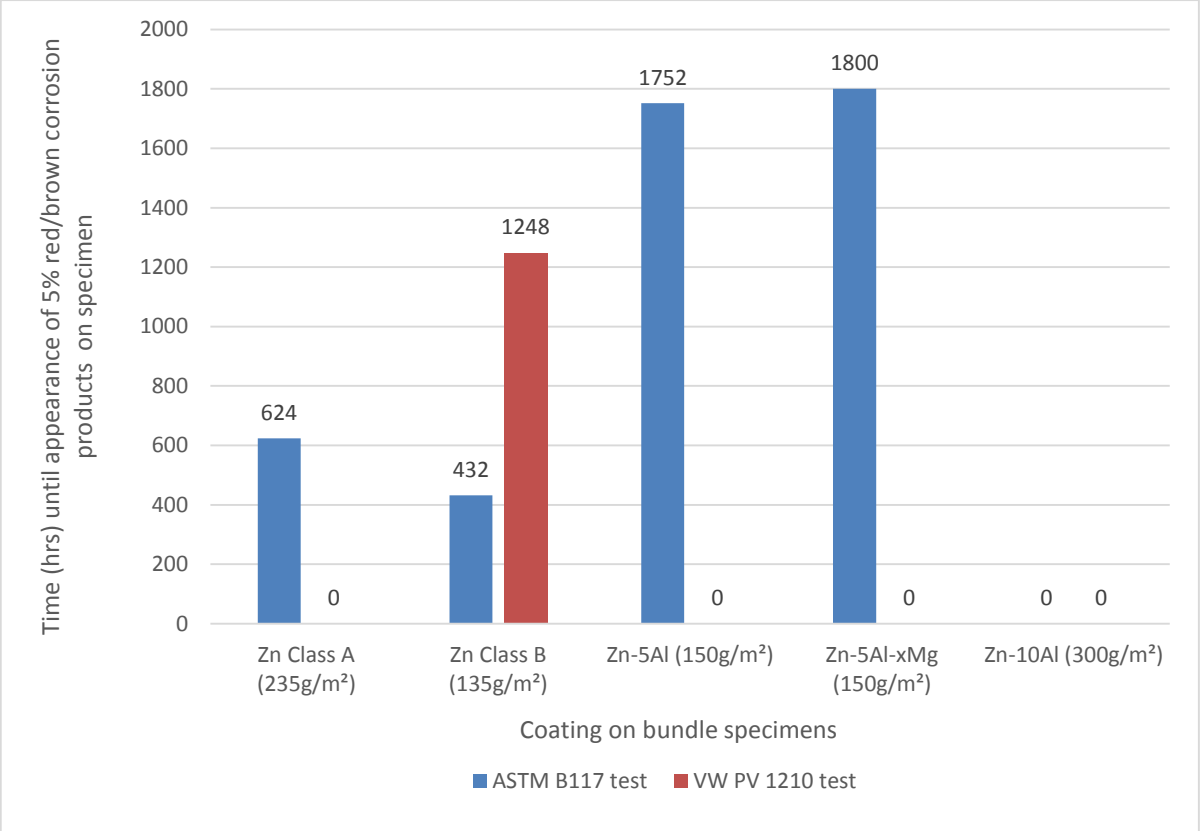


**Figure 7.1: Time taken for red/brown corrosion product appearance on 5% surface area of hot dip galvanized bundles during ASTM B117 and VW PV 1210 tests.**

**Figure 7.1** shows graphs representing the time elapsed until appearance of red/brown corrosion products on 5% surface area of bundle specimens during the ASTM B117 and VW PV 1210 salt spray tests. Each bundle comprised of 12 wires with either Zn Class A (235g/m²), Zn Class B (135g/m²), Zn-5Al (150g/m²), Zn-5Al-xMg (150g/m²) and Zn-10Al (300g/m²) hot dip coatings applied. The results show the superior corrosion performance of Zn-Al alloy coatings over Zn coatings in the salt spray tests. The presence of Al in the Zn-5Al (150g/m²), Zn-Al-xMg (150g/m²) and Zn-10Al (300g/m²) coatings led to improved barrier performance of corrosion products that form on the surface of the coatings [50].

Results of the ASTM B117 test show that there was no significant difference in the performance of the Zn-5Al (150g/m²) coating relative to the Zn-5Al-xMg (150g/m²) as red/brown corrosion products were observed on 5% surface area of the bundles after 1,752hrs and 1,800hrs respectively. However, the Zn-10Al (300g/m²) coating outperformed these coatings as red/brown corrosion products did not cover a 5% surface area of the bundles during the ASTM B117 test. This was due to the higher content of Al in the coating and the greater coating mass distribution of the coating. The greater coating mass distribution of the Zn Class A (235g/m²) coating also explains its improved corrosion performance over the Zn Class B (135g/m²) coating in the ASTM B117.

Red/brown corrosion products were primarily observed on specimens exposed to the ASTM B117 test. The only specimen to exhibit red/brown corrosion products on at least 5% of its surface area during the VW PV 1210 test was the Zn Class B (135g/$m^2$) coated bundle. A comparison of the difference in aggressiveness of the ASTM B117 test and the VW PV 1210 test may be made by comparing results of Zn Class B (135g/$m^2$) coated bundle. Red/brown corrosion products were observed on 5% specimen surface area after 432hrs and 1,248hrs in the ASTM B117 test and VW PV 1210 test respectively. Continuous specimen exposure to salt mist throughout the ASTM B117 created a harsher environment for specimens relative to the cyclic VW PV 1210 test where specimens were not continuously exposed to salt mist.

Although the bundles are composed of individual wires, the corrosion activity of the bundles was greater than that observed for the individual wire specimens. This is from the perspective of the appearance of red/brown corrosion products on the surface of the specimens during the salt spray tests. While no red/brown corrosion products were observed on individual wire specimens during both the ASTM B117 and VW PV 1210 tests, these corrosion products were observed on the bundles, and in some cases they covered more than 5% of surface area of bundle specimens as summarized in **Figure 7.1**.

The close proximity of wires that constitute the bundles exposes the bundles to crevice corrosion activity at the valleys that exist between adjacent wires. Crevice corrosion activity led to a greater dissolution of the protective hot dip coatings in the bundles relative to the individual wire specimens.

# 8. Results of Chapman's Peak Drive Environmental Exposure Test

Specimens suspended from Catch Fences 2, 23C and 38 along Chapman's Peak Drive were removed after 16 months and taken to the laboratory for inspection. All specimens installed at the catch fences at the beginning of the test were retrieved apart from the 22mm diameter rope coated with Zn-5Al as it could not be located when the specimens were collected from Catch Fence 38. The area surrounding Catch Fence 38 was searched but the specimen was not found.

**Figure 9.1** shows the appearance of specimens installed at Catch Fence 2 after the 16-month environmental exposure test. Rope and bundle specimens coated with various Zn-Al alloy coatings had minimal white corrosion products on their surface relative to specimens with Zn coatings. The 22 mm diameter rope coated with Zn exhibited red/brown corrosion products representative of corrosion of the underlying steel. Zn and Zn-5Al coated rope specimens installed at Catch Fence 23C displayed less corrosion products, as shown in **Figure 9.2**, than specimens installed at Catch Fence 2. However, specimens installed at Catch Fence 38 had more corrosion products on their surface than specimens installed at Catch Fences 2 and 23C based on the appearance of specimens in **Figure 9.3**.

It is clear from the results that Zn-Al coatings are more effective at protecting steel from corrosion attack. A similar conclusion was reached after exposing rope, bundle and wire specimens to ASTM B117 and VW PV 1210 salt spray tests in the laboratory. Results also show that local environmental conditions affect corrosion performance [26]. Although Catch Fences 2, 23C and 38 are found within 8km of each other along Chapman's Peak Drive there was a difference in appearance of the specimens installed at these catch fences when examined at the end of the environmental exposure period. Specimens installed at Catch Fence 38 exhibited the greatest corrosion damage, while specimens installed at Catch Fence 23C displayed minimal corrosion damage. The local environment at each catch fence is different, as described in **Section 3.5.3**. Catch Fence 23C is exposed to weather elements, meaning that there is no shelter from rain water or direct sunlight. Exposure to direct sunlight leads to an evaporation of moisture on the specimens that is required for corrosion to occur [26]. The location of Catch Fence 38 between a crevice in the mountain with a nearby water channel presents a damp environment where corrosion of the specimens is promoted. Catch Fence 2 is at the base of mountain where specimens are constantly shielded from weather elements, therefore moderate corrosion activity would be expected.

A main objective of carrying out the environmental exposure tests was to determine whether the accelerated laboratory corrosion tests were able to successfully determine the same ranking of the various coatings as is expected to occur during environmental exposure. Results of both the environmental exposure tests along Chapman's Peak Drive and ASTM B1117 and VW PV 1210 tests show that Zn-Al alloy coatings outperform Zn coatings. However, a relative ranking of corrosion performance of amongst the Zn-Al alloy coatings could not be made during the 16 month period during which the environmental test was carried out. A much longer exposure period would have been required in order to allow for distinctions in coating performance of the Zn-Al coatings to be observed.

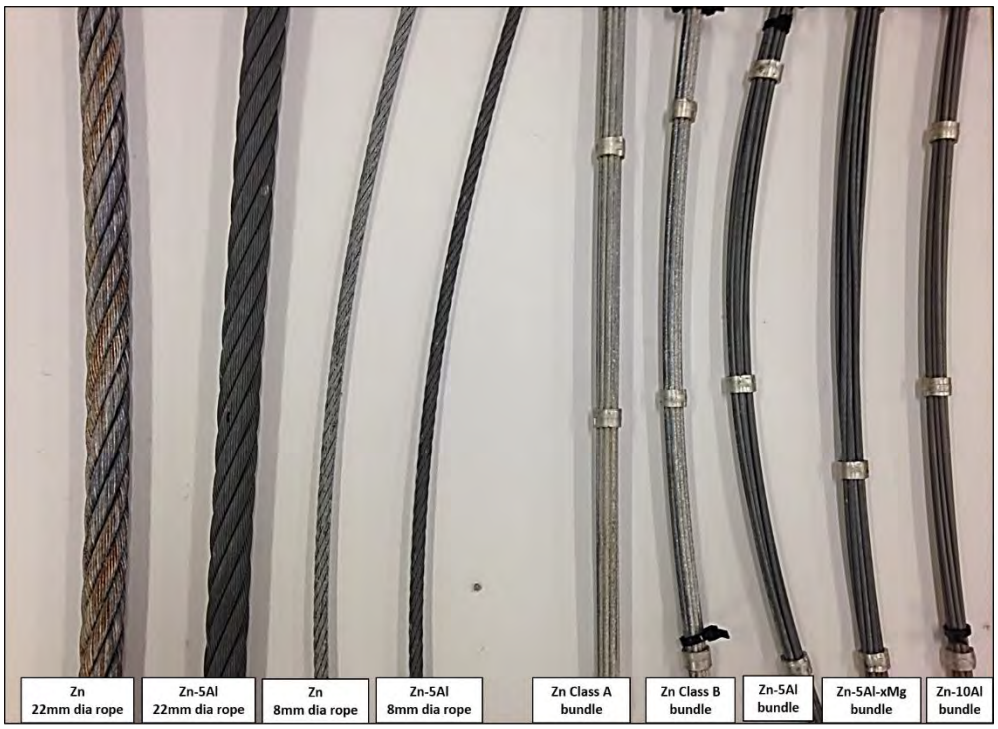


**Figure 9.1: Appearance of specimens installed on Catch Fence 2 after 16 month environmental exposure test along Chapman's Peak Drive.**


**Figure 9.2: Appearance of specimens installed on Catch Fence 23C after 16 month environmental exposure test along Chapman's Peak Drive.**

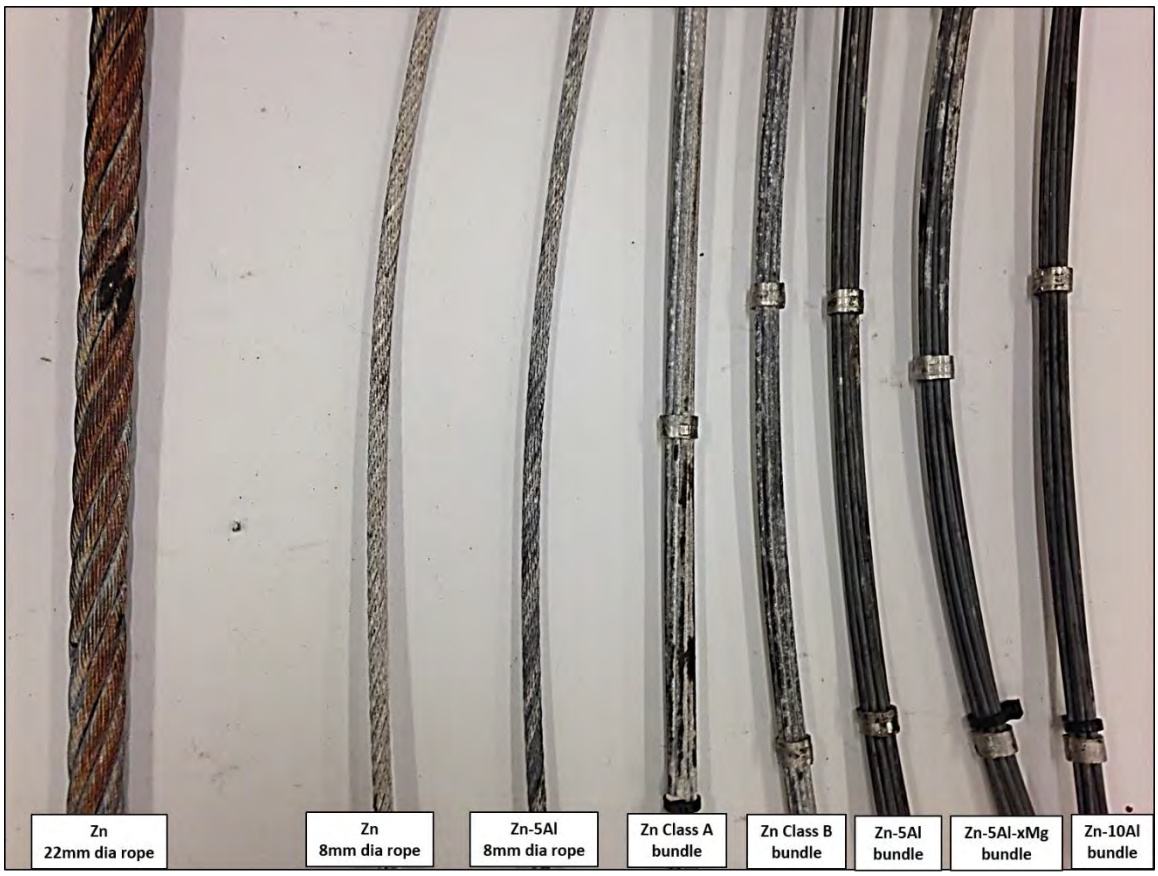


**Figure 9.3: Appearance of specimens installed on Catch Fence 38 after 16 month environmental exposure test along Chapman's Peak Drive.**

# 9. Summary and Conclusions

Salt spray tests present a controlled and reproducible method of evaluating corrosion performance of coatings in the laboratory [6]. This shortens the testing time, and subsequent expense associated with performance assessment of potential coating materials in harsh environments. Salt spray tests also provide an excellent tool for developing new coatings prior to actual environmental exposure and subsequent application [6,47,48].

The ASTM B117 and VW PV 1210 tests carried out in this study exposed specimens to harsh and moderate corrosion environments respectively. Results of the study presented in **Figures 4.1-4.7** and **5.1-5.14** show that Zn-Al alloy hot dip coatings provide steel with improved corrosion protection over Zn hot dip coatings. Eh-pH diagrams of Zn and Al reveal that in the neutral pH range ($6.5 < pH < 7.5$) Zn corrodes to form soluble products, comprising of $Zn^{2+}$ ions, while the corrosion of Al results in the formation of an inert $Al_2O_3$ oxide layer that provides the underlying steel with a better secondary barrier.

Test specimens exhibited better corrosion performance in the VW PV 1210 test relative to the ASTM B117 test as illustrated lower corrosion rates and cumulative mass loss results shown in **Figures 5.1-5.14**. This is due to the fact that in the less aggressive test (VW PV 1210 test), conditions were ideal for the development of a coherent passive layer, whereas in the ASTM B117 specimens were constantly exposed to a salt mist.

Environmental exposure tests allow the corrosion performance of coatings may be determined in the actual environment in which they will be used. The major drawback with these tests is that they are time consuming and thus not always practical to perform. Although the environmental exposure test in this study was carried out over 16months, a short period of time for tests of this nature, results still revealed that Zn-Al alloy coatings outperform Zn coatings on steel wire.

The following conclusions were drawn based on the results of this study:

1. Zn-Al alloy hot dip coatings provide steel with improved corrosion protection over Zn hot dip coatings in neutral pH environments. This conclusion is supported by qualitative results showing a faster development of red/brown corrosion products on the surface of Zn coated rope specimens relative to Zn-Al alloy coated rope, as described in **chapter 4** of this report. Quantitative results showing higher corrosion rates and cumulative mass loss of Zn coatings over Zn-Al alloy coatings on individual wire specimens, described in **chapter 5,** present further evidence of the superior corrosion performance of Zn-Al alloy coatings in comparison to Zn coatings**.**

2. On the basis of corrosion rates of individual wire specimens exposed to the ASTM B117 test, a ranking of corrosion performance amongst Zn-Al alloy coatings is as follows:
   Zn-10Al ($300g/m^2$) > Zn-5Al-xMg ($150g/m^2$) > Zn-5Al ($150g/m^2$)
   The Zn-10Al ($300g/m^2$) coating outperformed the Zn-5Al ($150g/m^2$) and Zn-5Al-xMg ($150g/m^2$) coatings owing to the higher Al content in the alloy. The presence of Mg in Zn-

5Al-xMg (150g/$m^2$) is responsible for its improved corrosion performance over Zn-5Al (150g/$m^2$).

3. The coating mass distribution of a coating has an impact on its service lifespan. Therefore, the thicker Zn Class A (235g/$m^2$) coating is expected to have a longer service lifespan relative to the thinner Zn Class B (135g/$m^2$) coating. Similarly, the Zn-10Al (300g/$m^2$) coating is predicted to have a longer service lifespan compared to the Zn-5Al-xMg (150g/$m^2$) and Zn-5Al (150g/$m^2$) coatings.

4. SEM micrographs showed that Zn-Al alloy coatings exhibit a two phase microstructure. On the basis of EDS analysis, the phases were identified as the Zn (η) phase and Zn-rich aluminium solid solution (β) phase. The Zn (η) phase has a lower negative free corrosion potential and will corrode preferentially. Corrosion products forming within Zn-Al coatings expand creating stress that leads to development of cracks within the coating.

5. The form of the steel material plays an impact on corrosion activity. A qualitative examination of corrosion products on specimens exposed to salt spray tests revealed that corrosion was most prolific in rope, followed by bundles and wires. Numerous crevices exist within the rope and bundle specimens which promote crevice corrosion.

6. The ASTM B1117 and VW PV 1210 salt spray tests presented a quick, reproducible and cost effective way of carrying out qualitative corrosion performance comparisons of coatings in the laboratory. However, findings from salt spray tests may not be used to accurately predict the service lifespan of coatings since there are many variables apart from weather conditions, such as mechanical wear, that impact coating service lifespan.

7. Although environmental exposure tests were all carried out along Chapman's Peak Drive the condition of the specimens varied based on the microclimatic conditions at the catch fences where specimens were installed. This highlighted the complexity of investigating corrosion performance in the environment.

8. Both the environmental exposure tests carried out along Chapman's Peak Drive and the ASTM B117 and VW PV 1210 salt spray tests show that Zn-Al alloy coatings outperform Zn coatings. However, unlike with the salt spray tests, a relative ranking of corrosion performance amongst the Zn-Al alloy coatings could not be determined from the 16 month environmental exposure test.

# 10. Recommendations

### Coating Mass Uniformity

The Zn and Zn-Al alloy coated wire specimens used in this study exhibited various coating thicknesses which made it difficult for firm conclusions on corrosion performance of the various coatings to be reached. Coating thickness is known to play a significant role on the expected lifespan of a coating. Therefore, the strength of an investigation of corrosion performance of Zn and Zn-Al alloy coatings may be increased by using coatings of identical thicknesses.

### Use of Electrochemical Tests to Investigate Corrosion Performance

A limited number of test specimens prevented electrochemical tests including electrochemical impedance spectroscopy (EIS) or measurement of galvanic potentials from being performed. Such tests may have provided may have given further evidence in support of results observed during the salts spray tests, and they could have also shed light on the corrosion mechanisms at play in the various Zn and Zn-Al alloy coatings.

### Impact of Cooling Rate on Microstructure of Zn-Al Alloy Coatings

This study had a large focus on how the composition of Zn-Al alloy coatings affects corrosion performance. However, corrosion performance of Zn-Al alloy coatings is also influenced by microstructural evolution during coating solidification. The impact of fast cooling and slow cooling of Zn-Al coatings during solidification on corrosion performance could also be investigated, similar to what was done in a study by Sugimaru et al. Sugimaru et al's investigation showed how slow cooling or air cooling led to development of a microstructure that was more resistant to corrosion in comparison to when the coating was water cooled during solidification [42].

### Characterization of Corrosion Products

A study on the characterization of corrosion products formed during the corrosion of Zn and Zn-Al alloy coatings could be performed using Raman microscopy and X-Ray diffraction (XRD). Chemical characterization of corrosion products, and developing an understanding of their formation mechanisms, are important factors in the development and improvement of protective metallic coatings [59].

# 11. Bibliography


1. Hard Assets Investor. Industrial metals. http://www.hardassetsinvestor.com/hard-assets-university/20-hard-assets-202-a-deeper-look-at-individual-commodities/548-industrial-metals.html?Itemid=4. Updated 2012. Accessed August 16, 2013.

2. World Steel Association. Crude steel production - december 2012. http://www.worldsteel.org/dms/internetDocumentList/statistics-archive/production-archive/steel-archive/Crude-steel-production-December-2013/document/Crude%20steel%20production%20December%202012.pdf. Updated 2012.

3. Askeland DR. *The science and engineering of materials.* 3rd ed. Boston: PWS Publishing Company; 1994.

4. ASM International. The effects and economic impact of corrosion. . 2000.

5. Fontana MG. *Corrosion engineering.* Third ed. Singapore: McGraw-Hill Book Company; 1987:556.

6. Simbi D. Corrections to MSc dissertation: Evaluation of corrosion behaviour of hot dip zn and zn-al alloys coatings on steel wire using field and laboratory tests. . 2014.

7. Chandler KA, Bayliss DA. *Corrosion protection of steel structures.* New York: Elsevier and Apllied Sciences; 1985:394.

8. *Ferrous wire handbook.* Connecticut, USA: The Wire Association International, Inc; 2008:1162.

9. Ailor WH, ed. *Atmospheric corrosion.* First ed. New York, USA: Wiley-Interscience; 1982.

10. Trethewey KR, Chamberlain J. *Corrosion for science and engineering.* 2nd ed. Harlow, Essex: Longman; 1995.

11. Tevera T. *The assessment of corrosion behaviour of zinc coated steel wire using a salt spray chamber.* [Bachelor of Science (Honours)]. University of Cape Town, South Africa; 2010.

12. Corrosion School. *Design and protection of corrosion prone plant.* Sandton: South African Corrosion Institute; 1984.

13. Schweitzer PA. *Corrosion and corssoion protection handbook.* New York: Marcel Dekker, Inc; 1983.

14. Honeycombe RWK. *Steels MIcrostructure and properties.* First Edition ed. London: Edward Arnold; 1981:244.

15. Gabe DR. *Coatings for protection.* London: Institute of Production Engineers; 1983.

16. Baboian R, ed. *Corrosion tests and standards, application and intepretation.* First ed. Fredericks, VA: American Society for Testing and Materials (ASTM); 1995.

17. Shrier LL, Jarman JA, Burstein GT. *Corrosion. volume 1.* 3rd ed. Oxford, England: Butterworth Heinemann.

18. Marder AR. The metallurgy of zinc-coated steel. *Progress in Materials Science*. 2000;45(3):191-271.

19. European Standards. DIN EN 10244-2, 2001 "non-ferrous metallic coatings on steel wire". . 2001.

20. Wirerope Works I. Bethlehem wire rope. . 2010.

21. Kalpakjian S. *Manufacturing engineering and technology.* 6th ed. New York: Prentice Hall; 2010.

22. Secretary of state's guidance for hot dip galvanizing processes. . 2004.

23. O'Donnell AJ. *An evaluation of the sacrificial protection afforded by continous galvanized coatings.* [DPhil (Metallurgy)]. University of Pretoria, South Africa; 1990.

24. Goodwin FE, Wright RN. The process metallurgy of zinc coated steel wire and galfan bath management. . 2001:135-139.

25. Zervoudis J, Anderson G. A review of bath alloy additives and their impact on the quality of the galvanized coating. .

26. Marder AR, Jordan CE. <br /> Fe-zn phase formation in interstitial-free steels hot-dip galvanized at 450°C: Part I 0.00 wt% al-zn baths. *Journal of Materials Science*. 1997;32(21):5593-5602.

27. Santana JJ, Fernandez-Perez BM, Morales J, Vasconelos HC, Souto RM, Gonzalez S. Characterization of the corrosion products formed on zinc in archipelagic subtropical environments<br /><br />Int. J. electrochem. sci., 7 (2012) 12730 - 12741. *International Journal of Electrochemical Science*. 2012;7:12730-12730 - 12741.

28. Al-Hinai AT, Al-Hinai MH, Dutta J. Application of eh-pH diagram for room temperature precipitation of zinc stannate microcubes in an aqueous media. *Materials Research Bulletin*. 2014;49:645-645-650.

29. Takeno N. <br />Atlas of eh-pH diagrams: Intercomparison of thermodynamic databases. . 2005;419.

30. Standards Australia. AS NZS 4534-2006 zinc and zinc aluminium-alloy coatings on steel wire. . 2006.

31. Elvins J, Spittle JA, Worsely DA. Microstructural changes in zinc aluminium alloy galvanising as a function of processing parameters and their influence on corrosion. *Corrosion Science*. 2005;47(11):2740-2759.

32. Yan L. Corrosion behaviour of hot dip zinc and zinc-aluminium coatings on steel in seawater. *Bulletin of Materials Science*. 2001;24(4):355-360.

33. Rosalbino F, Angelini E, Maccio D, Saccone A, Delfino S. Influence of rare earths additions on the corrosion behaviour of Zn–5Al (galfan) alloy in neutral aerated sodium sulphate solution. *Electrochimica Acta*. 2007;52(24):7107-7114.

34. Skoko Z, Popovic S, Stefanic G. Microstructure of Al–Zn and Zn–Al alloys. *Croatica Chemica Acta*. 2009;82(2):405-420.

35. Bluni ST, Marder AR, Goldstein JI. Surface characterization of hot-dip galfan coatings. *Materials Characterization*. 1994;33(2):93-97.

36. Eliot SA. Methods for metallographically revealing intermetallic formation at galfan/steel interfaces. *Materials Characterization*. 1993;30(4):295-297.

37. ASTM International. ASTM B750, 2012 "standard specification fro galfan (zinc-5% aluminium-mischmetal) alloy in ingot form for hot-dip coatings". . 2012. www.astm.org. doi: 10.1520/B0750-12.

38. Elvins J, Spittle JA, Worsley DA. Microstructual changes in zinc aluminium alloy galvanising as a function of processing parameters and their influence on corrosion. *Corrosion Science*. 2005;47(11):2740-2759.

39. Bluni ST, Notis MR, Marder AR. Nucleation characteristics and microstructure in off-eutectic al-zn alloys. *Acta Metallurgica et Materialia*. 1995;43(5):1775-1782.

40. ASM International. Binary alloy phase diagrams [electronic resource]. . 1990.

41. Zhu Y. General rule of phase decomposition in zn-al based alloys (II). *Materials Transactions*. 2004;45(11):3083-3097.

42. Ramus Moreira A, Panossian Z, Camargo PL, Ferreira Moreira M, da Silva IC, Ribeiro de Carvalho JE. Zn/55Al coating microstructure and corrosion mechanism. *Corrosion Science*. 2006;48(3):564-576.

43. Qiu P, Leygraf C, Wallinder I. Evolution of corrosion products and metal release from galvalume coatings on steel during short and long term atmospheric exposures. *Materials Chemsitry and Physics*. 2012;133(1):419-428.

44. Schmidt DP, Shawa BA, Sikora E, Shawa WW, Laliberte LH. Corrosion protection assessment of sacrificial coating systems as a function of exposure time in a marine environment. *Progress in Organic Coatings*. 2006;57:352–364.

45. Budruk AS, Balasubramaniam R, Gupta M. Corrosion behaviour of Mg–Cu and Mg–Mo composites in 3.5% NaCl. *Corrosion Science*. 2008;50:2423–2428.

46. Sugimaru S, Hikita N, Yoshie A, Tanaka S, Ohba H, Nishida S. Zinc alloy coated steel wire with high corrosion resistance. *Nippon Steel Technical Report*. 2007;96.

47. Enthone. Automotive update - cyclic corrosion testing. http://www.enthone.com/nl/docs/AutomotiveUpdate4-806CCT.pdf. Updated 2006. Accessed September, 20, 2010.

48. ASTM standard B117 2009, " standard practice for operating salt spray (fog) apparatus". . 2009. doi: 10.1520/B0117-09.

49. ASTM Interational. ASTM D1141, 1998 "standard practice for the preparation of substitue ocean water". . 1998. www.astm.org. doi: 10.1520/D1141-98R13.

50. Q Panel Lab Products. Q-FOR CYClic tester operating manual. . Revised 11 July 2003.

51. WireCo WorldGroup. Wire rope user's handbook. . 2008.

52. SurTec. SurTec 451 - chemcial deburring. .

53. Baker K. University of Cape Town.

54. Struers. Metallographic preparation of zinc coatings. .

55. *Energy-dispersive X-ray microanalysis, an introduction.* Middleton, Wisconsin: NORAN Instruments; 1983.

56. Geobrugg. RXI and AXI rockfall barriers stop rocks that would even overwhelm concrete galleries. .

57. Volovitch P, Vu TN, Allely C, Abdel Aal A, Ogle K. Understanding corrosion via corrosion product characterization: II. role of alloying elements in improving the corrosion resistance of zn-al-mg coatings on steel. *Corrosion Science*. 2011;53(8):2437-2445.

58. Bierwagen G, Tallman D, Li J, He L, Jeffcoate C. EIS studies of coated metals in accelerated exposure. *Progress in Organic Coatings*. 2003;46(2):149-158.

59. Antunes RA, Costa I, Araujo de Faria DL. <br />Characterization of corrosion products formed on steels in the first months of atmospheric exposure. *Materials Research*. 2003;6(3).

# Acknowledgements

First of all, praise be to God for his goodness. He makes all things possible.

I continue my thanks with my supervisor, Professor Rob Knutsen, for his guidance and support throughout my postgraduate years at the University of Cape Town. I could not have come this far without him. I am forever a better person by having passed through his hands.

Various other acknowledgements are made to:

Miranda Waldron at the Electron Microscopy unit for assistance with scanning electron microscopy.

Glen Newins and his team at the Mechanical Engineering workshop for constantly and efficiently assisting me with various material preparations.

Simon Norton of the Chemical Investigation Services for introducing me to the wonderful world of metallic corrosion and for providing advice and reading materials whenever I made a request.

All the staff and my colleagues at the Centre for Materials Engineering who made every day in the lab a pleasant experience of laughter and learning. I will miss them all.

To Faatin Bux , a huge THANK YOU for your patience and assistance during the final printing of this report!

I thank my parents and family for their constant support and encouragement. Their love pulled me through the toughest of times; they are my anchor through every storm I navigate.

Finally, I thank the love of my life, Amanda Mashanyare. You make every day a happy day. I look forward to ‘forever and a day’ at your side.